

**Femtosecond Carrier Dynamics In III-V Semiconductors Grown
At Low Substrate Temperatures**

by

Yiorgos K. Kostoulas

Submitted In Partial Fulfillment
of the
Requirements for the Degree

Reviewed for Classification 1/19/96
(Date)

Doctor of Philosophy

UNCLASSIFIED


R. L. McCrory, Jr.

Authorized Derivative Classifier

Supervised by

Professor Philippe M. Fauchet

Department of Physics and Astronomy
The College
Arts and Sciences

University of Rochester
Rochester, New York

1995

Curriculum Vitae

Yiorgos Kostoulas was born on August 26, 1966. He attended the Aristoteleio Panepistimio Thessalonikis in Greece from 1984 to 1989, where he received a Bachelor of Science Degree in Physics. After an internship at CERN, in the summer of 1989, he started graduate studies in the University of Rochester on September 1989, under the guidance of Professor A. Melissinos. In 1989 he was awarded the Erasmus Fellowship and in 1993-1994 he was a recipient of the Link Foundation Fellowship. His research work has included the Brookhaven National Laboratory Experiment 840 -a coherent production of any pseudoscalar (or scalar) that couples to two photons- from May 1989 to December 1990. Subsequently he directed his efforts in the field of Optical Nonlinearities in III-V Semiconductors. Among the areas he has worked on are: Femtosecond Nonlinearities and Hot Carrier Dynamics in GaAs, Refractive Index Spectral hole burning in InP, Femtosecond Carrier Dynamics in Porous Silicon, and Sub-Picosecond Carrier Trapping Times In III-V Compounds Grown At Low Substrate Temperatures, from May 1992 to present. He was a teaching assistant in the Department of Physics from January 1993 to May 1993. This work was supervised by Professor Philippe M. Fauchet.

Acknowledgments

This work wouldn't have been possible without the support of the Laboratory of Laser Energetics and the Center for Optoelectronics and Imaging. Both LLE and COI provided us with facilities and personnel so there are numerous people to thank: Shirley Steinberg, Ronda Salomon, Dick Fellows, Linda Clement, LaDona Black and everybody in the electronics shop. This support was matched by the people of the Physics Department: Betty Cook, Barbara Warren, Ovide Coriveau, Marj Chapin, and Kenn Harper. I would also like to express my gratitude to the faculty of the Department of Physics both for instruction during the years I spend in the University of Rochester and for the insights that I will carry with me as I move onward. The interactions and collaborations that I have enjoyed with fellow students and staff have also been invaluable. I am grateful to Dr. John Soures of LLE, to Prof. Dan Watson for his support and encouragement during my stay in Rochester, to Prof. Gary Wicks for making all his resources readily available, and to my advisor Prof. Philippe Fauchet for his continuous guidance. I would also like to thank Mike Koch for making his expertise in MBE always available. My appreciation goes to my fellow graduate students Kamil Burak Üçer and Ahmad Ibrahim Lobad whose help would be hard to overestimate. Finally, my special thanks go to my parents, Dionysia and Kostas, whose support eventhough from a distance, has made this thesis possible.

ABSTRACT

Studies on carrier dynamics, trapping and recombination are presented, in III-V compounds grown at low substrate temperatures (LT-III/Vs). We have used femtosecond pump-probe, and up-conversion luminescence spectroscopy in order to determine the dynamics of photoexcited carriers in a variety of semiconductor compounds of the As and P family (LT-GaAs, LT-InP and LT-GaInP). Changes in the absorption coefficient and refractive index are measured over a wide spectral range (570 nm - 900 nm) and at different injected carrier densities ($\sim 10^{16}$ - 10^{19} cm^{-3}).

Complementary experimental techniques such as pump-probe and up-conversion luminescence, show that in the low temperature grown III-V compounds, it is carrier trapping that takes place in a sub-picosecond time scale with carrier recombination following at longer times. In spite of their different electrical properties, these materials show very similar optical response near the band edge.

No spectral hole burning is observed in the LT-III-V compounds studied. Carrier scattering spreads the distribution to the bottom of the conduction band within our 100 fs time resolution. Carrier trapping leads to induced absorption due to the photoionization of the defects by the probe photons. For the

lowest growth temperatures, the trapping times were found to be 0.45 ps, 0.35 ps, for InP and GaInP grown at 200°C, and 1.4 ps for GaAs as grown at 195°C.

Table of Contents

Curriculum Vitae	ii
Acknowledgments.....	iii
Abstract.....	iv
List of Figures.....	vi
List of Tables.....	vii
Chapter 1: Introduction.....	1
1.1 Technological Motivation	1
1.2 Survey of the Material Properties.....	5
1.3 Outline of Thesis.....	25
References.....	26
Chapter 2: Experimental Considerations.....	31
2.1 Laser Systems.....	31
2.2 Sample Preparation.....	35
2.3 Experimental Methods	38
References.....	48
Chapter 3: Femtosecond Carrier Dynamics In Low Temperature Grown InP.....	50
3.1 Introduction.....	50
3.2 Refractive Index Spectral Hole Burning	52
3.3 Carrier Trapping and Recombination.....	59
References.....	72
Chapter 4: Carrier Dynamics In low Temperature Grown Ga _{0.51} In _{0.49} P Above and Below The Conduction Band Edge.....	75
4.1 Introduction.....	75
4.2 Carrier Dynamics In Conventionally Grown GaInP	77
4.3 Carrier-Carrier Scattering In Conventionally Grown GaAs and GaInP	86
4.4 Carrier Dynamics In Low-Temperature Grown GaInP	96
4.5 Spectral Hole Burning In Conventionally and Low Temperature Grown GaInP	101
4.6 Carrier Trapping vs Recombination In Low-Temperature Grown GaInP	104
4.7 Conclusions	109

References	110
Chapter 5: Ultrafast Photo-Response of Low Temperature Grown GaAs	113
5.1 Introduction.....	113
5.2 LT-GaAs Grown at 250°C.....	117
5.3 LT-GaAs Grown at 195°C	118
5.4 Carrier Dynamics Below the Band Edge	125
References.....	133
Chapter 6: Conclusions and Future Directions.....	135
References.....	139

List of Figures

Chapter 1:	
1.1 Electron and hole photoionization of the EL2 defect	6
1.2 Proposed density of states for GaAs as-grown at 200°C	11
1.3 Proposed density of states for annealed GaAs	14
1.4 Free carrier concentration and mobility of LT-InP	18
1.5 Band structure of LT-GaInP	21
Chapter 2:	
2.1 Schematic of the 2 eV based amplified laser system.....	32
2.2 Schematic of the Ti:Sapphire laser cavity	34
2.3 Procedure for lift-off of the InP thin films.....	37
2.4 Diagrammatic representation of the pum-probe measurements	40
2.5 Extraction of n and k from the measured T and R values.....	44
2.6 The up-conversion luminescence experimental set-up.....	47
Chapter 3:	
3.1 Spectral hole burning in a semiconductor	53
3.2 Refractive Index Spectral Hole Burning in GaAs.....	55
3.3 Refractive Index Spectral Hole Burning in InP	56
3.4 No spectral hole burning is observed in LT-InP.....	58
3.5 Time resolved bandedge luminescence of LT-InP.....	61
3.6 Differential transmission of LT-InP samples	63
3.7 200°C grown InP at different carrier densities	65
3.8 200°C grown InP vs n-type normally grown material, at 2 eV	67
3.9 Trap saturation at high carrier densities.....	70

Chapter 4:	
4.1	Band edge luminescence of conventionally grown GaInP 78
4.2	Carrier dynamics at 2 eV in conventionally grown GaInP 81
4.3	2 eV/WLC measurements of conventionally grown GaInP 85
4.4	Carrier-carrier scattering in GaAs at low carrier density 89
4.5	Carrier-carrier scattering in GaAs at high carrier density 91
4.6	Carrier-carrier scattering in conventionally grown GaInP 94
4.7	ΔT_{\max} vs carrier density in conventionally grown GaInP 95
4.8	Carrier dynamics in LT-grown GaInP 98
4.9	Response of 200°C grown GaInP at 620 nm and 750 nm 100
4.10	Spectral hole burning in conventionally and LT-grown GaInP . 103
4.11	300°C and conventionally grown GaInP response at 840 nm ... 105
4.12	Response of 200°C as-grown and annealed samples (840 nm) . 108
Chapter 5:	
5.1	2 eV/WLC measurements on 250°C as-grown GaAs..... 116
5.2	2 eV/WLC measurements on 195°C as-grown GaAs..... 119
5.3	Single exponential fit of the 890 nm response 121
5.4	2 eV/WLC measurements on 195°C annealed GaAs 122
5.5	Comparison of the banedge response of four GaAs samples 124
5.6	1.55 eV/WLC measurements on the 195°C as-grown GaAs 126
5.7	1.55 eV/WLC measurements on the 195°C annealed GaAs 128
5.8	1.55 eV/WLC measurements on the 250°C as-grown GaAs 130
5.9	1.55 eV/WLC measurements on the 500°C grown GaAs..... 131
Chapter 6:	
6.1	Expected behavior of other III-Vs grown at lowtemperature 138

List of Tables

Chapter 1:	
Table I	Photoconductive Materials With Carrier Lifetimes and Mobilities..... 3
Table II	Material Parameters of Annealed LT-GaAs..... 16
Chapter 4:	
Table III	Material Parameters for GaInP and GaAs 79

CHAPTER 1

Introduction

1.1 Technological Motivation

The development of ultrashort optical pulses has led to the emergence of new techniques for the generation and detection of subpicosecond electrical transients. Laser-triggered, ultrafast photoconductive switching [1] and electro-optic sampling [2] are techniques that have demonstrated a capability for subpicosecond or near-terahertz response/bandwidth. Currently, the limitations imposed on these techniques are mainly due to the long lifetime of the photo-generated carriers. To achieve significantly shorter carrier lifetimes, various methods have been employed in the past with different degrees of success. A partial list includes introduction of deep levels through doping with compensating impurities, use of amorphous or polycrystalline [3] materials, bombardment with high-energy particles and ion implantation, and use of II-VI materials such as CdTe grown by metal-organic vapor phase epitaxy (MOVPE) [4]. Unfortunately all of these methods suffer from inherent limitations. For instance, doping with compensating impurities introduces deep levels and hence reduces the carrier lifetime. In the case of GaAs:Cr, carrier lifetimes of ~60 ps have been found [5]. While shorter than for intrinsic materials, the lifetimes realized by this process limit the electrical pulse widths that can be generated to a few tens of picoseconds.

In the case of the amorphous and polycrystalline materials, it is their low carrier mobility that acts as the limiting factor. Amorphous silicon is one such material that has been extensively studied as a photoconductor [6]. However, due to disorder, the charge transport takes place through the extended band tail states, resulting in a very low drift mobility ($\sim 1 \text{ cm}^2/\text{Vsec}$). This implies a poor conversion efficiency from the applied bias to the peak amplitude of the generated pulse.

The use of damage induced by high energy particles in order to create deep level trapping/recombination centers can also lead to short carrier lifetimes. For instance, the free-carrier lifetime in O^+ implanted Si-on-Sapphire (SOS) decreases as the implantation dose increases. In studies of SOS experiencing doses above $3 \times 10^{14} \text{ cm}^{-2}$, the measured carrier lifetime reached a limit of 600 fs [7]. Proton bombardment has been also used to decrease the carrier lifetime in InP and GaAs. Carrier lifetimes reaching down to $\sim 100 \text{ fs}$ for very high doses of $\sim 10^{16} \text{ cm}^{-2}$ have been reported in the case of InP [8]. Two problems are associated with this technique: First, as the implantation dose increases, the carrier mobility decreases leading to low responsivity, a problem similar to that encountered in amorphous materials, and second, the degradation of the ion-implanted materials at room temperature.

Very fast switching times ($\sim 480 \text{ fs}$) have been achieved with II-VI materials, such as CdTe.[9] In addition the responsivity of this material is relatively high since the carrier mobility is $\sim 180 \text{ cm}^2/\text{Vsec}$. The main problem is the difficulty

Table I. Photoconductive materials with carrier lifetimes and mobilities.

Material	Carrier Lifetime (ps)	Mobility (cm ² /V's)
GaAs:Cr	50-100	1000
Ion-implanted InP	2-4	200
Ion-damaged SOS	0.6	30
Amorphous silicon	0.8-20	1
MOCVD CdTe	0.45	180

Table I. Various photoconductive materials with their carrier lifetimes and mobilities. (After Gupta et. al., IEEE J Quantum Electron., **QE-28**, 2464 (1992)).

to integrate II-VI materials with the relatively mature III-V semiconductor device technology. Table I lists some of these materials and their typical lifetimes together with their mobilities.

An alternative approach that seems to overcome the above limitations is the growth of III-V semiconductors at low substrate temperatures. For epitaxial growth of III-V semiconductor layers by molecular beam epitaxy (MBE), the substrate temperature T_g , the group V/III flux ratio and the growth rate are the important parameters determining the growth mechanism and the quality of the epitaxial layers. Varying the growth temperature in order to optimize growth conditions, has been used extensively. Between 1978 and 1983 a small number of papers([10, 11]) reported the first attempts to grow GaAs at substrate temperatures lower than the standard 600°C but at the same growth rate. The resulting material exhibited an abrupt decrease in mobility and carrier concentration, and was also “optically dead” (i.e. it was not luminescent). Colin Wood, one of the pioneers in MBE, would refer to this type of GaAs as “wooden”, perhaps in reference to his early crystal growths. In order to compensate, Metzger and Calawa [12] reduced the growth rate and defined the growth conditions [13] for what is now known as LT-GaAs: T_g of about 200°C, growth rate of about 1 $\mu\text{m/h}$ and As-stable growth conditions (As:Ga beam equivalent pressure ratio of 10:1). This type of material has a high density of point defects, due to the growth at low temperature. These defects act as trapping/recombination centers, reducing the carrier lifetime to ~ 400 fs. The

resulting material is also of high crystalline quality (the low growth rate allows enough time to the ad-atoms to move to their lattice sites) and therefore of high carrier mobility ($\mu \sim 1000 \text{ cm}^2/\text{V}\cdot\text{sec}$). These properties, together with high resistivity (after annealing at 600°C for 10 minutes) make this material the most suitable candidate for the opto-electronic applications mentioned earlier, without any of the deficiencies encountered in the previous attempts to shorten the carrier lifetime.

This success has led to the commercialization of LT-GaAs based, high-speed optoelectronic devices as is demonstrated by the spin-off of Picometrix, Inc. Additionally, other III-V materials such as LT-InP, InGaP, AlGaAs, InAlAs and InGaAs have been investigated in an effort to understand better the fundamental properties of these compounds and to identify candidates suitable for optoelectronic devices at the optical communications wavelength of $1.55 \mu\text{m}$. In this work we will concentrate on three different III-Vs that have very different electrical properties when grown at low substrate temperatures: LT-InP, LT- $\text{Ga}_{0.51}\text{In}_{0.49}\text{P}$, and LT-GaAs.

1.2 Survey of the Material Properties

LT-GaAs

The dominant point defects in LT-GaAs are *EL2*-related defects. In an attempt to supply a background for the understanding of the material properties of LT-GaAs,

we summarize the major characteristics of the *EL2* defect in GaAs. The *EL2* defect is the dominant defect in melt grown GaAs. It is commonly present in concentrations of $1-2 \times 10^{16} \text{ cm}^{-3}$ both in liquid encapsulated Czochralski (LEC)- and Bridgman-grown crystals. *EL2* is present in concentrations of 10^{14} cm^{-3} in vapor phase epitaxy (VPE) GaAs. However, it is not present in liquid phase epitaxy (LPE) grown layers or in molecular beam epitaxy (MBE) layers (the defects in LT-GaAs are *EL2*-like, i.e. they exhibit most but not all of the *EL2* properties). The *EL2* defect basically controls the electrical and optical properties of GaAs and its existence makes it possible to achieve thermally stable semi-insulating (SI) GaAs-the key material in integrated circuit technology.

The *EL2* defect is created under As-rich conditions. Its concentration can be controlled to some extent by stoichiometry during crystal growth. For the range of As/Ga over which monocrystalline (melt grown or epitaxial) GaAs can be grown, the concentration of *EL2* varies by less than an order of magnitude. Lagowski *et al.* [14] linked *EL2* with an arsenic antisite defect. As_{Ga} has a double donor character, and according to the mass action law its creation can be strongly suppressed by intentional doping with shallow donors. This leads to a variation of the *EL2* concentration by more than three orders of magnitude (nearly constant at $\sim 10^{16} \text{ cm}^{-3}$ for a free electron concentration up to $5 \times 10^{16} \text{ cm}^{-3}$ and reducing to less than 10^{13} cm^{-3} when the free electron concentration exceeds $2 \times 10^{17} \text{ cm}^{-3}$). These results lead to a two-step mechanism for the creation of the *EL2* defect:

- i. the creation of Ga vacancies under As-rich conditions (during GaAs solidification at $\sim 1250^\circ\text{C}$), and
- ii. the migration of As atoms and their interaction with gallium vacancies, leading to the creation of antisite As-related defects (during post solidification cooling at $\sim 800^\circ\text{C}$).

The *EL2* defect has a deep donor character. The *EL2* thermal activation energy was determined to be at 0.75 eV below the conduction band E_c [15] using Hall measurements. This means that the ground state of configuration $EL2^{0/+}$ is roughly placed in the middle of the GaAs energy gap ($EL2^{0/+}$ represents *EL2* in the neutral charge state when the $E_c - 0.75$ eV level is occupied and in the singly positive charge state after giving up an electron). The second ionization level, $EL2^{+/++}$, lies at 0.52 eV above the top of the valence band

The near infrared absorption spectrum related to *EL2* in neutral charge state was first published by Martin [16]. After the part corresponding to the intracenter transitions was identified (between 1.0 eV and 1.3 eV) [17], the spectrum corresponding to photo-ionization of the *EL2* was isolated. It consists of three bands with energy thresholds at about 0.8 eV, 1.0 eV and 1.3 eV, related to photo-ionization to the Γ , L, and X points of the GaAs Brillouin zone. The *EL2* optical cross section, both for photo-ionization to the conduction band ($EL2^0 \rightarrow EL2^+ + e$ in the conduction band) σ_n^0 , and for electron capture from the valence band ($EL2^+ + e$ in the valence band $\rightarrow EL2^0$) σ_p^0 , was determined by Silverberg *et al* [18]. Their data for room temperature can be seen in **Figure 1.1**. The cross

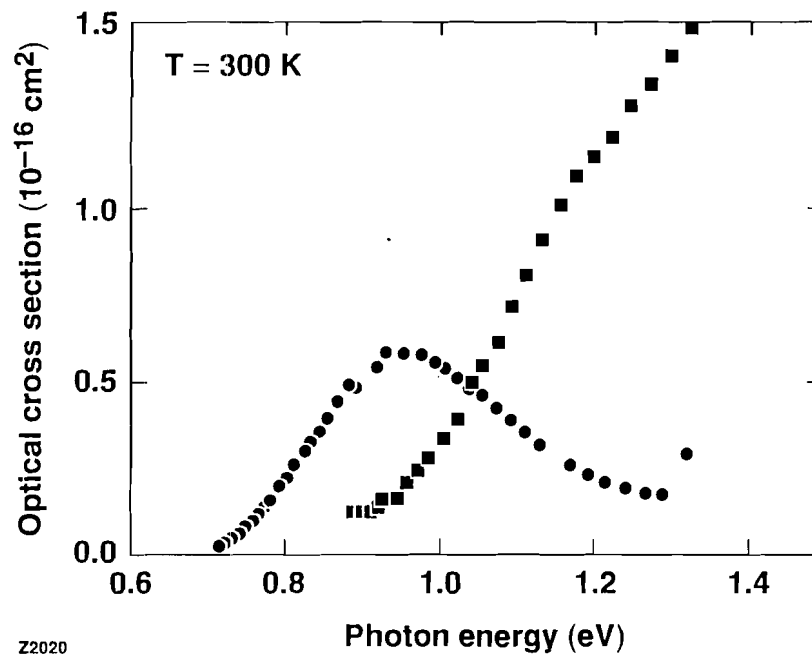


Figure 1.1 Room temperature electron (squares) and hole (circles) cross-sections of the EL2 in GaAs (After Silverberg et. al. [18]).

section at room temperature, for 1.2 eV photons, is $0.3 \times 10^{-16} \text{ cm}^2$ and 10^{-16} cm^2 for hole and electron photo-ionization respectively.

The most characteristic feature -the signature- of the *EL2* defect is its metastable state. It occurs at low temperatures (<130 K) under illumination with light of 1.0-1.3 eV. Its spectrum is identical to the intracenter absorption spectrum. The *EL2* transition from its neutral ground state to the metastable state occurs without change of the defect charge state. The de-excitation of the *EL2* from its metastable state takes place thermally and it is accelerated in the presence of free electrons, due to an ‘‘Auger-like’’ process. Optically induced relaxation of the metastable state has also been studied but results are not yet conclusive. Due to the existence of the metastable state, the near infrared absorption of *EL2* can be quenched under illumination with white light.

A theory has been proposed recently in order to explain the metastable state of the *EL2* defect. According to Dabrowski and Scheffler [19] the metastable transition arises when a neutral As_{Ga} absorbs a photon of $\sim 1.1 \text{ eV}$ energy and moves from the Ga lattice site into an interstitial location. This process creates a $\text{V}_{\text{Ga}}\text{-As}_i$ defect complex. A perturbation in the local environment of the defect can preclude the existence of the metastable state, as has been observed in plastically deformed and neutron and electron irradiated samples. In these cases, an increase has been observed in the density of As_{Ga}^0 and As_{Ga}^+ defects, but the near infrared absorption is not quenched by white light illumination, i.e. no metastable state exists. The defects in LT-GaAs are also of similar nature.

In the MBE growth of GaAs, the growth rate is determined by the Ga flux incident on the sample, while the As flux and the substrate temperature determine the surface reconstruction. These three parameters determine if the growing GaAs surface is As- or Ga- stabilized (i.e. has an excess of As or Ga). As the growth temperature is reduced, a smaller As-to-Ga flux ratio is needed in order to achieve As stabilized growth conditions. For the growth of LT-GaAs, it is usually 10:1 As:Ga, ensuring As-rich conditions. Additionally, the Ga or As adatoms do not have enough time to move to their respective equilibrium lattice sites before they are incorporated into the growing film. These growth conditions lead to an increased number of defects in the film, such as As_{Ga} , V_{Ga} , and As_i .

In studying LT-GaAs, we need to distinguish two forms: the as-grown material and the annealed material, which have quite different properties. The parameters quoted refer to samples grown at $\sim 200^\circ\text{C}$ and the standard annealing conditions are at 600°C for 10 min under As overpressure.

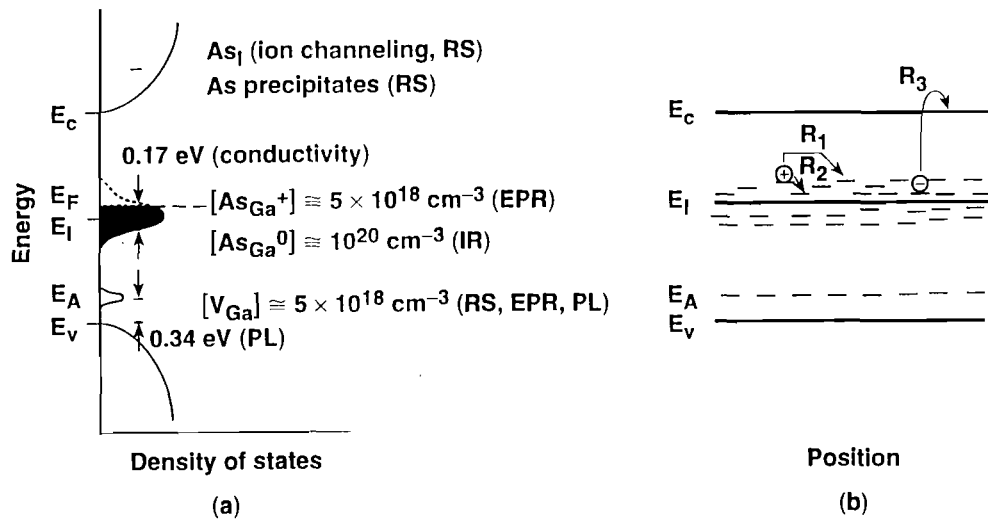
As more arsenic is incorporated into the sample at low growth temperatures, the stoichiometry of the material changes. The resulting as-grown GaAs is found to be 1at%-2at% As-rich. This leads to an increase in the lattice constant by $\Delta a/a_0 \sim 10^{-3}$. The larger lattice constant causes pseudomorphic growth of the LT epilayer, with a pseudomorphic thickness that reduces with reducing growth temperature. For 200°C , the pseudomorphic thickness is $\sim 2 \mu\text{m}$, above which the epilayer becomes polycrystalline. The density of the dominant As_{Ga} defect is $\sim 10^{20} \text{ cm}^{-3}$ as it was determined by IR absorption. This defect has

an energy level 0.75 eV below the conduction band minimum. Such a large density of point defects leads to the creation of a defect band via two possible mechanisms. The first is called disorder broadening. In this mechanism, the energy of the deep levels associated with the defects is perturbed by a change in their local environment, as, for instance, by some other nearby charged defect or crystal imperfection. The disordered distribution of these other defects (especially charged ones) represents a fluctuating potential that shifts the energy levels of the defect under consideration, leading to an energy spread of the deep levels and the formation of the deep-level band. The second mechanism involves the wave function overlap of the defect states. The greater the density of defects, the greater the wave function overlap, and hence, the greater the spread of the defect energy band. This is analogous to the tight binding approximation used to describe the formation of energy bands in crystals. The contribution of this mechanism to the formation of an As_{Ga} defect band in LT-GaAs is expected to be small since these defects are spaced, on average, a distance $\geq 20 \text{ \AA}$ apart in the as-grown and annealed material. The width of this band is estimated from conductivity measurements to be $\sim 0.17 \text{ eV}$ in the as-grown material. Of these defects, $\sim 5\%$ are ionized, leading to a concentration of As_{Ga}^+ of $\sim 5 \times 10^{18} \text{ cm}^{-3}$, as determined by electron paramagnetic resonance (EPR).

The IR absorption shows the same characteristics as that of the *EL2* defect i.e. it begins at 0.75 eV, and has the two changes of slope observed in the absorption of *EL2*. It can be quenched only partially, leading to the conclusion that

only part (~10%) of the As_{Ga}^0 defects are *EL2* defects. For the as-grown material, the conduction at room temperature is due to hopping of holes in the defect band. Therefore, the electrons from the As_{Ga} ionized defects must be bound to compensating acceptors. The defects that act as such are the Ga vacancies, V_{Ga} , which have an acceptor level at 0.34 eV above the valence band edge. A density of states diagram for the as-grown material can be seen in **Figure 1.2**. The room temperature resistivity of the as-grown material is low, ~100 Ω cm, for growth at 200°C.[20] The mechanism responsible for such low resistivity is nearest neighbor hopping of holes in the 0.75 eV defect band. At higher temperatures, the conductivity is due to free electrons in the conduction band, with a mobility of 1000 cm^2/Vsec . Between 0°C to -90°C, the conductivity can be described by a temperature activated mechanism resulting in a defect band width of 0.17 eV with a mobility of ~1 cm^2/Vsec . At even lower temperatures, the mobility is again of the order of 1 cm^2/Vsec and the conductivity is due to variable range hopping ($\log\sigma \sim T^{-1/4}$).

The incorporation of more As in the material and the monotonic increase in point defect density with decreasing growth temperature lead also to a monotonic reduction of the band edge luminescence. At a growth temperature of ~300°C, the band edge luminescence is already below detectable levels. In contrast, the deep level luminescence at ~1.16 eV appears to increase slightly in intensity as the growth temperature is reduced. This deep level peak is associated with the conduction band-to- V_{Ga} transition. After annealing under As overpressure, the



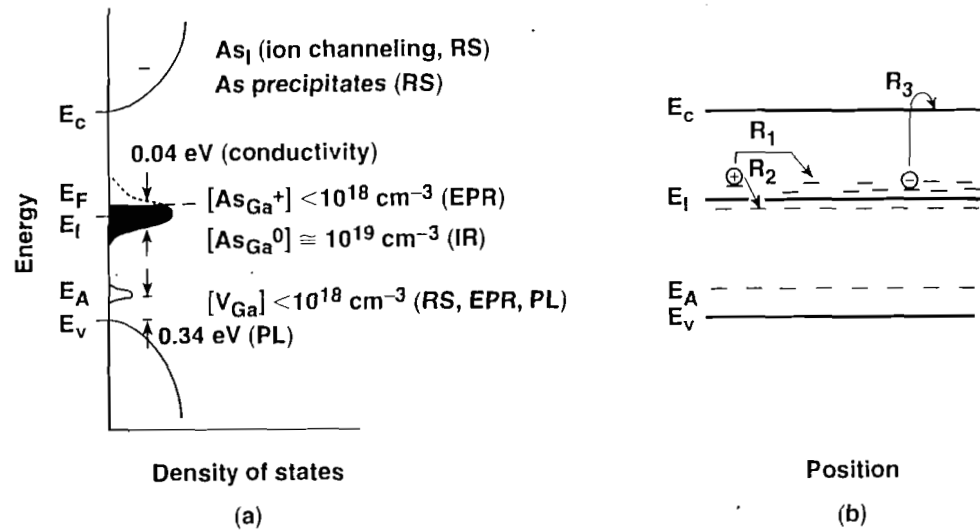
Z2021

Figure 1.2 Model for as-grown LT-GaAs. (a) Density of states and (b) band diagram. The techniques used to identify the defects are shown in parentheses. R_1 , R_2 , and R_3 represent nearest neighbor hopping, variable range hopping, and thermal activation conduction (after Smith, F. W. PhD Thesis, MIT 1990).

amount of excess As in the epilayer does not change but rather redistributes itself in the GaAs crystal matrix, and As precipitates are formed [21]. The average diameter of the precipitates is 60 Å and their density is of the order of 10^{17} cm^{-3} to 10^{18} cm^{-3} (for higher annealing temperatures and/or longer times, the diameter of the precipitates as well as their average spacing increases) [22].

The lattice constant is reduced monotonically with increasing annealing temperature, until it becomes indistinguishable from that of the conventionally grown material. The density of the As_{Ga}^0 is reduced by about an order of magnitude, to $\sim 10^{19} \text{ cm}^{-3}$. The density of As_{Ga}^+ drops below levels detectable by EPR i.e. $< 10^{18} \text{ cm}^{-3}$, but the persistence of hole hopping conductivity at room temperature indicates that it is still appreciable. As a result of the anneal, the width of the defect band is also reduced to 0.04 eV. Annealing also leads to a slower band edge optical response of LT-GaAs. The carrier lifetime increases from ~ 2 ps to ~ 10 ps [22] as the average As precipitate diameter increased from 400 Å to 900 Å, with 30 second anneals at temperatures ranging from 650°C to 1000°C [22]. Annealing of the material leads also to a much higher resistivity of $\sim 10^6 \Omega \cdot \text{cm}$. A schematic of the annealed LT-GaAs density of states diagram is depicted in **Figure 1.3** and its properties are summarized in Table II.

Two models have been proposed in order to explain the semi-insulating properties of the annealed LT-GaAs: the buried Schottky barrier model [23] and the arsenic antisite defect model [24]. The former explains the semi-insulating properties in terms of overlapping depletion regions around As precipitates formed



Z2022

Figure 1.3 Model for annealed LT-GaAs. (a) Density of states and (b) band diagram. The techniques used to identify the defects are shown in parentheses. R_1 , R_2 , and R_3 represent similar conduction mechanisms as in figure 1.2 (after Smith, F. W. PhD Thesis, MIT 1990).

Table II. Material parameters of annealed LT-GaAs

	GaAs	Annealed LT-GaAs
Structure	Crystalline	Crystalline
Stoichiometry	$\text{Ga}_{0.5}\text{As}_{0.5}$	~1 at % excess As $\text{Ga}_{0.495}\text{As}_{0.505}$
Resistivity	~ 0.3-20 $\Omega\text{-cm}$	~ $10^6 \Omega\text{-cm}$
Breakdown field	~ $3 \cdot 10^4 \text{ V cm}^{-1}$	~ $5 \cdot 10^5 \text{ V cm}^{-1}$
Trap density	$< 10^{15} \text{ cm}^{-3}$	~ 10^{19} cm^{-3}
Trapping time	~1 ns	< 1 ps

Table II. Summary of the material parameters of low tetmperature LT-GaAs grown at $\sim 200^\circ\text{C}$.

upon annealing, while the latter attributes the semi-insulating properties to the residual As_{Ga} defects which pin the Fermi level close to the mid-gap. The effect of doping on the dynamics of As clustering in LT-GaAs has also been studied extensively. It has been observed that the precipitates tend to accumulate in the n -doped regions and deplete from the p -doped regions on annealing.

Melloch [25] suggested that the dynamics of cluster formation can be qualitatively understood based on the charged states of the As interstitial and using thermodynamic arguments in which the crystal attempts to minimize the chemical potential during the anneal. The As interstitial has two positive charge states, +1 and +3. It is a “negative U” defect and it goes directly between these two charge states without a +2 charge state. In n -type material the As-precipitates are negatively charged and will attract positive As interstitials. In p -type material, the precipitates are positively charged and will repel positively charged As interstitials. However, there is still a short range attraction that will allow As precipitates to form in p -type LT-GaAs. Therefore, during coarsening there will be a preferential growth of the As precipitates on the n -GaAs side of a pn junction. In addition, a precipitate in an electric field will not be stable because if it thermally emits an As interstitial, the interstitial will be swept away by the electric field due to its positive charge. That explains the formation of As precipitates in Si δ -doped planes and in between Be- δ -doped planes [26].

LT-InP

InP is the second most important III/V binary after GaAs. Because of its direct band gap, smaller than that in GaAs, it is primarily used for a variety of light sources and optoelectronic detectors. Its very high carrier mobilities make InP an attractive material for fabricating high-speed devices. As in the case of GaAs, both bulk and epitaxial technologies are now mature, economically viable, and allow the fabrication of structures with properties desirable for commercial applications.

When growth at low temperatures is attempted, the case of InP is quite different from that of LT-GaAs. Even though the same prescription has been followed in an effort to create semi-insulating InP layers of good crystalline quality and short carrier trapping/recombination time, the resulting material is heavily n-type [29]. Such high electron concentration in LT-InP is mainly related to non-stoichiometric effects. The species of native defects in phosphorus-rich InP are P_i (phosphorus interstitial), P_{In} (phosphorus antisite defect), and V_{In} (In vacancy). Of these only P_{In} is a donor. Because the phosphorus atom is much smaller than the In atom, P can easily occupy an In vacancy under P-rich conditions. This can lead to up to ~6% excess P at growth temperatures of 200°C [27]. In the growth temperature range from 265°C to 500°C the concentration of residual carriers dramatically increases with decreasing growth temperature as can be seen in **Figure 1.4**. As the growth temperature is reduced even further, the concentration saturates at about $4 \times 10^{18} \text{ cm}^{-3}$ [28]. The mobility follows a similar behavior: it is $\sim 2500 \text{ cm}^2/\text{Vsec}$ at the highest growth temperatures, and drops

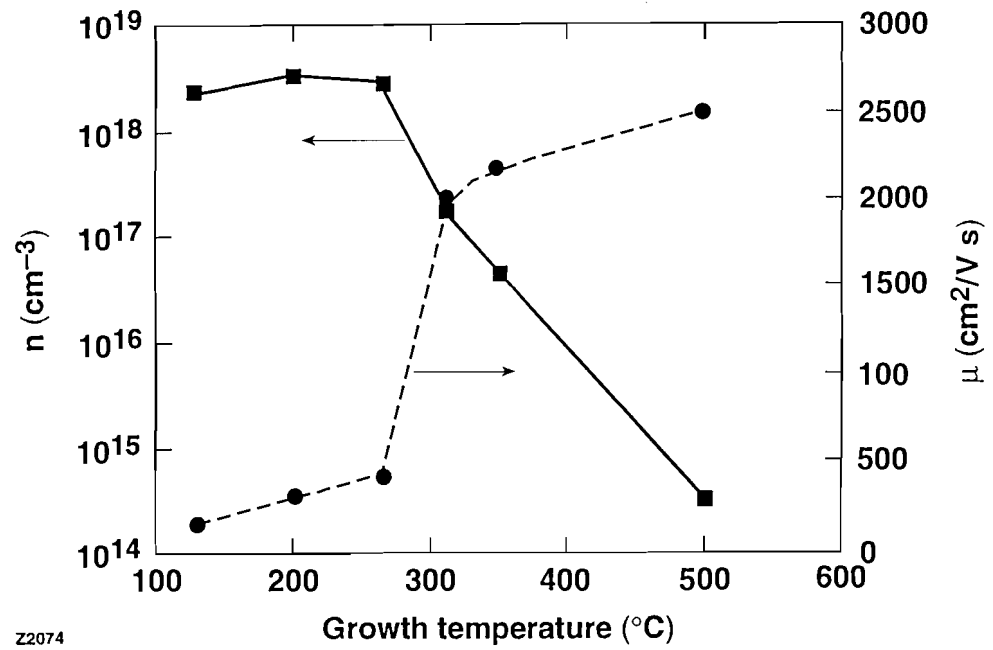


Figure 1.4 Room-temperature free carrier concentration n and mobility μ in undoped InP epilayers as a function of the growth temperature (from Dreszer et. al. [28]).

down to $<500 \text{ cm}^2/\text{Vsec}$ for temperatures between 300°C and 200°C . The defect responsible for these properties is the P_{In} interstitial which acts as a double donor. Its first ionization level, P_{In}^+ , which is degenerate with the conduction band at 0.11 eV above the conduction band minimum, has been identified by far infrared absorption under hydrostatic pressure [28]. This level gives rise to the high electron concentration via auto-ionization. Its second ionization level, $\text{P}_{\text{In}}^{++}$, lies at 0.23 eV below the conduction band Γ point [28]. The resistivity of the as-grown material is very low, $\sim 0.02 \Omega\text{cm}$ at room temperature [29]. Doping with Be, in an attempt to create semi-insulating LT-InP, has not achieved the desired results. The material remains n-type even at the highest doping densities of $\sim 10^{19} \text{ cm}^{-3}$ [29]. *Ex-situ* annealing of as-grown LT-InP at 500°C for 30 min can lead to an increase in resistivity of the undoped and Be-doped material by a factor of 6 and 60 respectively [29]. The formation of phosphorus precipitates has also been observed [30,31]. They consist of the alpha-white cubic form of phosphorus [31] which is insulating and their size ranges from 3 nm [31] up to 50 nm [30] for annealing at $\sim 600^\circ\text{C}$ for a few minutes.

LT-GaInP

$\text{Ga}_{0.49}\text{In}_{0.51}\text{P}$ (hereafter referred to as GaInP), with a band gap of $\sim 1.89 \text{ eV}$, is lattice matched to GaAs and thus epitaxial layers and devices made of this material are compatible with semi-insulating GaAs substrates and the relatively

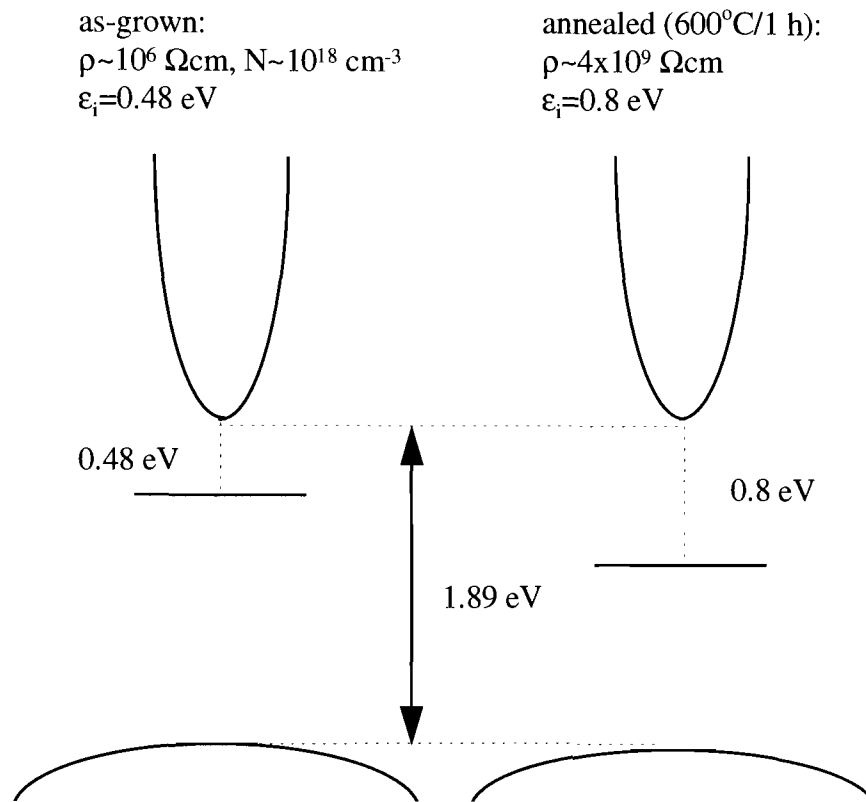


Figure 1.5 Band structure and defect levels of as-grown and annealed GaInP grown at a substrate temperatures of 200°C.

mature GaAs technology. With both n-type and p-type doping available, and a relatively high band gap of ~ 1.9 eV, many device applications have been proposed and implemented. For example, a high valence band discontinuity with GaAs (~ 0.24 eV [32]) and a low Be diffusion coefficient make GaInP an attractive emitter material for GaInP/GaAs/GaAs heterojunction bipolar transistors. Most of the work on deep levels in GaInP has been done for samples grown using LPE, VPE, and OMVPE. In LPE layers the deficiency of phosphorus can cause the appearance of an electron trap with a thermal activation energy of 0.39 eV. Sulfur doping introduces a DX-like electron state with a thermal activation energy in the range of 0.37-0.4 eV. This state exhibits all the characteristics of the DX center in $\text{Al}_x\text{Ga}_{1-x}\text{As}$ such as carrier freeze-out and persistent photoconductivity. Epilayers grown by gas source molecular beam epitaxy (GSMBE) at $\sim 550^\circ\text{C}$ have defects associated with both anion and cation vacancies. The phosphorus vacancy, V_p , as identified by electrical measurements, is an electron trap located at 0.28 eV below the conduction band edge [33]. Cathodoluminescence measurements have shown two luminescence bands at 1.34 eV and at 1.7 eV [34]. Their shift with temperature helps their identification as Column III and Column V vacancies. The former comprises a transition between the conduction band and a defect level located 0.5 eV above the valence band. This defect is associated with a Ga and/or In vacancy. The 1.7 eV band is due to a transition from a phosphorus vacancy at 0.2 eV below the conduction band to the valence band.

Unfortunately, very few studies have been done in order to determine the properties of the material when grown at temperatures lower than $\sim 550^\circ\text{C}$ [35]. Growth temperatures as low as 150°C have been attempted, but most of the characterization has been done on samples grown at 200°C [35]. In all cases the samples were of good crystalline quality as was determined by reflection high-energy electron diffraction (RHEED). The growth rate of the epilayers was $0.5 \mu\text{m/h}$. For the epilayers grown at 200°C , the lattice constant was found to be slightly larger than that of the material grown at high temperatures, due to the excess phosphorus in the material. After annealing at 600°C for 1 hour, the lattice constant reduces but is still larger than in normally grown epilayers. The experimental room temperature values for resistivity ρ , and mobility μ , of the 200°C as-grown epilayer, are $8.7 \times 10^5 \Omega\text{cm}$ and $120 \text{ cm}^2/\text{Vsec}$ [35]. A numerical solution of the Boltzmann transport equation yields an ionized defect concentration of $\sim 10^{18} \text{ cm}^{-3}$ [35]. The large resistivity of the as-grown material indicates that the density of defects is not large enough to produce hopping conductivity as in the case of LT-GaAs. The activation energy of the defect determined from the slope of the Arrhenius plot, is 0.48 eV , i.e. the defect involved has a $T=0$ transition at $E_c - 0.48 \text{ eV}$.

Annealing at 600°C for 1 hour produces material with even higher resistivity. It is extrapolated from higher temperature measurements to be $4 \times 10^9 \Omega\text{cm}$ at room temperature, with an activation energy of 0.8 eV . Cross-sectional transmission electron microscopy showed no formation of P-precipitates after

annealing, but showed phase separation in the as-grown material, manifested in the form of a “precipitate-like” microstructure. **Figure 1.5** shows a schematic of the band structure and defect levels of the LT-GaInP material.

Other LT-III/Vs

The success of LT-GaAs has led to the study of the properties of a variety of other semiconductors, grown at low substrate temperatures. Other As-based III-Vs include AlGaAs, InAlAs, and InGaAs. AlGaAs grown at 250°C and annealed at 600°C for 20 minutes is of extremely high resistivity ($\sim 10^{11}$ Ωcm) with the mobility being between 0.1 and 10 cm^2/Vsec [36]. In AlGaAs/GaAs superlattices, precipitate accumulation and depletion zones have been observed caused by diffusion of As from AlGaAs to GaAs. Layers of $\text{In}_{0.52}\text{Al}_{0.48}\text{As}$ lattice matched on InP (band gap at ~ 1.45 eV), are single crystalline and of high resistivity ($\sim 10^7$ Ωcm) when grown at substrate temperatures of $\sim 150^\circ\text{C}$ and annealed at 500°C for 10 min [37]. In an effort to extend the set of useful materials to include the wavelengths that are important to the optical communications industry, i.e. 1.3 μm and 1.5 μm , $\text{In}_x\text{Ga}_{1-x}\text{As}$ has also attracted much attention. When lattice matched to InP ($x=0.53$) it was found to be single crystalline for growth temperatures down to 125°C. Below 200°C, the electron concentration increases to 10^{18} cm^{-3} and the mobility falls from 10^4 to 10^3 cm^2/Vsec . This behavior was attributed to a 32 meV donor level. The resistivity did not change after a 500°C anneal for 1 hour [38]. Unfortunately, these properties make GaInAs

unsuited for photodetector applications. Various approaches have been used to increase the resistivity while maintaining short carrier lifetimes and similar bandgap energies. For example, the addition of a small mole fraction of Al in the alloy will improve the resistivity while altering the bandgap only to a small extent. The growth of lattice mismatched $\text{In}_x\text{Ga}_{1-x}\text{As}$ on GaAs also yields material of high resistivity. For $x=0.25$, the resistivity and mobility decrease as growth temperatures is reduced to 160°C . After annealing at 600°C for 15 minutes under As over pressure, both these properties improved dramatically [39].

On the side of the phosphides, another material that has attracted attention is GaP. As-grown at 190°C , the material is single crystal and its dark resistivity is too high to be measured on a high impedance Hall effect system. Under intense illumination it is of the order of $10^6 \Omega\text{cm}$. Annealing at 700°C for 1 hour did not produce significant strain reduction [40].

1.3 Outline of thesis

Out of the III-V semiconductors grown by MBE, GaAs is the most important material, and as such it is the one that has been studied the most when grown at low temperatures. After the initial success with GaAs, attention turned to a variety of III-Vs grown at low substrate temperatures. From the previous description of material parameters, we can see that even though the same

prescription is followed for the growth of all III-Vs at low substrate temperatures, not all of them have the same properties. For example, LT-GaAs is of low resistivity as-grown and becomes high resistivity after annealing. LT-InP is heavily n-type as-grown and annealed. LT-GaInP, on the other hand, is high resistivity both as-grown and annealed. These material properties are expected to play an important role in the optical response of these materials. In the following chapters we study each material with the appropriate ultrafast laser system and make a comparison with their normally grown counterparts. After a description of the experimental methods and laser systems in chapter 2, our results on LT-InP are presented in chapter 3. Chapter 4 deals with LT-GaInP and in chapter 5 our results on LT-GaAs are presented. Conclusions and future directions make up chapter 6.

References

1. D. H. Auston, IEEE J. Quantum Electron. **QE-19**, 639 (1983).
2. J. A. Valdmanis and G. Mourou, IEEE J. Quantum Electron. **QE-22**, 69 (1986).
3. D. H. Auston, P. Lavallard, N. Sol, and D. Kaplan, Appl. Phys. Lett. **36**, 66 (1980).
4. M. C. Nuss, D. W. Kisker, P. R. Smith, and T. E. Harvey, Appl. Phys. Lett. **54**, 57 (1989).
5. C. H. Lee, A. Antonetti, G. Mourou, Opt. Commun. **21**, 158, (1977).

6. D. H. Auston, P. Lavallard, N. Sol, D. Kaplan, Appl. Phys. Lett. **36**, 66, (1980).
7. D. R. Grischkowsky, M. B. Ketchen, C. C. Chi, I. N. Duling, N. J. Halas, J. M. Halbout, P. G. May, IEEE J. Quantum Electron. **24**, 221, (1988).
8. K. F. Lambert, S. Juen, L. Palmetshofer, and R. A. Hopfel, Appl. Phys. Lett. **59**, 926, (1991).
9. M. C. Nuss, D. W. Kisker, P. R. Smith, and T. E. Harvey, Appl. Phys. Lett. **54**, 57 (1989).
10. T. Murotani, T. Shimano and S. Mitsui, J. Cryst. Growth, **45**, 302, 1978.
11. R. Stall, C. Wood, P. Kirchner, and L. Eastman, Electron. Lett., **16**, 171, 1980.
12. G. Metze, and A. Calawa, Appl. Phys. Lett., **42**, 818, 1983.
13. F. Smith, A. Calawa, C.-L. Chen, M. Manfra, and L. Mahoney, Electron. Device Lett. **9**, 77, 1988.
14. J. Lagowski, H. C. Gatos, J. M. Parsey, K. Wada, M. Kaminska, and W. Walukiewicz, Appl. Phys. Lett. **40**, 342, (1982).
15. C. H. Henry, and D. V. Lang, Phys. Rev. B **15**, 989, (1977).
16. G. M. Martin, Appl. Phys. Lett. **39**, 747, (1981).
17. M. Kaminska, M. Skowronski, J. Lagowski, J. M. Parsey, and H. C. Gatos, Appl. Phys. Lett. **43**, 302, (1983).
18. P. Silverberg, P. Omling, and L. Samuelson, Appl. Phys. Lett. **52**, 1689, (1988).

19. J. Dabrowski, and M. Scheffler, *Phys. Rev. Lett.* **60**, 2183, (1988).
20. D. C. Look, D. C. Walters, G. D. Robinson, J. R. Sizelove, M. G. Mier, and C. E. Stutz, *J. Appl. Phys.* **74**, 306, (1993).
21. M. R. Melloch, N. Otsuka, J. M. Woodall, A. C. Warren, and J. L. Freeouf, *Appl. Phys. Lett.* **57**, 1531, (1990).
22. E. S. Harmon, M. R. Melloch, J. M. Woodall, D. D. Nolte, N. Otsuka, and C. L. Chang, *Appl. Phys. Lett.* **63**, 2248, (1993).
23. A. C. Warren, J. M. Woodall, J. L. Freouf, D. Grischkowski, D. T. McInturff, M. R. Meloch, and N. Otsuka, *Appl. Phys. Lett.* **57**, 1331, (1990).
24. D. C. Look, D. C. Walters, M. O. Manasreh, J. R. Sizelove, C. E. Stutz, and K. R. Evans, *Phys. Rev. B* **42**, 3578, (1990).
25. M. R. Melloch, N. Otsuka, K. Mahalingam, C. L. Chang, J. M. Woodall, G. D. Pettit, P. D. Kirchner, F. Cardone, A. C. Warren, and D. D. Nolte, *J. Appl. Phys.* **72**, 3509, (1992).
26. M. R. Melloch, N. Otsuka, K. Mahalingam, C. L. Chang, P. D. Kirchner, J. M. Woodall, and A. C. Warren, *Appl. Phys. Lett.* **61**, 177, (1992).
27. K. Xie, C. R. Wie and G. W. Wicks, *Mat. Res. Soc. Symp. Proc.* **241**, 265 (1992).
28. P. Dreszer, W. M. Chen, K. Seendripu, J. A. Wolk, W. Walukiewicz, B. W. Liang, C. W. Tu, and E. R. Weber, *Phys. Rev. B.* **47**, 4111, (1993).
29. B. W. Liang, and C. W. Tu, *Mat. Res. Soc. Symp. Proc.* **241**, 283 (1992).

30. G. N. Maracas, K. T. Shiralagi, R. A. Puechner, F. Yu, K. T. Choi, J. S. Bow, R. Ramamurti, M. J. Kim and R. W. Carpenter, *Mat. Res. Soc. Symp. Proc.* **241**, 271 (1992).
31. A. Claverie, J. Crestou, and J. C. Garcia, *Appl. Phys. Lett.* **62**, 1638, (1993).
32. A. Ginoudi, E. C. Paloura, and N. Frangis, *J. Appl. Phys.* **75**, 2980 (1994).
33. Z. C. Huang, C. R. Wie, J. A. Variano, M. W. Koch, and G. W. Wicks, *Mat. Res. Soc. Symp. Proc.* **325**, 137 (1994).
34. R. E. Viturro, J. A. Variano, and G. W. Wicks, *Mat. Res. Soc. Symp. Proc.* **325**, 513 (1994).
35. D. C. Look, Y. He, J. Ramdani, N. El-Masry, and S. M. Bedair, *Appl. Phys. Lett.* **63**, 1231 (1993).
36. A. C. Campbell, G. E. Crook, T. J. Rogers, and B. G. Steerman, *J. Vac. Sci. Tech.* **B8**, 305 (1990).
37. R. A. Metzger, A. S. Brown, W. E. Stanchina, M. Lui, R. G. Wilson, T. V. Kargodorian, L. G. McCray, and J. A. Hanige, *J. Cryst. Growth.* **111**, 445 (1991).
38. H. Künzel, J. Bötcher, R. Gribis, and G. Urmann, *Appl. Phys. Lett.* **61**, 1347, (1992).
39. S. Gupta, J. F. Whitaker, S. L. Williamson, G. A. Mourou, L. Lester, K. C. Hwang, P. Ho, J. Mazurowski, and J. M. Ballingall, *J. Electron. Mat.* **22**, 1449, (1993).

40. J. Ramdani, Y. He, M. Leonard, N. El-Masry, and S. M. Bedair,
Appl. Phys. Lett. **61**, 1646 (1992).

CHAPTER 2

Experimental Considerations

2.1 Laser Systems

The laser systems used in the measurements presented in this thesis are a copper-vapor-laser (CVL) amplified, colliding-pulse modelocked (CPM) dye laser, and a Ti:Sapphire laser. Here we will briefly touch upon the characteristics of these systems.

The first system is based on the CPM laser,[1] which gives pulses as short as 50 fs, energies of ~ 100 pJ/pulse at a repetition rate of 100 MHz, centered at a wavelength of 620 nm. The output of the CPM laser is amplified in a six-pass, CVL-pumped, dye amplifier.[2] After the fourth pass, the laser beam goes through a saturable absorber dye jet, in order to eliminate amplified spontaneous emission and pulses that are not amplified due to the different repetition rate between the CPM and CVL laser systems. The output of the amplifier is compressed by a prism sequence, positioned at the exit point of the amplifier, in order to provide pulse-width limited time-bandwidth product. This system gives pulse energies of ~ 10 μ J, as short as 80 fs, at a repetition rate of 8.5 kHz. Part of the amplifier output is then focused on a 1.25 mm thick ethylene glycol jet, where it generates a white light continuum (WLC). The wide spectral tunability (0.5 - 1.0 μ m) of these WLC pulses is fully exploited in our femtosecond spectroscopy measurements.

The duration of the CVL pulse is ~ 25 ns, and it is during this interval that energy is stored in the amplifier dye. This is, therefore, the time span during which the six passes of the CPM beam should take place. We need, therefore, a reliable electronic circuit, in order to synchronize the CPM and the CVL lasers. The synchronization electronics along with the laser system are shown in **Figure 2.1**. Additionally, the CVL laser needs to be prevented from being turned off, if the CPM laser is disturbed. The synchronization is accomplished by a gating discriminator, in which the 100 MHz output from a photodiode detecting the CPM pulses is gated by an 8.5 kHz, 15 ns, TTL signal. A digital delay is used to adjust the triggering phase of the CVL, so that the six passes of the CPM beam coincide with the peak of the CVL output pulse on the gain dye cell. Protection from shut-down is accomplished by means of a coincidence unit, which is used to trigger the CVL only when the CPM is off.

The Ti:Sapphire laser[3] is a folded cavity design, pumped by an “All lines” Ar⁺ laser (Coherent Laser Group, model Innova 100). It produces 90 fs pulses at a repetition rate of 85 MHz and with an energy of ~ 10 nJ. An intracavity, two prism sequence, provides the proper amount of group velocity dispersion for production of transform limited pulses, and an adjustable slit is used to tune the central wavelength of the light pulses from 800 nm to 900 nm. A schematic of the cavity is shown in **Figure 2.2**.

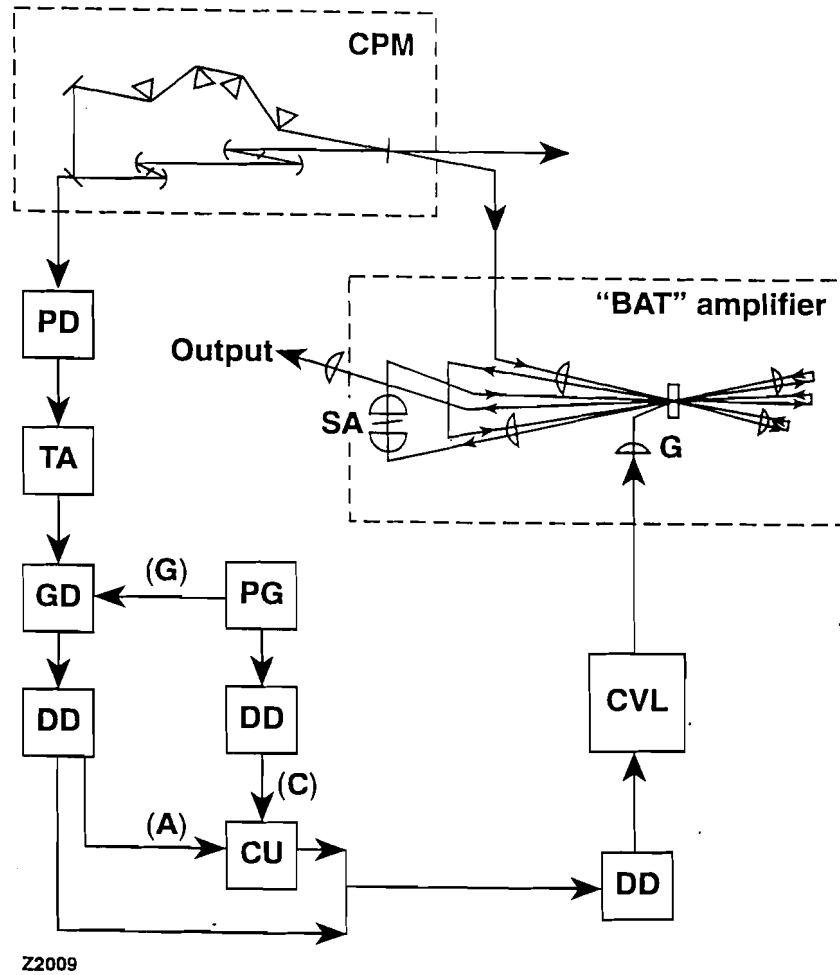


Figure 2.1 Schematic of the CVL-amplified CPM laser together with synchronization electronics. PD = photodiode, TA = timing amplifier, GD = gating discriminator, PG = pulse generator, DD = digital delay, CU = coincidence unit, BS = beam splitter.

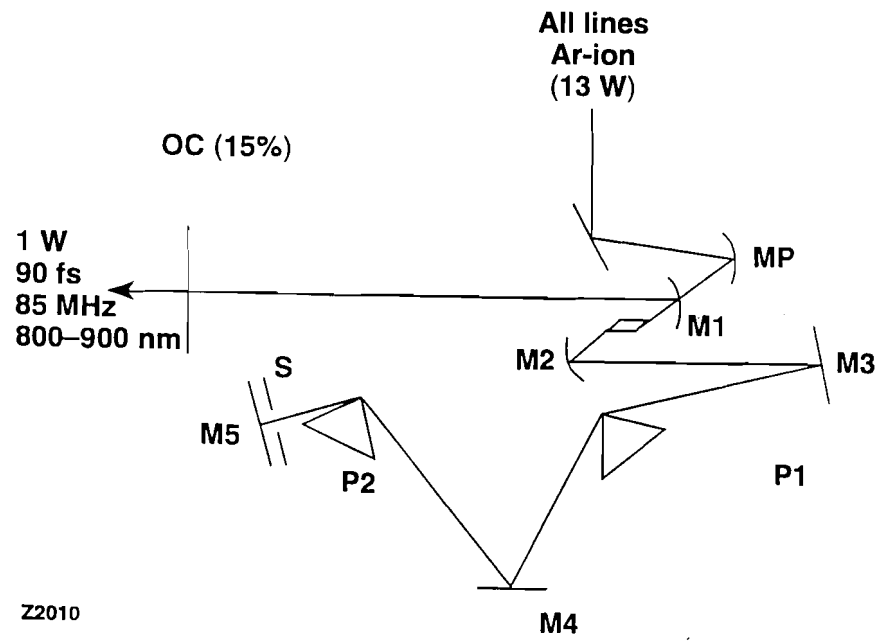


Figure 2.2 Schematic of the Ti:Sapphire laser cavity. OC = output coupler, M1, M2, M3, M4, and M5 = cavity mirrors, P1, P2 = prisms, S = tuning slit.

2.2 Sample Preparation

The thin film samples used in our measurements were grown by Solid Source Molecular Beam Epitaxy (SSMBE) at The Institute of Optics of the University of Rochester. The method used to remove the substrate differs, depending on the epilayer, but all are based on a technique developed by Yablonovitch et. al. for GaAs [5].

We will start our description of the sample preparation with the case of GaAs. Two 0.3 μm thick layers of this material were prepared, at growth temperatures of 250°C and 195°C. After growth, a piece of each was *in situ* annealed at 600°C for 10 min. A 0.8 μm thick layer of $\text{Al}_{0.8}\text{Ga}_{0.2}\text{As}$ was stacked between the epilayer and the substrate and served as a lift-off layer. A solution of 25 mg wax (Apiezon W) dissolved in 100 ml of trichloroethylene was applied uniformly on the epilayer side. After annealing at $\sim 100^\circ\text{C}$ for $< 1/2$ h, the sides of the sample were exposed, and the sample was stored in dilute ($\sim 20\%$) HF acid, at 0°C. At this high Al concentration, HF etches the AlGaAs layer a few orders of magnitude faster than it attacks GaAs. A selectivity of $\sim 10^7$ has been measured between AlAs and $\text{Al}_{0.4}\text{Ga}_{0.6}\text{As}$, with the onset of etching occurring very suddenly at about 40% to 50% Al composition [5]. The annealing condition produces the right amount of tension and curvature for the LT-GaAs film. The slight up-lifting of the epilayer edges permits the resulting H_2 gas to diffuse from the etching zone, allowing the etching process to continue unimpaired. Typically, after ~ 24 h in this

environment, the AlGaAs layer has been etched away completely, and the LT-GaAs epilayer floats off. The layer, supported by the wax, is then carefully placed on a sapphire window where it remains attached due to van der Waals forces. The wax is then removed by submerging the whole structure in trichloroethylene for five minutes. We have chosen sapphire instead of glass due to its excellent thermal conductivity which minimizes thermal effects. The electronic quality of the epitaxially grown films is unaffected by this lift-off process [5].

The processing of the LT-InP samples was slightly different, as can be seen in **Figure 2.3**. A 0.2 μm thick InP layer was grown, at temperatures of 200°C and 300°C, on top of a 0.5 μm $\text{Ga}_{0.47}\text{In}_{0.53}\text{As}$ stop-etch layer, grown on an InP substrate. HCl acid is used to etch selectively InP, while a solution of $\text{H}_2\text{SO}_4:\text{H}_2\text{O}_2:\text{H}_2\text{O}:5:1:1$ is used to etch only the GaInAs layer. First, a small amount of the same wax solution used for the GaAs samples is applied on the LT-InP epilayer, in such a manner that a narrow perimeter of the LT-InP epilayer is left exposed to the acid. The sample is then dipped in HCl for a few seconds in order to create a mesa structure by etching away the narrow part of the LT-InP not covered by the wax. The wax is then removed and re-applied in order to cover both the remaining LT-InP and the GaInAs exposed in the previous step. Wax that possibly has spilled over the side of the substrate is removed by rubbing slightly the sides on fine sand paper. Then the InP substrate is removed by placing the sample in HCl for a few minutes. Lapping of the substrate down to $\sim 200 \mu\text{m}$ can speed up

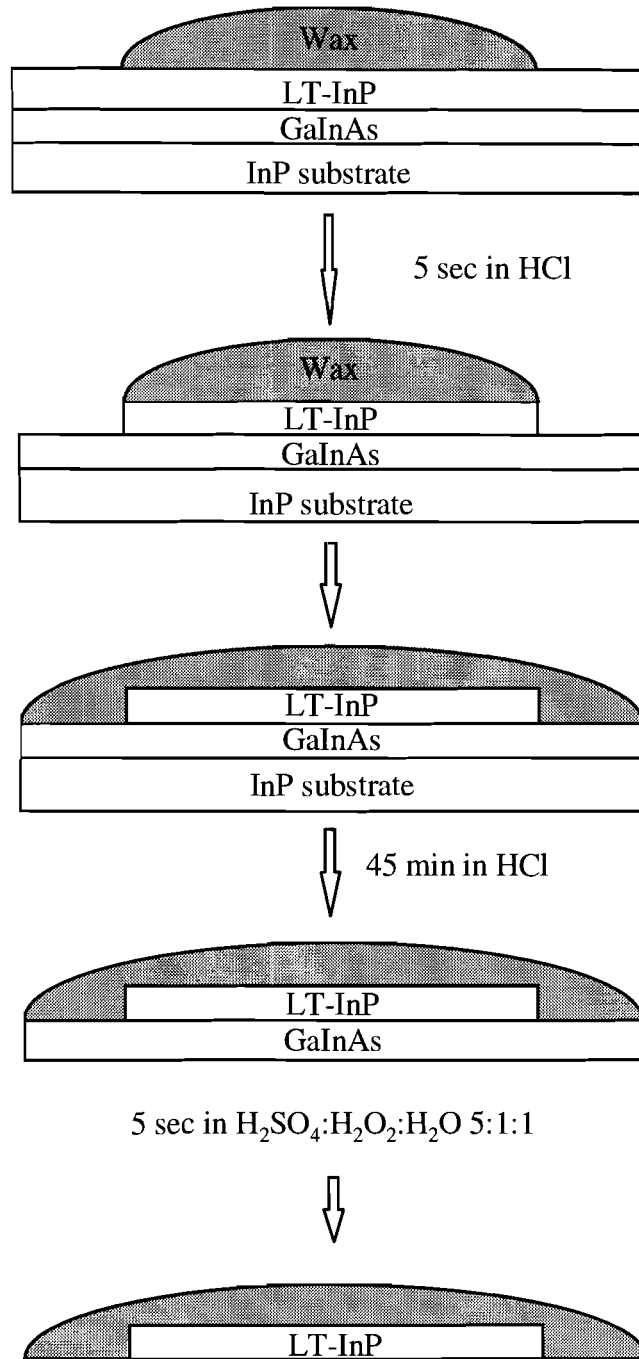


Figure 2.3 Selective etching of the InP samples used in this study. The $0.2 \mu\text{m}$ thin film, supported by the wax, is placed on a sapphire window where it stays attached via van der Waals forces.

this process. This is desired since a long exposure in the HCl environment will affect the LT-InP epilayer even if it is covered by wax. This is evident by presence of small holes in samples treated for ~50 minutes and also by the appearance of small air bubbles during etching of the substrate. Lapping the substrate down to an even smaller thickness not only reduces etching time, but also makes the sample difficult to handle. A subsequent dip for ~10 sec in a $\text{H}_2\text{SO}_4:\text{H}_2\text{O}_2:\text{H}_2\text{O}:5:1:1$ solution, completely etches the GaInAs layer, leaving only the LT-InP on the wax. As in the GaAs case, the sample is van der Waals attached on a sapphire window.

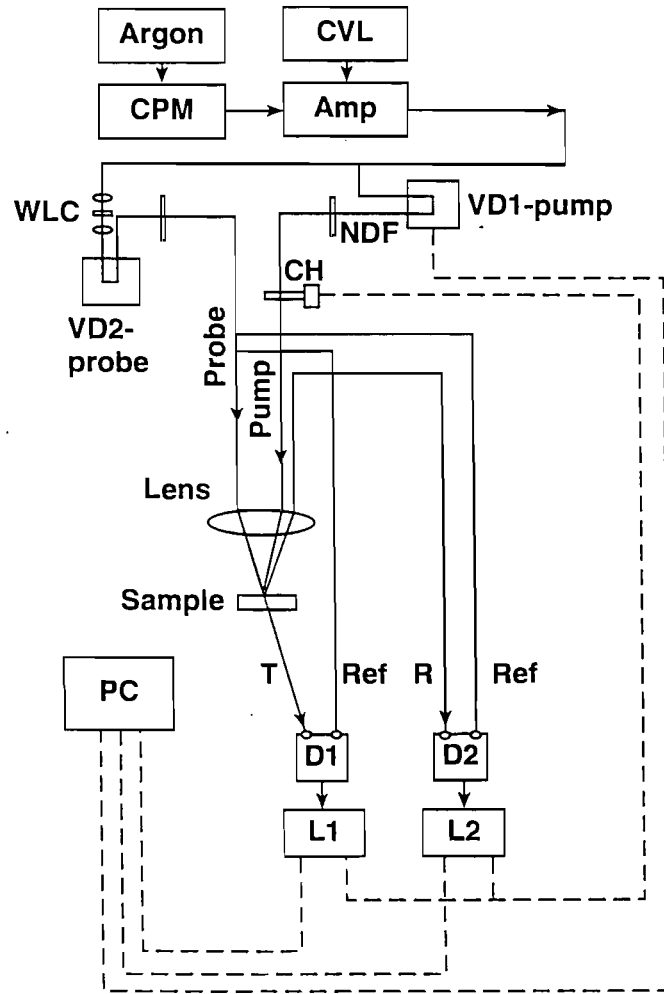
A slightly different method was used in the case of $\text{Ga}_{0.51}\text{In}_{0.49}\text{P}$. The epitaxial layers were directly grown on GaAs substrates, which were then lapped down to ~100 μm thickness. After wax was applied on the epilayer, the samples were placed in a solution of $\text{H}_2\text{SO}_4:\text{H}_2\text{O}_2:\text{H}_2\text{O}:5:1:1$ at 0°C , in order to etch selectively the GaAs substrate at an etching rate of ~8 $\mu\text{m}/\text{hour}$. The 200°C , as-grown and annealed, $\text{Ga}_{0.51}\text{In}_{0.49}\text{P}$ samples, were prepared by using $\text{NH}_4\text{OH}:\text{H}_2\text{O}_2:1:30$ as a selective etch, reducing the processing time significantly.

2.3 Experimental Methods

Both the pump-probe and the up-conversion luminescence techniques are used extensively to study the dynamics of excitations in a variety of materials and

physical systems. In this section we will give a brief description of both experimental set-ups.

Illustrated in **Figure 2.4** is the complete 2-eV-pump/WLC-probe experimental arrangement. A simpler version of it has been used for the degenerate pump-probe measurements with the Ti:Sapphire system. About 4% of the amplified CPM pulse was split off as a ≤ 100 fs pump pulse at 620 nm (~ 2 eV). The remainder was used to generate a white light continuum in a flowing jet of ethylene glycol, from which a wavelength tunable probe pulse was selected by means of interference filters of 10 nm or 25 nm bandwidth. This allowed the probe wavelength to be chosen in the range of 570 nm to 900 nm. Typical cross-correlation measurements of the pump and probe pulses at 620 nm yielded widths of 80 fs. When the probe is extracted from the WLC, it is usually slightly longer by $\sim 15\%$ - 20% . Both pump and probe pulses are focused on the sample (at near normal incidence) using the same lens. The polarization of the pump was rotated by means of a half-wave plate to 90° with respect to that of the probe in order to reduce coherent artifacts. The variable delay was achieved by diverting the pump into a retroreflector mounted on a computer controlled, stepper-motor driven, translation stage. The transmitted and reflected beams were collected simultaneously by focusing lenses on two different photodiodes. Each of these photodiodes was part of a subtraction scheme that made possible the measurement of only the pump-induced changes in the transmission, ΔT , and reflection, ΔR , of the sample and simultaneously was compensating for noise in the probe pulse train.



Z2008

Figure 2.4 Experimental arrangement. Solid lines represent optical paths, while dashed lines represent computer interfaces and electrical connections. WLC = white light continuum, VD1, VD2 = variable delays, IF = interference filter, NDF = neutral density filter, T = transmitted probe beam, R = reflected probe beam, REF = reference beam, D1, D2 = difference photodiodes, PC = personal computer, L1, L2 = lock-in amplifiers, and CH = chopper.

The resulting ΔT and ΔR were induced in phase with the modulation of the pump beam by an optical chopper, and were measured by two lock-in amplifiers. The outputs of these amplifiers were read at each point of the variable time delay, and averaged over many sweeps of the pre-determined time window. The control of the two lock-in amplifiers, of the stepper motor, and the averaging of the raw data, was implemented by a personal computer. The intensity of the pump pulse was varied by up to three orders of magnitude, and the injected carrier density was estimated from the energy per pulse, the absorption coefficient of the sample at the pump wavelength, the measured focal spot size and the sample thickness. Typical carrier densities range from 10^{17} cm^{-3} to 10^{19} cm^{-3} . Due to the relatively low repetition rate, it was difficult to achieve a good S/N ratio at lower carrier densities, and in order to achieve carrier densities less than 10^{16} cm^{-3} , we used the unamplified CPM. Uncertainties in the beam parameters and/or in the absorption coefficient of some of the samples, as well as the efficient surface recombination on un-passivated samples [6], make the overall uncertainty of the absolute carrier density about $\pm 50\%$.

Together with ΔT and ΔR , we also measure carefully T_0 and R_0 , the undisturbed transmission and reflectivity, at each probe wavelength. With this information at hand, we can determine $T(\tau)$ and $R(\tau)$ as a function of the time delay τ , from the relations: $T(\tau) = T_0(1 + \Delta T/T_0)$ and $R(\tau) = R_0(1 + \Delta R/R_0)$. The samples used in this thesis are thin films on thick transparent substrates and show clear Fabry-Perot fringes, especially when the probe wavelength is in the

transparency regime of the material. These fringes can obstruct the extraction of physical information since both ΔT and ΔR can contribute to the observed signal. In order to avoid this problems we transformed our data from $T(\tau)$ and $R(\tau)$ to $n(\tau)$ and $k(\tau)$, where n and k are the real and imaginary part of the index of refraction, by reversing the Fabry-Perot formulas. The transmission T and reflection R at normal incidence and at wavelength λ , are given by [7]:

$$T = \frac{n_3}{n_1} \frac{\tau_{12}^2 \cdot \tau_{23}^2 \cdot e^{-2k\eta}}{1 + \rho_{12}^2 \cdot \rho_{23}^2 \cdot e^{-4k\eta} + 2 \cdot \rho_{12} \cdot \rho_{23} \cdot e^{-2k\eta} \cdot \cos(\phi_{23} + \phi_{23} + 2\rho\eta)} \quad (1)$$

$$R = \frac{\rho_{12}^2 + \rho_{23}^2 \cdot e^{-4k\eta} + 2 \cdot \rho_{12} \cdot \rho_{23} \cdot e^{-2k\eta} \cdot \cos(\phi_{23} + \phi_{23} + 2\rho\eta)}{1 + \rho_{12}^2 \cdot \rho_{23}^2 \cdot e^{-4k\eta} + 2 \cdot \rho_{12} \cdot \rho_{23} \cdot e^{-2k\eta} \cdot \cos(\phi_{23} + \phi_{23} + 2\rho\eta)} \quad (2)$$

where

$$\tau_{12} = \left[\frac{4 \cdot n_1^2}{(n_1 + n)^2 + k^2} \right]^{1/2} \quad (3)$$

$$\tau_{23} = \left[\frac{4 \cdot (n + k)^2}{(n_3 + n)^2 + k^2} \right]^{1/2} \quad (4)$$

$$\rho_{12(23)} = \left[\frac{(n_{1(3)} - n)^2 + k^2}{(n_{1(3)} + n)^2 + k^2} \right]^{1/2} \quad (5)$$

$$\tau_{12} = \left[\frac{4 \cdot n_1^2}{(n_1 + n)^2 + k^2} \right]^{1/2} \quad (6)$$

$$\eta = \frac{2 \cdot \pi \cdot d}{\lambda} \quad (7)$$

Here n and k are the real and imaginary parts of the refractive index of the film, d is the thickness of the film, $n_1=1$ is the refractive index of air, and n_3 is the refractive index of the sapphire window which is given by [8]:

$$n_3 = \left[1 + \frac{1.023798 \cdot \lambda^2}{\lambda^2 - 0.00377588} + \frac{1.058264 \cdot \lambda^2}{\lambda^2 - 0.0122544} + \frac{5.280792 \cdot \lambda^2}{\lambda^2 - 321.3616} \right]^{1/2} \quad (8)$$

with λ in units of μm . Equations (1) and (2) are solved numerically, in order to calculate the absorption coefficient α that is related to the imaginary part k of the refractive index through: $\alpha=4\pi k/\lambda$. Typical T and R traces are shown in **Figure 2.5(a)**, while the calculated n and α are shown in **Figure 2(b)**. Our system allowed detection of changes as small as 10^{-5} . The extraction of n and k from the experimental values of T and R requires the use of initial guesses for the values of n_0 and k_0 , the unperturbed real and imaginary parts of the refractive index. These

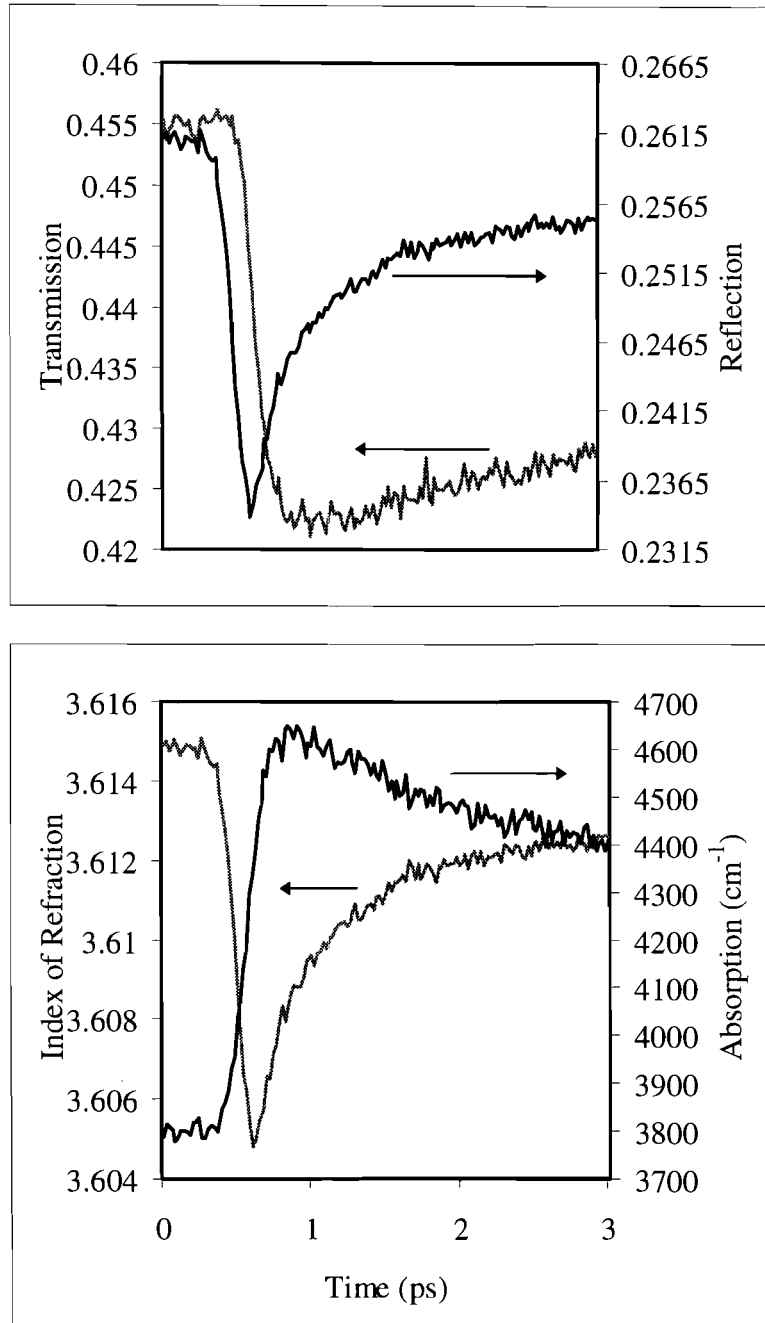


Figure 2.5 Measured reflection and transmission (a) and calculated index of refraction and absorption coefficient (b) using the Fabry-Perot formulas, of a LT-GaInP film grown at 200°C.

initial guesses are taken from the existing literature, and while they are well known for GaAs [9] and InP [9], they are still under study in the case of GaInP [10]. We have found that the calculated values of n and k are sensitive to variations in these initial guesses and also to uncertainties in the film thickness (mostly Δn).

The time resolved differential reflection has also been measured in bulk LT-GaAs and LT-InP. The reflectivity at normal incidence is given by:

$$R = \frac{(n-1)^2 + k^2}{(n+1)^2 + k^2} \quad (9)$$

Then the change of the refractive index is related to the change in reflection by

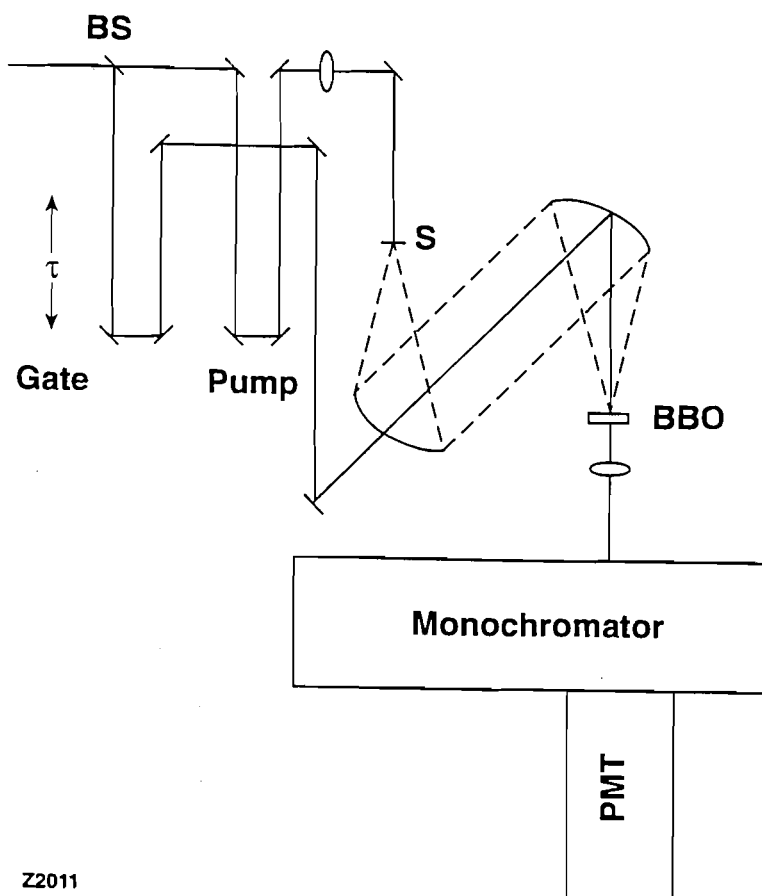
$$\begin{aligned} \Delta R &= \left(\frac{\partial R}{\partial n} \right)_{R_0} \cdot \Delta n + \left(\frac{\partial R}{\partial k} \right)_{R_0} \cdot \Delta k \\ &= \frac{4 \cdot (n_o^2 - k_o^2 - 1)}{(n_o + 1)^2 + k_o^2} \cdot \Delta n + \frac{8 \cdot n_o \cdot k_o}{(n_o + 1)^2 + k_o^2} \cdot \Delta k \end{aligned} \quad (10)$$

where n_o (k_o) is the undisturbed real (imaginary) part of the refractive index of the sample. This type of reflectivity measurements is mostly sensitive to probe wavelengths near that of the pump, since probe light with penetration depth much longer than that of the pump cannot detect the change effectively, due to the small

interaction length. For the pump, and consequently for the probe wavelengths used in our measurements, it is $n_o > 10k_o$, and this leads to:

$$\Delta n = \frac{(n_o^2 - 1)}{4} \cdot \frac{\Delta R}{R_o} \quad (11)$$

The schematic of the up-conversion luminescence set-up is shown in **Figure 2.6**. A 50%-50% beam splitter was used to create the gate and pump pulses. A retroreflector, mounted on a computer controlled, stepper motor driven, translation stage, introduces a variable time delay on the gate pulse train. The pump beam is focused on the sample with a 40 cm focal length lens, in order to excite the sample. The luminescence photons, emerging in a point-source-like fashion from the back surface of the sample, are then collected with two off-axis parabolic mirrors. The first mirror collimates the luminescence and the second focuses it on a BBO crystal. The gate beam, after passing through a hole in the first mirror, is focused by the second mirror on the BBO crystal, in order to up-convert the luminescence through sum-frequency generation. The two off-axis parabolic mirrors are aligned so that the focal spot on the sample is imaged on the BBO crystal. This set-up utilizes the luminescence transmitted through the sample. Re-absorption of the luminescence photons is not significant since the absorption length at the luminescence photon energies is much larger than the sample



Z2011

Figure 2.6 Schematic of the up-conversion luminescence set-up. BS = 50/50 beam splitter, S = sample, BBO = β -Barium Borate, PMT = photomultiplier. The luminescence photons, together with the gate beam are up-converted in the BBO crystal. The resulting ultraviolet photons are then dispersed with the monochromator and counted with the PMT

thickness. The up-converted UV photons are then focused on the entrance slit of a monochromator and detected using photon-counting techniques. Both the rise time and the decay time of the luminescence can be used to extract information about the carrier dynamics.

References

1. J. A. Valdmanis, and R. L. Fork, IEEE J. Quantum Electron. **QE-22**, 112 (1986).
2. W. N. Nighan Jr., and P. M. Fauchet, *Applications of Ultrafast Laser Pulses in Science and Technology*, SPIE Proc. **1268**, 79 (1990).
3. D. E. Spence, P. N. Kean, and W. Sibbett, Opt. Lett. **16**, 42 (1991).
4. B. C. Tousley, Ph.D. Thesis, Department of Electrical Engineering, Unniversity of Rochester, (1993).
5. E. Yablonovitch, T. Gmitter, J. P. Harrison, and R. Bhat, Appl. Phys. Lett. **51**, 2222 (1987).
6. J. F. Young, K. Wan, A. J. Springthorpe, and P. Mandeville, Phys. Rev. B **36**, 1316 (1987).
7. M. Born and E. Wolf, *Principles of Optics*, (Pergammon, Oxford, 1985) p. 630.
8. I. H. Malitson, J. Opt. Soc. Am. **52**, 1377 (1967).

9. *Handbook of the Optical Constants of Solids*, ed. by E. D. Palik, (Academic, London, 1985) p. 429.
10. M. Möser, R. Winterhoff, C. Geng, I. Queisser, F. Scholz, and A. Dornen, *Appl. Phys. Lett.* **64**, 235 (1994).

CHAPTER 3

Femtosecond Carrier Dynamics In Low Temperature-Grown Indium Phosphide

3.1 Introduction

Electron and hole populations can be monitored through the band to band absorption saturation. Before evolving toward a quasi-equilibrium, the electron-hole distribution is expected to be peaked at the excitation energy, giving rise to a dynamic spectral hole burning effect, i.e. a preferential bleaching at the excitation energy. This absorption saturation is the result of filling of the states connected via the excitation photons. As the as-excited carrier distribution thermalizes, the carriers spread over a wide spectral distribution in the conduction band and the spectral hole disappears.

With the advent of the femtosecond lasers, it has been possible to observe in real time the spectral hole burning associated with the absorption saturation of valence-to-conduction band transitions. The absorption spectral hole burning was first directly observed near the band edge of bulk GaAs by Oudar [1] and also later by Hunsche [2] and in intrinsic and doped quantum wells by Knox [3,4] and its recovery was used to deduce the dwell times of the carriers in the as-excited states. Later such hole burning was observed for excitation high (~ 2 eV) in the

conduction band of GaAs by pump and continuum-probe measurements [5-7]. When the Kramers-Krönig relations are applied, a dynamic spectral hole burned in the absorption spectrum gives rise to a spectral resonance in the index of refraction [8]. Changes in the index of refraction are readily observable in an optically thick sample for which $\Delta R \sim \Delta n$ (see chapter 2 page 52) and information about refractive nonlinearities and carrier dynamics can be extracted.

If pump and probe measurements are performed at the same wavelength, the recovery of the bleaching yields information on the dwell time of the carriers in the as-excited states. Both equal-pulse correlation and non-linear pump-probe techniques have been used to measure the time it takes for carriers to scatter out of the initially excited states. When the excitation takes place high in the conduction band and states close to the band edge are probed, the rise time of the signal also contains information about the carrier cooling [9,10]. When pump-probe spectroscopy is used to study the carrier trapping time or lifetime, complications arise from carrier relaxation which can contribute significantly to the observed signal decay.

The decay of the band edge luminescence, on the other hand, can provide transparent information about the carrier trapping time or lifetime.

In this chapter we use these two complementary methods to study the dynamics of photoexcited carriers in low-temperature grown InP. By contrasting the results from the two methods we find that carrier trapping and not recombination is the ultrafast effect in this material.

3.2 Refractive Index Spectral Hole Burning

For a conventionally grown III-V semiconductor, the pump pulse at $t \sim 0^+$ causes a sharp reduction of the absorption at the pump wavelength due to state filling. By means of the Kramers - Krönig relations this dynamic bleaching will cause a spectral resonance in the index of refraction. For an optically thick semiconductor (thickness \gg absorption length at the pump photon energy), a change in reflectivity is proportional to a change in the index of refraction and the above mentioned resonance should therefore be evident in the reflectivity data. The manifestation of such a spectral resonance is a short-lived negative dip at $\tau \sim 0^+$ for probe photon energies smaller than the pump. At the zero point of the spectral resonance, which takes place when $\lambda_{\text{probe}} = \lambda_{\text{pump}}$, we expect no spectral features at $t \sim 0^+$. When the probe photon energy becomes larger than that of the pump, we probe the positive part of the spectral resonance and we would anticipate a short-lived positive feature to appear in the reflectivity right after carrier injection. This can be seen in **Figure 3.1** where a schematic of the absorption and refractive index spectral hole burning is depicted.

Figure 3.2 shows the time resolved differential reflection of an intrinsic bulk GaAs sample grown at normal temperatures measured using the CPM/CVL laser system (T. Gong, Ph.D. Thesis [11]). The probe wavelength varies from 600 nm to 700 nm and the injected carrier density is $2\text{-}3 \times 10^{18} \text{ cm}^{-3}$. The data at 600 nm and 620 nm exhibit a short-lived positive spike right after carrier injection,

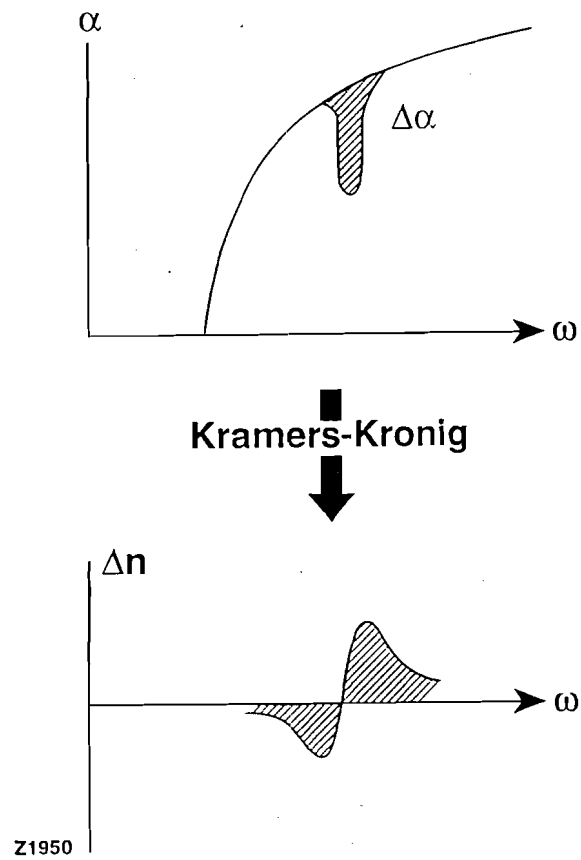


Fig. 3.1 Schematic representation of spectral hole burning caused by the absorption bleaching induced by the pump pulse, and of the corresponding resonance in the index of refraction. As the photo-injected carrier distribution spreads, the resonance disappears.

whereas the data at 680 nm and 700 nm exhibit a negative spike. No fast feature is observed at a probe wavelength of 650 nm. These positive and negative spectral features observed right after carrier injection are a clear demonstration of the refractive index spectral hole burning. In reflectivity measurements, the probe wavelength cannot be varied much compared to that of the pump since the penetration depth increases or decreases quickly leading to a small overlap and consequently to a small interaction length in the sample. The relatively large width of the spectral hole (~ 200 meV) indicates that carrier-carrier scattering has redistributed electrons in the Γ valley within the pulse width. In addition, the zero point of the spectral resonance appears to be at 650 nm instead of the pump wavelength of 620 nm. This peculiarity is due to the influence of intervalley scattering which leads to an apparent accumulation of carriers in the Γ valley at an energy ~ 30 meV below the X-valley minimum, causing the peak of the spectral resonance to appear at ~ 650 nm [12].

After ~ 200 fs, the resonance disappears because carriers leave the initial excited Bloch states by various scattering processes. The similar gradual rise of Δn on a picosecond time scale in the 600 nm - 700 nm spectral range is due to band filling which is controlled in part by the slow return of carriers from the L valley.

Having the GaAs differential reflectivity measurements as a benchmark, we proceed to investigate the behavior of bulk InP grown at normal temperatures under the same experimental conditions. The corresponding data for an injected carrier density of $8 \times 10^{18} \text{ cm}^{-3}$ are depicted in **Figure 3.3**. Again the spectral

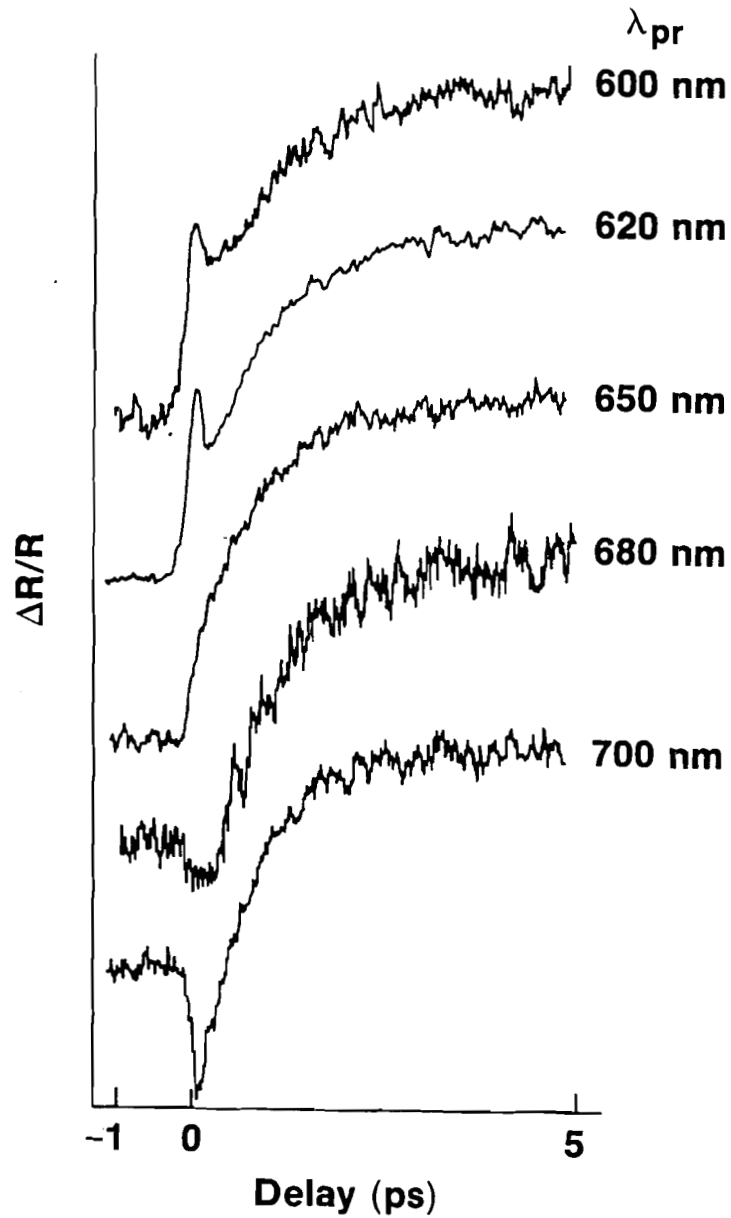


Fig. 3.2 Transient spectral hole burning: as the probe wavelength varies around 2 eV, we clearly see the positive and negative part of the spectral resonance at $\tau \sim 0^+$ for conventionally grown GaAs [after T. Gong, Ph.D Thesis, Princeton University 1991).

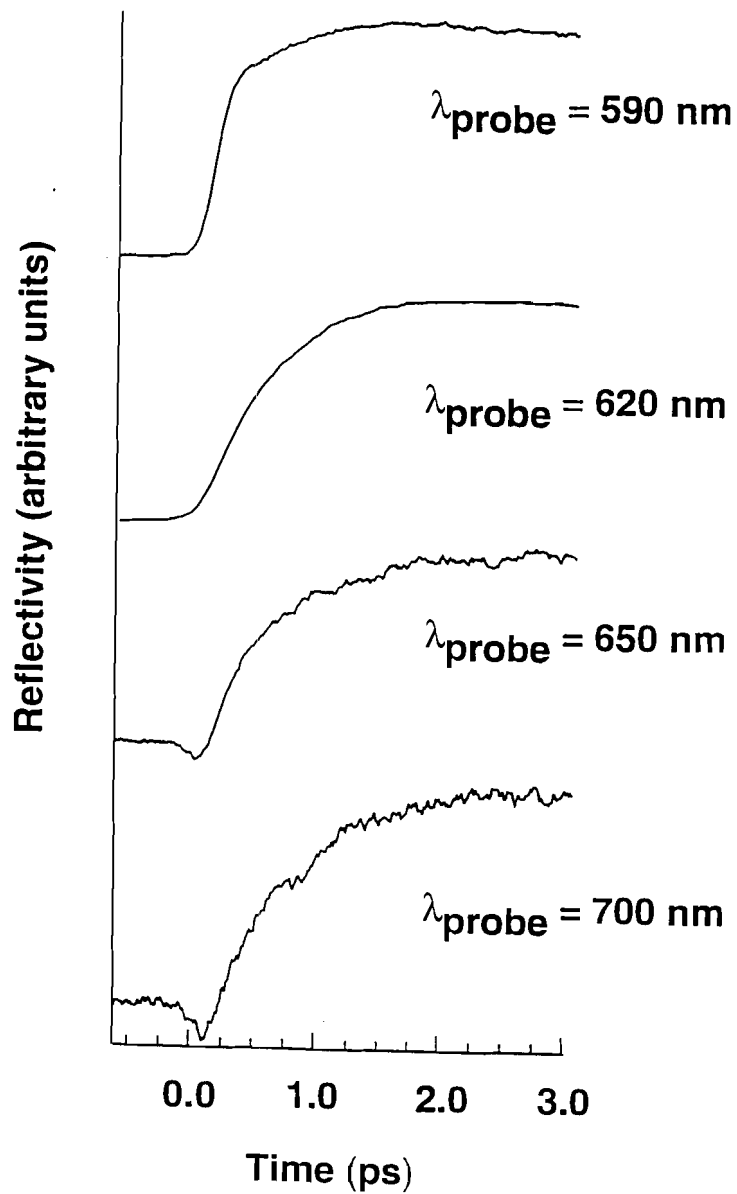


Fig. 3.3 Transient spectral hole burning in the case of conventionally grown InP substrate (comp. Figure 3.2). The high injected carrier density ($\sim 10^{19} \text{ cm}^{-3}$) leads to a significant spread of the carrier distribution within the pulse width. This prevents the resolution of the falling edge of the 590 nm signal at $\tau \sim 0^+$ fs.

resonance is clearly visible. The band structure of InP is different than that of GaAs. The X and L valley minima are at higher energies than in GaAs and therefore, no significant intervalley transfer can take place. As a result, the zero of the spectral resonance is at the pump wavelength of 620 nm. At the smaller probe photon energies the negative part of the spectral resonance is clearly visible. As the photon energy is increased above that of the pump, only the rise time of the resonance can be resolved as can be seen from the much faster rise of the signal at 590 nm compared to that at 620 nm. The reason for that is the fast thermalization through carrier-carrier scattering at these high injected carrier densities. This leads to an appreciable spread of the injected carrier distribution within the probe pulse width. As the excited carriers undergo fast relaxation, the positive contribution of bandfilling [13] to the index of refraction becomes prominent. The negative part of the spectral resonance is not affected by this change of sign. The positive part of the spectral resonance on the other hand, is overwhelmed by the contribution of bandfilling which obstructs the resolution of its falling edge.

The same measurements are performed on a 5 μm thick LT-InP layer grown at 200°C, and can be seen in **Figure 3.4**. This sample is polycrystalline and has ~7% excess phosphorus due to the growth at low substrate temperatures [14]. Under the same experimental conditions the LT-InP sample exhibits a totally different behavior. As the probe wavelength is varied we observe no transient spectral hole burning: the change in reflectivity right after carrier injection is always negative. For all probe wavelengths the signal recovers on a fast time scale

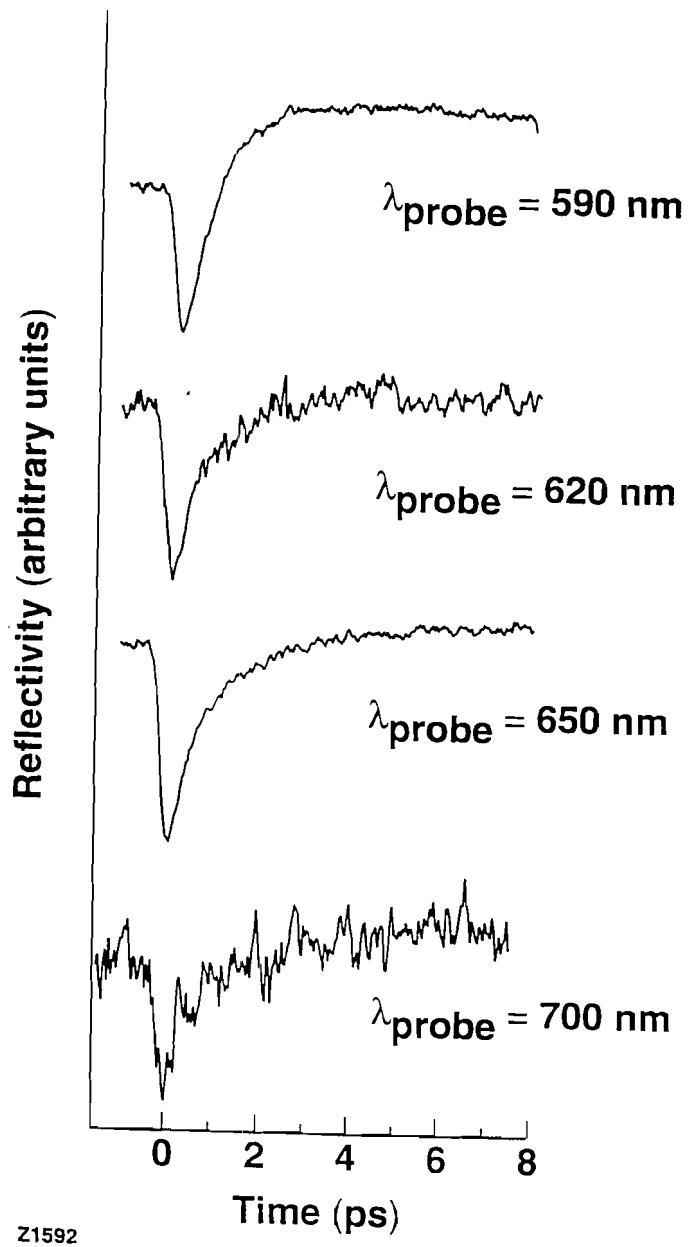


Fig. 3.4 Similar measurements as in Figure 3.3 for InP grown at a substrate temperature of 200°C. In this case the change in reflectivity is negative for all probe wavelengths clearly showing the lack of spectral hole burning.

(~1 ps) and reaches a positive plateau. A similar behavior has been observed at 2 eV by Gupta et al. [15] in single crystalline LT-GaAs grown at 200°C. This negative change in reflectivity for all probe wavelengths is a characteristic signature of free carrier absorption, but this is not compatible with transmission experiments on LT-InP films as we will see below. The existence of a defect band in the LT-material which affects our data through the integration over all energies in the Kramers-Krönig relations complicates the interpretation of the reflectivity measurements.

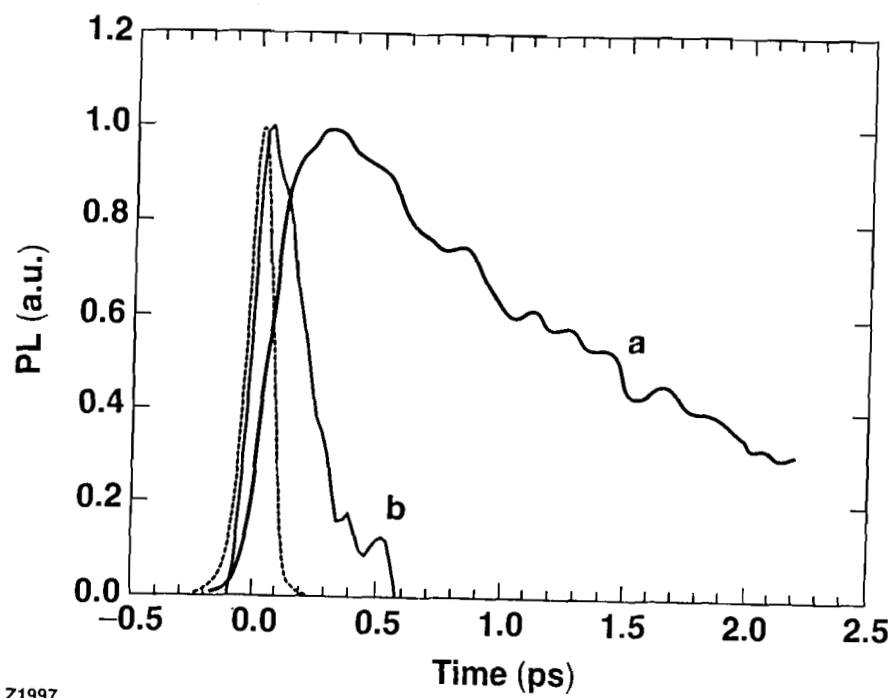
3.3 Carrier Trapping vs Carrier Recombination

In order to avoid the complications introduced by the Kramers-Krönig relations and to investigate more thoroughly the carrier trapping/recombination lifetimes in LT-InP, we performed up-conversion luminescence experiments in conjunction with 2-eV-pump/WLC-probe differential transmission measurements, on two LT-InP thin films grown at 200°C and 300°C. No annealing was performed and X-ray diffraction measurements show both samples to be of good crystalline quality. Their thickness was 0.2 μm which is approximately equal to one absorption length for the 2 eV pump photons, ensuring fairly uniform

excitation. The InP films were lifted off according to the method described in chapter 2.

Figure 3.5 shows the result of the up-conversion luminescence measurements. The carrier density generated by the pump pulse was $\sim 10^{17} \text{ cm}^{-3}$. The peak of the luminescence was found to be at 880 nm ($\sim 1.40 \text{ eV}$), slightly displaced towards energies higher than the bandgap of the normally grown material (1.34 eV). This is in contrast to what has been observed in the case of LT-GaAs where the peak is at the same energy as in its normally grown counterpart.[16] The difference results from bandfilling, as low-temperature grown InP is n-type due to the incorporation of excess phosphorus in the material.[17] The luminescence efficiency of the 200°C sample is about one order of magnitude less than that of the 300°C sample. This is due to the incorporation of more phosphorus at the lower growth temperature which leads to a larger density of point defects and therefore to an enhancement of the non-radiative recombination.

For excitation high in the conduction band, the carrier thermalization time can be extracted from the rise time of the band edge luminescence. From their measurements Zhou et al. [18] have extracted a carrier thermalization time of 800 fs in normally grown InP under excitation with 2 eV photons. In our measurements, on the other hand, the rise time of the luminescence is pulse-width limited for both samples, consistent with a strong carrier scattering mechanism that leads to a near-Maxwellian distribution within our time resolution [19,20]. This pulse width limited relaxation may be the result of the interaction of the



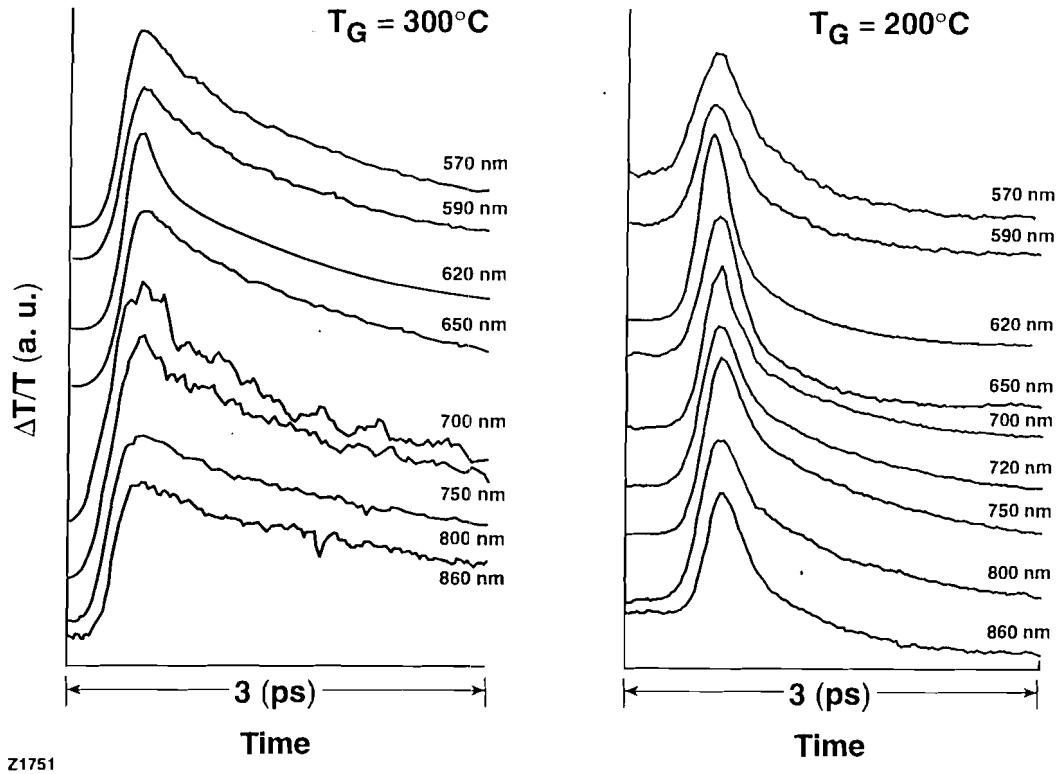
Z1997

Fig. 3.5 Up-conversion photoluminescence traces of (a) the 300°C sample and (b) the 200°C sample. The signal is measured at the peak of the photoluminescence. The pulse width limited rise time indicates a carrier distribution that extends to the bottom of the conduction band within our time resolution.

photoexcited carrier distribution with a cold Fermi sea of electrons of higher density already present in the conduction band. (An extremely fast initial scattering time of ~ 25 fs has been observed in n-type GaAs arising from the coupled phonon-plasmon modes) [20]. The fact that a pulse width limited thermalization has also been observed in other LT-III/Vs that are of high resistivity, indicates that other scattering mechanisms, such as defect ionization scattering can also contribute to this effect. The relaxation of carriers to the band edge within the pump pulsewidth shows that in the thin film samples, as in the polycrystalline sample, no spectral hole is observed.

The up-conversion luminescence signal decays exponentially with a time constant (without deconvolution) of 0.45 ps for the 200°C sample and 1.6 ps for the 300°C sample. These time constants are due to *carrier trapping and not recombination*, as will be seen from the pump-probe measurements. A similar carrier trapping time has also been observed in the case of GaAs grown at 200°C [16].

The differential transmission measurements are shown in **Figure 3.6**. The carrier density generated by the pump pulse was $\sim 10^{19}$ cm⁻³ for these measurements. We observe a pulse-width limited rise time of the bleaching signal for both samples, at all probe wavelengths from 570 to 860 nm. The photoexcitation of a nearly monoenergetic electron distribution in the conduction band of conventionally grown GaAs using 2 eV photons induces a bleaching signal with a slow rise at probe wavelengths close to the band edge [20,21]. This effect is

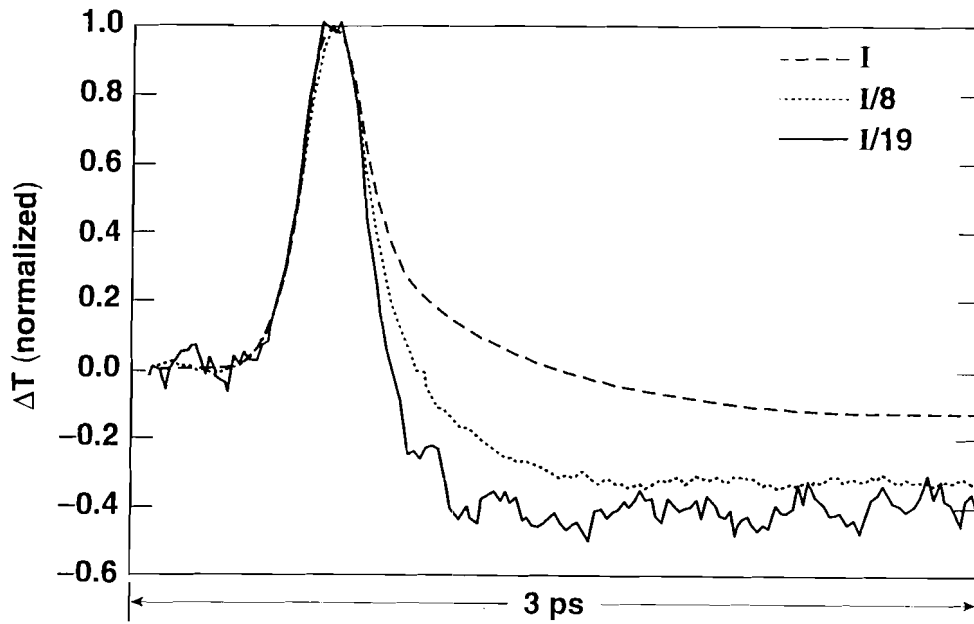


Z1751

Fig. 3.6 Differential transmission measurements on the same samples as in Figure 3.5. The fast decay of the bleaching is due to carrier trapping with the recombination taking place in a much longer time scale.

caused by the cooling of the photo-generated carriers down to states near the bottom of the conduction band. Such behavior is not observed in low temperature grown InP, indicating that the carrier distribution broadens significantly within our time resolution. This wavelength-independent, pulsewidth limited rise time is consistent with what we observe from the luminescence measurements and confirms that the carrier distribution extends to the bottom of the conduction band in a time less than the excitation pulse.

In the case of the 200°C sample, the recovery of the signal is qualitatively similar for all probe wavelengths. The bi-exponential decay has a fast component of ~150 fs and a slower component of ~650 fs. A bi-exponential decay of the bleaching signal is also observed in the case of the 300°C sample but the amplitude of the fast component becomes smaller at longer probe wavelengths and the slower time constant is longer, ~2 ps. Trap saturation largely contributes to these longer time constants, as will be seen below. The fast component is attributed to cooling of the photo-excited carriers in the conduction band while the slower component, which is close to the time constant observed in the up-conversion luminescence measurements, describes carrier trapping. The fast decay of the signal is partly the result of electron-electron interactions between a cold Fermi sea and the hot distribution of photo-excited carriers, which results an efficient channel for carrier relaxation [20,22]. This can be seen also in **Figure 3.7**, where we plot the 620-620 nm pump-probe trace at three injected carrier densities differing by more than an order of magnitude. The initial decay of the bleaching is faster at lower injected

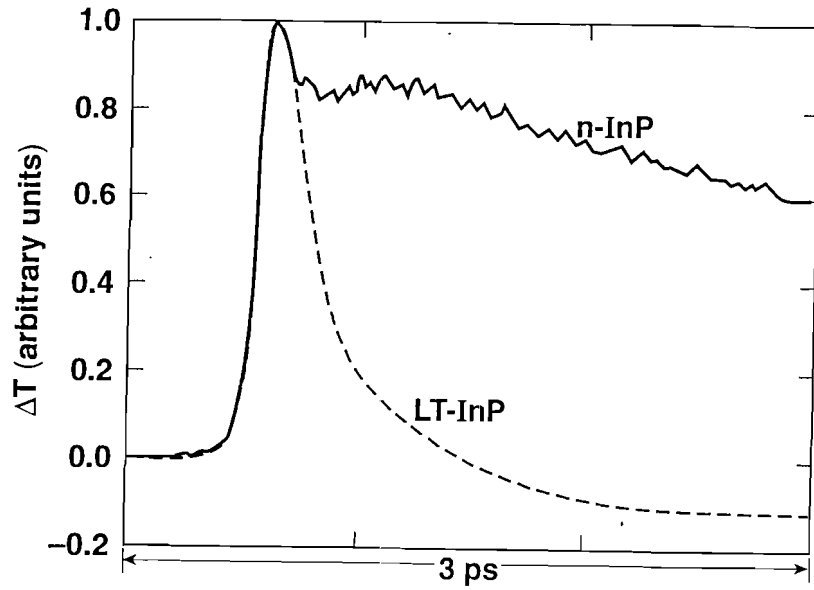


Z1846

Fig. 3.7 Differential transmission measurements on the 200°C sample at 620 nm and three injected carrier densities: The initial decay of the bleaching becomes faster as the carrier density is decreased. The traces are normalized with respect to their peaks for comparison.

carrier densities since the number of photo-injected hot electrons interacting with the cold Fermi sea at the bottom of the conduction band is smaller, resulting in a faster temperature equilibration. We note that intervalley scattering does not contribute significantly to the fast recovery of the signal in the case of InP, since 2 eV photons excite electrons in the conduction band with an excess energy below the intervalley scattering threshold.

In an attempt to deduce the contribution of carrier-carrier scattering to the fast carrier relaxation observed in our experiments, we performed differential transmission measurements at 2 eV on a normally grown InP film which was intentionally n-type doped to $N_d=5 \times 10^{18} \text{ cm}^{-3}$. The results are contrasted with those of the 200°C sample in **Figure 3.8**. Both traces are taken under similar injected carrier densities ($\sim 10^{19} \text{ cm}^{-3}$) and are normalized to their peak values for comparison. Even though both samples have a similar density of residual electrons in their conduction bands, their response at 2 eV is markedly different. A small partial relaxation is observed right after photo-excitation in the n-type InP sample, followed by a slow recovery due to bandfilling. A small increase of the transmission observed at longer time delays is probably due to the return of carriers from the satellite valleys. Even though in InP carriers injected with 2 eV do not have enough excess energy for intervalley scattering, at high injected carrier densities, electron-electron scattering causes the tail of the carrier distribution to extend to energies high enough for intervalley transfer. In the 200°C grown sample, on the other hand, the initial carrier relaxation is of much larger amplitude.



Z2072

Fig. 3.8 A comparison between the response at 620 nm of the 200°C grown sample and of a conventionally grown but n-type doped to same carrier density. There is little recovery in the n-type material indicating that defect scattering contributes significantly to the observed relaxation in the low temperature grown material.

These differences indicate that other scattering mechanisms such as ionized impurity scattering contribute significantly to the fast relaxation observed in the In the sample grown at 200°C, the bleaching observed immediately after photo-injection turns into induced absorption (i.e. negative transmission plateau) after 1 ps. This plateau does not decay for tens of picoseconds and has also been observed in femtosecond transmission spectroscopy measurements close to the band gap of GaAs as-grown at 250°C [23].

Even if we assume that the energy of each photon absorbed during the excitation process is transferred to the lattice through multi-phonon, non-radiative recombination, the change in the optical properties of the material due to lattice heating cannot account for the observed induced absorption. For a photo-excited carrier density of $n \sim 10^{19} \text{ cm}^{-3}$, a pump photon energy of 2 eV and taking the heat capacity of InP at 298 K to be $0.32 \text{ J g}^{-1} \text{ K}^{-1}$ [24], we find a lattice temperature increase of $\Delta T \sim 2 \text{ K}$ if all carriers recombine non-radiatively. Since the bandgap energy depends on temperature as $E_g(T) = E_g(0) - aT^2/(T+b)$ with $E_g(0) = 1.421 \text{ eV}$, $a = 3.63 \cdot 10^{-4} \text{ eV/K}$ and $b = 162 \text{ K}$ [25], an increase in the lattice temperature by $\sim 2 \text{ K}$, will cause an increase of the absorption coefficient by $\sim 30 \text{ cm}^{-1}$. A lattice temperature increase by $\sim 2 \text{ K}$ is an overestimate, since it assumes that *all* photo-excited carriers *recombine* non-radiatively. Therefore the actual induced absorption due to lattice heating is expected to be even smaller than 30 cm^{-1} . This can not explain our experimental results which at 620 nm and at an injected carrier of $\sim 10^{19} \text{ cm}^{-3}$ show an increase in absorption by a factor of $\sim 1000 \text{ cm}^{-1}$. We

conclude that the large induced absorption plateau is caused by re-absorption of the probe photons by the carriers trapped in the defects. From the magnitude of the induced absorption we can estimate the absorption cross section: with $\Delta\alpha \sim 1000 \text{ cm}^{-1}$ and for $n \sim 10^{19} \text{ cm}^{-3}$, we find $\sigma = \Delta\alpha/n \sim 10^{-16} \text{ cm}^2$. Even though the nature of these traps is not known at present, their photo-ionization cross-section is similar to that of the *EL2* defect in GaAs [26]. We conclude that the photo-excited carriers are first undergoing a fast trapping process, with recombination following at a longer time scale ($\gg 10 \text{ ps}$). The decay constant of the luminescence signal, therefore, describes the trapping time and not the lifetime of the photo-excited carriers. The fast carrier lifetime observed in LT-grown GaAs [23] and LT-grown InGaAs [27] may also be interpreted in the same way.

The induced absorption plateau is also observed in the case of the 300°C sample but at longer time delays. This is due to the saturation of the traps at the high injected carrier densities used in our pump-probe measurements. In **Figure 3.9** we compare the change in transmission at 620 nm in the 200°C and 300°C samples, at injected carrier densities of $\sim 10^{16} \text{ cm}^{-3}$, i.e. three orders of magnitude smaller than the 2-eV-pump/WLC-probe measurements depicted in figure 3.6. After normalizing both traces to their peak values for comparison, we see that the signal recovers in both samples at the same rate. In other words, when the injected carrier density is lower than the density of point defects in both samples, their behavior is identical. The decay of the bleaching in the sample grown at 200°C changes only slightly as the injected carrier density is increased from 10^{16} cm^{-3} to

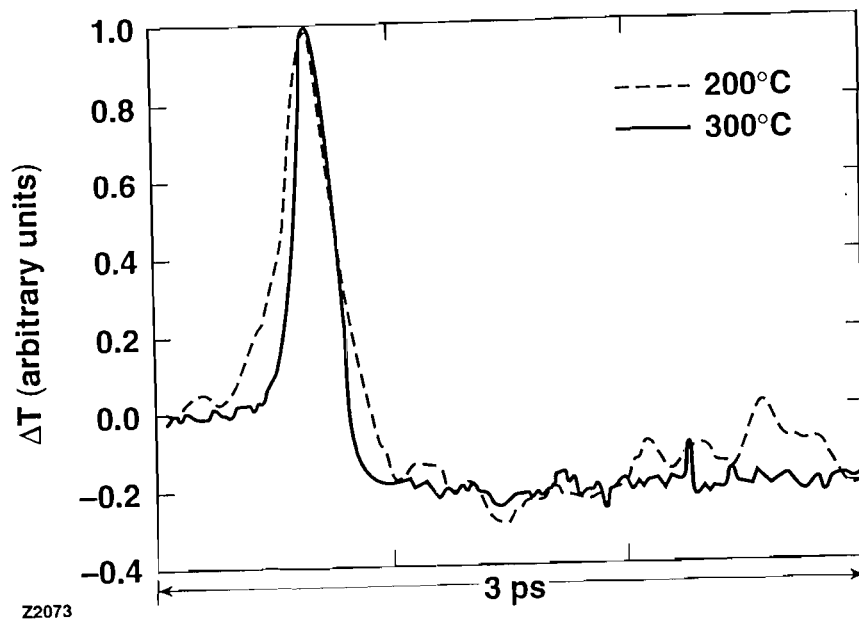


Fig. 3.9 Saturation of the traps at high injected carrier densities is evident when the recovery of the bleaching at 620 nm is found to be identical for both the 200°C and the 300°C samples at $N_{inj} \sim 10^{16} \text{ cm}^{-3}$.

10^{19} cm^{-3} indicating that the density of the traps is $\geq 10^{19} \text{ cm}^{-3}$ in this sample. In the sample grown at 300°C , on the other hand, a similar estimate leads to a trap density of mid- 10^{17} cm^{-3} .

In conclusion, we have presented the results of differential reflection, transmission, and up-conversion luminescence measurements on optically thick and thin LT-InP films grown at 200°C and 300°C . Even though the electronic and structural properties of this material differ appreciably from those of LT-grown GaAs, the optical response is very similar.

No spectral hole is observed in the reflectivity measurements within our time resolution. This is consistent with the pulse width limited rise time of the band edge luminescence and of the band edge photo-induced bleaching measurements.

Trapping of photoexcited carriers takes place in a subpicosecond time scale with time constants of 0.45 ps for the 200°C sample and 1.6 ps for the 300°C sample. Carrier recombination takes place on a much longer time scale. A strong scattering mechanism appears to dominate the carrier dynamics in the first 100 fs after photo-excitation. This relaxation is mostly due to mechanisms such as defect ionization scattering as can be seen from a comparison with an n-type film, grown at high ($\sim 500^\circ\text{C}$) temperature.

Re-absorption of the probe photons by the trapped carriers leads to induced absorption at time delays greater than ~ 1 ps. The trap photo-ionization cross-section is $\sim 10^{-16} \text{ cm}^2$ at 2 eV. Saturation of the traps is observed at high

injected carrier densities, leading to a slower recovery of the bleaching for samples grown at the higher substrate temperatures.

References

1. J. L. Oudar, D. Hulin, A. Migus, A. Antonetti, and F. Alexandre, *Phys. Rev. Lett.* **55**, 2074 (1985).
2. S. Hunsche, H. Heesel, A. Ewertz, H. Kurtz, and J. H. Collet, *Phys. Rev. B* **48**, 17818 (1993).
3. W. H. Knox, D. S. Chemla, G. Livescu, L. E. Cunningham, and J. E. Henry, *Phys. Rev. Lett.* **61**, 1290 (1988).
4. W. H. Knox, C. Hirlimann, D. A. B. Miller, J. Shah, D. S. Chemla, and C. V. Chang, *Phys. Rev. Lett.* **56**, 1191 (1986).
5. C. H. Brito-Cruz, R. L. Fork, and C. V. Shank, *IQEC Technical Digest*, p. 82 (1987).
6. R. W. Schoenlein, W. Z. Lin, E. P. Ippen, and J. G. Fujimoto, *Appl. Phys. Lett.* **51**, 1442, (1987).
7. W. Z. Lin, R. W. Schoenlein, J. G. Fujimoto, and E. P. Ippen, *IEEE J. Quantum Electron.* **QE-24**, 267 (1988).
8. D. C. Hutchings, M. Sheik-Bahae, D. J. Hagan, and E. W. Van Stryland, *Opt. Quantum Electron.* **24**, 1 (1991).

9. J. Shah, B. Deveaud, T. C. Damen, W. T. Tsang, A. C. Gossard, and P. Lugli, *Phys. Rev. Lett.* **59**, 2222 (1987).
10. J. N. Sweetser, T. J. Duhn, L. Waxer, I. A. Walmsley, S. M. Shank and G. W. Wicks, *Appl. Phys. Lett.* **63**, 3461, (1993).
11. T. Gong, "Femtosecond Nonlinearities And Hot Carrier Dynamics In GaAs", Ph. D. Thesis Princeton University, (1991).
12. J. -Y. Bigot, M. T. Portella, R. W. Schoenlein, J. E. Cuningham, C. V. Shank, *Phys. Rev. Lett.* **65**, 3429 (1990).
13. B. R. Bennett, R. A. Soref, and J. A. Del Alamo, *IEEE J. Quantum Electron.* **QE-26**, 113 (1990).
14. K. Xie, C. R. Wie and G. W. Wicks, *Mat. Res. Soc. Symp. Proc.* **241**, 265 (1992).
15. S. Gupta, J. F. Whitaker, and G. A. Mourou, *IEEE J. Quantum Electron.* **QE-28**, 2464 (1992).
16. X. Q. Zhou, H. M. van Driel, W. W. Rühle, Z. Gogolak, and K. Ploog, *Appl. Phys. Lett.* **61**, 3020 (1992).
17. P. Dreszer, W. M. Chen, K. Seendripu, J. A. Wolk, W. Walukiewitz, B. W. Liang, C. W. Tu, and E. R. Weber, *Phys. Rev. B.* **47**, 4111, (1993).
18. X. Q. Zhou, G. C. Cho, U. Lemmer, W. Kütt, K. Volter, and H. Kurz, *Sol. State Electron.* **32**, 1591 (1989).
19. A very fast luminescence rise time could also arise from recombination of electrons from the large cold electron reservoir with the photogenerated

holes. The pump-probe measurements shown in Fig. 2, however, support the interpretation in the text.

20. T. Gong, P. Mertz, W. L. Nighan Jr., and P. M. Fauchet, *Appl. Phys. Lett.* **59**, 721–723 (1991).
21. T. Gong, W. L. Nighan Jr. and P. M. Fauchet, *Appl. Phys. Lett.* **57**, 2713, (1990).
22. T. Gong, P. M. Fauchet, J. F. Young, and P. J. Kelly, *Phys. Rev. B* **44**, 6542 (1991).
23. E. S. Harmon, M. R. Melloch, J. M. Woodall, D. D. Nolte, N. Otsuka, and C. L. Chang, *Appl. Phys. Lett.* **63**, 2248 (1993).
24. U. Piesbergen, “Semiconductors and Semimetals,” in *Physics of III-V Compounds*, edited by R. K. Willardson and A. C. Beer (Academic Press, NY, 1966), Vol. 2, p. 52.
25. “Properties of Indium Phosphide,” *EMIS Datareviews Series*, Vol. 6, (INSPEC Institution of Electrical Engineers, London, 1991).
26. G. C. Valley, T. F. Boggess, J. Dubard, and A. L. Smirl, “Picosecond Pump-Probe Techniques to Measure Deep-Level, Free-Carrier, and Two Photon Cross Sections in GaAs,” *J. Appl. Phys.* **66**, 2407 (1989).
27. B. C. Tousley, S. M. Mehta, A. I. Lobad, P. J. Rodney, P. M. Fauchet, and P. Cooke, “Femtosecond Optical Response of Low Temperature Grown $\text{In}_{0.53}\text{Ga}_{0.47}\text{As}$,” *J. Electron. Mater.* **22**, 1477 (1993).

CHAPTER 4

Femtosecond Carrier Dynamics In Low Temperature-Grown

$\text{Ga}_{0.51}\text{In}_{0.49}\text{P}$

4.1 Introduction

The success of LT-GaAs in a variety of applications has prompted the study not only of other As-based, low temperature grown III-V compounds, but also of the P-based materials. In the previous chapter we discussed the results of pump-probe and up-conversion luminescence spectroscopy on LT-InP. The optical response of this material is similar to that of LT-GaAs, even though their electrical properties are quite different. We have seen that InP when grown at low temperatures ($\sim 200^\circ\text{C}$) is heavily n-type due to the donor nature of the P_{In} antisite defect, which has an energy level degenerate with the conduction band. This does not change even after annealing at high temperatures.

Another phosphorus based material of technological importance is the ternary $\text{Ga}_{0.51}\text{In}_{0.49}\text{P}$. It is lattice matched to GaAs and thus epitaxial layers made of this material are compatible with the relatively mature GaAs technology. With both n- and p-type doping available and a relatively wide band gap of 1.9 eV, many device applications have been proposed and are implemented. For example, a high valence band discontinuity with GaAs and a low Be diffusion coefficient,

make GaInP an attractive material for GaInP/GaAs/GaAs heterojunction bipolar transistors [1]. However, a common problem in many semiconductor materials is the lack of a stable, semi-insulating form. In the case of GaInP, growth at low substrate temperatures can solve this problem effectively.

When as-grown between 150°C and 250°C, low-temperature Ga_{0.51}In_{0.49}P (LT-GaInP) is weakly n-type with a room temperature resistivity of $\sim 9 \times 10^5 \Omega\text{cm}$, a mobility of 120 cm²/Vs, and a donor activation energy of 0.48 eV.² The lattice constant is increased by 0.05%, which corresponds to a $\sim 47\%$ In content.[3] After annealing at 600°C for 1 hour, the resistivity increases to $10^9 \Omega\text{cm}$ and the activation energy to 0.8 eV.[2,3] These properties, if accompanied by a short carrier trapping time, make LT-GaInP an attractive candidate for fast photoconductive switch and metal-insulator field-effect (MISFET) transistor applications. In this chapter we show that the carrier trapping time in this material is < 1 ps, depending on the growth temperature and the annealing conditions, and that the point defects caused by the low temperature growth are directly responsible for this ultrafast response.

We make use of the 2-eV-pump/WLC-probe system in order to investigate carrier dynamics in samples grown at 500°C, 300°C, and 200°C. Due to the proximity of the band gap luminescence to the pump photon energy, it is impossible to perform up-conversion luminescence measurements with this system. The noise introduced from the doubled pump photons obscures the low level photon counting of the band gap luminescence.

4.2 Carrier Dynamics in High Temperature Grown GaInP

In order to investigate properly the dynamics of carriers in LT-grown GaInP, we first attempt a characterization of the material grown at normal substrate temperatures of $\sim 500^\circ\text{C}$. In Table I we summarize the material parameters for GaInP. The corresponding values of GaAs are quoted for comparison.

The sample that was used in this study was grown by gas source molecular beam epitaxy (GSMBE) at a substrate temperatures of 500°C . X-ray diffraction measurements showed good crystalline quality. The thickness was $0.5\ \mu\text{m}$, which is approximately equal to one absorption length for 2 eV photons. The GaAs substrates were selectively etched (see chapter 2), and the epitaxial layers were attached to sapphire windows using van der Waals forces. In order to verify that the substrate was completely removed after the etching process, we performed CW luminescence measurements exciting the sample with the 514 nm Ar^+ laser line. This measurement was also used to determine the band gap of the epitaxial layer. The results are shown in **Figure 4.1**. There is no evidence of the GaAs substrate in the CW luminescence trace and the band gap energy of the GaInP layer is found to be 1.89 eV at room temperature. In all the experiments reported here, the excitation energy is 2 eV. From the material parameters of Table I we calculate the carrier kinetic energies to be: $\epsilon_e^{\text{hh}} = 89\ \text{meV}$, $\epsilon_e^{\text{lh}} = 68\ \text{meV}$, for the

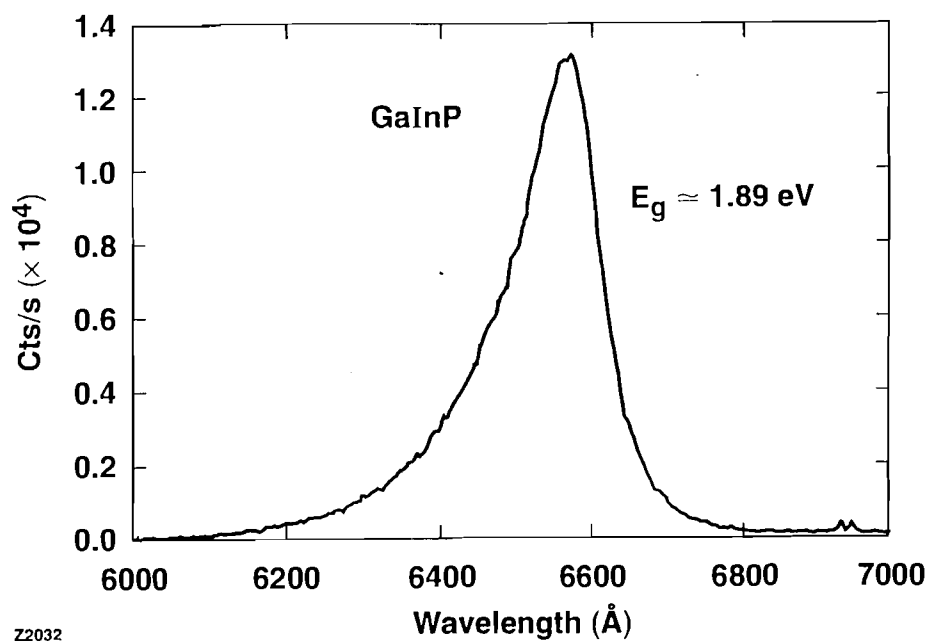


Fig. 4.1 CW luminescence measurement of the conventionally grown GaInP film. The excitation was the 514 nm line of an Ar⁺ laser. There is no trace of the GaAs substrate, and the peak of the luminescence is at 1.89 eV. This value is also considered to be the band gap of the GaInP film.

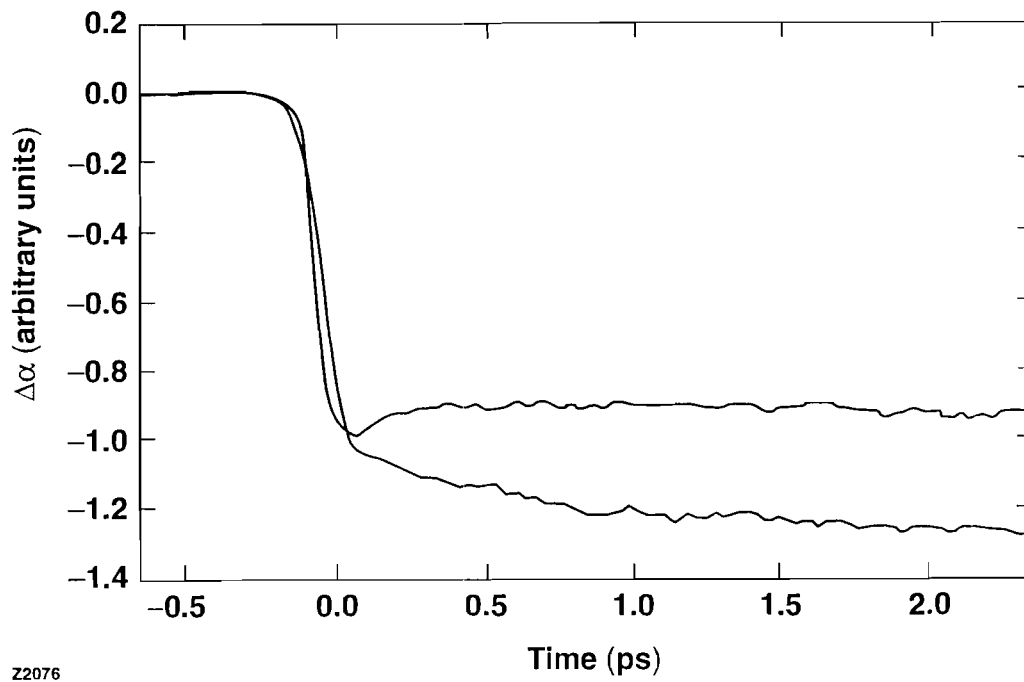
	Ga _{0.51} In _{0.49} P ⁽⁴⁾	GaAs ⁽⁵⁾
$m_{e\Gamma}^*$	0.11 m_0	0.067 m_0
m_{eL}^*	0.15 m_0	0.55 m_0
m_{eX}^*	0.23 m_0	0.85 m_0
m_{lh}^*	0.18 m_0	0.082 m_0
m_{hh}^*	0.43 m_0	0.45 m_0
E_Γ	1.89 eV	1.424 eV
E_L	2.56 eV	1.708 eV
E_X	2.23 eV	1.900 eV
Δ	0.113 eV	0.33 eV

Table III. Material parameters for GaInP and for GaAs: the effective masses, m^* , of the Γ , X, and L valleys and the heavy- and light-hole bands are given. The band edge positions are measured with respect to the valence band edge, and Δ is the spin-orbit splitting.

electrons from the heavy and light holes, and $\epsilon_{hh} = 22$ meV, and $\epsilon_{lh} = 42$ meV for the heavy and light holes respectively. With a value of $\Delta=0.11$ eV, excitation of carriers from the spin-split off band at the bottom of the conduction band is also allowed. The vanishing density of states though, renders the effect of this transition negligible. The satellite valleys are at much higher energies, as can be seen from Table I, so that for 2 eV photon excitation we can ignore intervalley scattering.

Numerous pump-probe and equal-pulse correlation experiments have been performed to date, and theoretical analysis attempted, in order to explore the contributions of the fundamental carrier scattering processes to the measured results in both quantum wells and the bulk. While the near band gap regime has been studied extensively in quantum wells, in the bulk the attention has been almost exclusively focused to excitation far from the band edge. Excitation close to the band edge has been recently addressed in the work of Bair et. al.⁶ on GaInAs and of Ulman et. al.[7] on Al_{0.1}Ga_{0.9}As. Our experiments belong to the same category.

In **Figure 4.2** are depicted the results of the 2 eV pump-probe measurement at two injected carrier densities ($N_{inj} \sim 5 \times 10^{16} \text{ cm}^{-3}$ and $\sim 10^{19} \text{ cm}^{-3}$). The behavior at the low injected carrier density is what might be expected for excitation above the gap of a direct gap semiconductor. The initial hole burning peak is short-lived as can be seen by the small relaxation right after



Z2076

Fig. 4.2 Differential absorption measurements at 620 nm on the 500°C at injected carrier densities of $5 \times 10^{16} \text{ cm}^{-3}$ and $\sim 10^{19} \text{ cm}^{-3}$.

carrier injection. This results from scattering of carriers out of their initial excited states. The relatively large width of the peak is due to the fact that carriers leave slowly the as-excited states through carrier-carrier and LO-phonon scattering. Taking into account the spectral extend of the 100 femtosecond pulses at 2 eV, the electron distributions excited from the heavy and light hole bands overlap, creating an effective carrier distribution that extends from ~ 100 meV to ~ 50 meV above the band edge. Fast carrier-carrier scattering will also broaden this distribution during photo-excitation. Thus, the phase space available for scattering is appreciably reduced. This leads to the observed small amplitude and relatively slow relaxation.

Exciting carriers close to the bottom of the conduction band, allows the observation of the effects of Fermi level increasing with carrier density to be observed. In Figure 4.2(b) we show the same experiment performed at an injected carrier density of $\sim 10^{19}$ cm $^{-3}$. This value is determined from the beam spot size, the average power and the absorption coefficient at 2 eV. At these high densities, the small fast relaxation disappears. Instead, the bleaching continues to increase slowly after photoexcitation. This is the result of the slow relaxation of holes towards the bottom of the valence band. At $N_{inj} \sim 10^{19}$ cm $^{-3}$, electron thermalization through carrier-carrier scattering takes place in less than 100 fs.^{8,9} Thus, the electron distribution is expected to contribute the most to the observed bleaching within the pump pulsewidth. Because of their mass, heavy holes are excited in a relatively narrow energy range even for a wide distribution of wave vectors. Therefore, the relaxation in energy of the heavy holes is not dramatic [7].

Additionally, the initial average hole energy (~ 22 meV) is very close to the thermal energy, indicating that heavy hole relaxation is minimal. The light holes on the other hand, have an average thermal energy of 42 meV and as they relax to the heavy hole band through intervalence band scattering, the bleaching increases. A simple calculation of the band filling factor shows that at these high injected carrier densities, the contribution of the heavy hole transition to the percentage change of absorption is twice that of the light hole, leading to a net positive contribution to bleaching. The limited phase space available for hole scattering due to the high injected carrier density, also slows down the relaxation of holes. Recent measurements on GaAs,[10] have shown that heavy holes thermalize with the lattice at ~ 500 fs.

For excitation low in the conduction band additional effects such as band gap renormalization and Coulomb enhancement, have to be taken into account. Both processes increase the excited carrier density, and band renormalization also broadens the excited distributions. Coulomb enhancement is a band edge phenomenon, and for sufficiently high excitation energy ceases to be important. Band renormalization in contrast, continues to grow in importance for hotter initial electron distributions, and the canceling effect of Coulomb enhancement becomes smaller. The bandgap will shrink and band renormalization will slow the apparent relaxation and broaden the carrier distribution. It seems likely that this aspect of band gap renormalization will make its greatest contribution for excitation higher in the conduction band, and not at the band edge. Bair [6] have performed Monte

Carlo simulations for similar conditions in the case of GaInAs. They have shown that for a cooling carrier distribution the effects of the two processes are opposite, with bandgap renormalization slowing the carrier relaxation. Additionally, the dominant contributions to the observed signal for the first 400 fs are from the heavy holes, in contrast to excitation at higher energies where holes contribute only on much shorter time scales.

In order to examine in more detail the carrier dynamics at high injected carrier densities we performed pump-probe measurements with 2 eV pump and WLC probe. The results are shown in **Figure 4.3**. The absorption change is extracted from the transmission and reflection measurements by inverting the Fabry-Perot formulas as described in Chapter 2. We observe absorption bleaching at all wavelengths from 570 nm to 670 nm. In agreement with the results of Figure 4.2, we do not observe any relaxation at any wavelength. Instead the behavior is qualitatively the same for all probe wavelengths. This is due to the large density of injected carriers which saturates the involved transitions within the pulse width. In spite of the fact that the band gap is at 1.89 eV, (656 nm), we observe bleaching at ~40 meV below the gap (670 nm probe wavelength). This is due to the renormalization of the bandgap. Using an empirical formula [11], the reduction of the bandgap due to band gap renormalization is

$$\Delta E_g(N) = \frac{c}{\epsilon_s} \left(1 - \frac{N}{N_{cr}} \right)^{1/3}, \quad N \geq N_{cr}$$

$$\Delta E_g(N) = 0, \quad N \leq N_{cr}$$

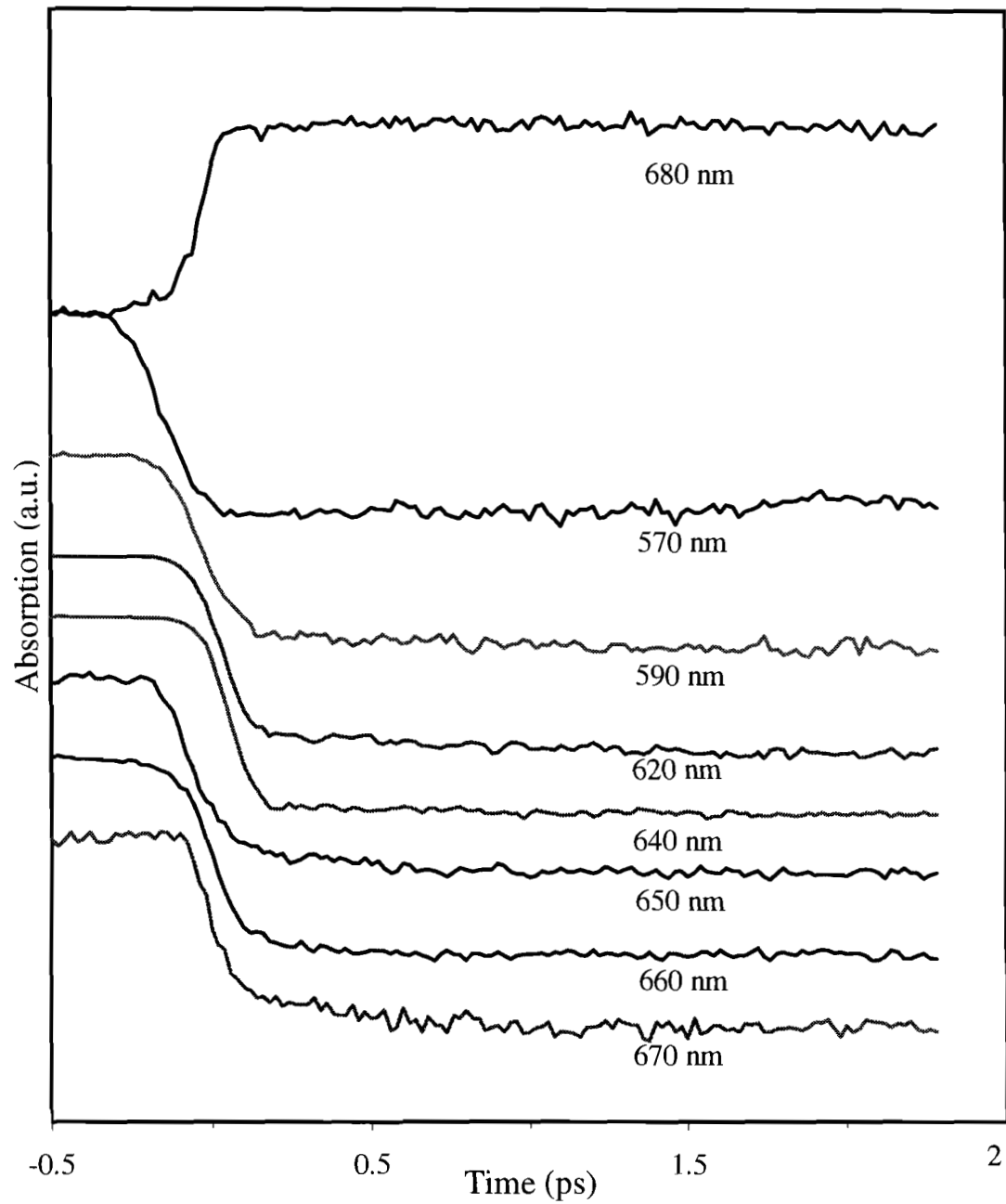


Fig. 4.3 Absorption change in normally grown GaInP with a 2 eV pump. We observe bleaching at 670 nm (~ 40 meV below the bandedge) and induced absorption at 680 nm.

where ϵ_s is the static dielectric constant of the material, c is a fitting parameter and N_{cr} is a critical carrier density. The values of some of these parameters were extrapolated from those of GaAs since there are no data available for GaInP. Using the above formula, we estimate the band gap renormalization to be 32 meV, in good agreement with our results. At 680 nm the probe photons are not energetic enough to cause a transition to the conduction band even after renormalization, and we observe an increase in absorption. This increase is due to free carrier absorption which becomes possible after carrier injection. The absorption change at 680 nm is 462 cm^{-1} , and for an injected carrier density of 10^{19} cm^{-3} we estimate the free carrier absorption cross section to be $\sigma = \sigma_e + \sigma_h = \Delta\alpha/n \sim 5 \times 10^{-17} \text{ cm}^2$.

4.3 Carrier-Carrier Scattering in Conventionally Grown GaAs and GaInP

Time resolved spectroscopy of semiconductors has been one of the most useful tools in the study of the dynamics of non-equilibrium carriers. Laser excitation of semiconductors results in generation of electrons and holes with relatively well defined kinetic energies in the conduction and valence bands respectively. If the exciting pulse duration is less than or comparable to the fastest scattering mechanisms then one should be able to monitor the evolution from

nonthermal to thermal distributions through carrier-carrier interaction among the photoexcited carriers. At low injected carrier densities ($< 10^{15} \text{ cm}^{-3}$) this transition takes on the order of picoseconds.¹² When the injected carrier density is higher ($> 10^{17} \text{ cm}^{-3}$, more typical of semiconductor devices), the thermalization time is much shorter ($< 100 \text{ fs}$), as was found by a variety of optically based experiments.[13-16]

Femtosecond bleaching experiments provide information about the dwell time of the photogenerated carriers in the optically coupled states. The role of carrier-carrier scattering is difficult to identify from the temporal behavior of the bleaching signal since it is more complicated than carrier-phonon scattering and it does not lead to an exponential recovery of the bleaching. In a degenerate femtosecond pump-probe experiment, very fast scattering mechanisms such as carrier-carrier interaction will significantly broaden the as-excited electron distribution before absorption of the pump pulse is completed. This affects the maximum bleaching, $\Delta\alpha_{\text{max}}$, since the faster the carriers leave the as-excited states, the smaller the amplitude of the bleaching is. Thus, we come to the conclusion that by monitoring $\Delta\alpha_{\text{max}}$ under various excitation conditions, we can directly study carrier-carrier scattering. For example, it has been reported that $\Delta\alpha_{\text{max}}$ varies sublinearly with increasing injected carrier density in the case of intrinsic GaAs[17] and superlinearly in n-type GaAs.[18]

In the present work we employ an experimental technique that allows us to monitor carrier-carrier scattering with improved sensitivity. This technique consists

of monitoring the maximum absorption bleaching $\Delta\alpha_{\max}$, in the presence of an additional electron-hole distribution. Two pulses, the pump and the probe, are fixed at $\tau \sim 0^+$, i.e. on the maximum of the absorption bleaching, $\Delta\alpha_{\max}$. A third pulse, the pre-pump, centered at the same wavelength as both pump and probe pulses, injects an additional electron-hole plasma at different time delays with respect to the pump pulse. As the time delay increases, this additional carrier distribution relaxes towards the bottom of the conduction band and affects $\Delta\alpha_{\max}$ accordingly. Since $\Delta\alpha_{\max}$ is a direct measure of carrier-carrier scattering, this type of experiments is designed to measure the dependence of this scattering process on both carrier density and carrier temperature. First, we examine the behavior of normally grown GaAs under these experimental conditions. This material, being investigated extensively, serves as a benchmark for a comparison with GaInP.

In **Figure 4.4** we present a three-pulse experiment performed on the intrinsic GaAs thin film at the low carrier density regime. Both pump and pre-pump pulses inject $N \sim N_{\text{pre}} \sim 3 \times 10^{16} \text{ cm}^{-3}$ carriers. The inset shows the signal measured in a conventional pump and probe arrangement and the arrow indicates the time delay in which $\Delta\alpha_{\max}$ is monitored. When an additional $3 \times 10^{16} \text{ cm}^{-3}$ carriers are present, $|\Delta\alpha_{\max}|$ is reduced by 5%. As the delay between the pre-pump and pump pulses increases, there is a very fast partial recovery of the maximum bleaching, followed by a 10 ps decay. The initial maximum bleaching reduction results from enhanced electron-electron scattering, thus, it directly measures the efficiency of carrier-carrier scattering.

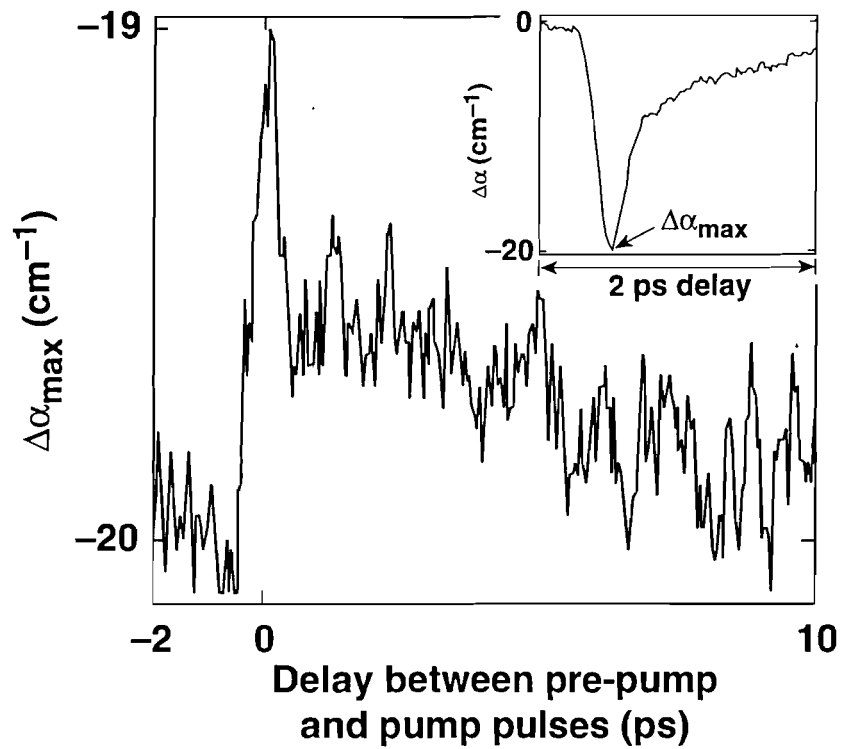


Fig. 4.4 Three-pulse experiment on i-GaAs thin film ($d \sim 0.2 \mu\text{m}$) at low injected carrier densities ($N \sim N_{\text{pre}} \sim 3 \times 10^{16} \text{cm}^{-3}$). The inset shows where $\Delta\alpha_{\max}$ was monitored.

When the same experiment is performed at the high carrier density regime ($N \sim N_{\text{pre}} \sim 5 \times 10^{18} \text{ cm}^{-3}$), the result is strikingly different as can be seen in **Figure 4.5**. When pre-pump and pump pulses overlap temporally we see again a decrease in $|\Delta\alpha_{\text{max}}|$ due to enhanced electron-electron scattering. After ~ 1 ps however, a fast recovery causes the signal to change sign and then slowly reach a plateau. The dwell time of the electrons increases because electron-electron scattering becomes less efficient in the presence of a high density, thermalized electron distribution resulting an increase in $|\Delta\alpha_{\text{max}}|$. When the carrier density is reduced this plateau is seen to decrease with respect to the fast feature. At $\sim 10^{17} \text{ cm}^{-3}$, the reversal of the signal sign does not take place at all.

Two important conclusions can be deduced from Fig. 4.4. First, electron-electron scattering is detectable even for carrier densities as low as $3 \times 10^{16} \text{ cm}^{-3}$. Second, the interaction between the two electron distributions (with $3 \times 10^{16} \text{ cm}^{-3}$ each) is more efficient when all electrons are in similar Bloch states. In GaAs, the 2 eV photons excite three nearly monoenergetic electron distributions from the heavy hole(hh:c), light hole(lh:c) and spin-split-off(so:c) bands. Of these distributions, the hh:c and lh:c have excess energy above the intervalley scattering threshold. As the time delay between the pre-pump and pump pulses increases, most of the hh:c and lh:c carriers injected by the pre-pump pulse transfer to the satellite valleys. Scattering between electrons in the X and L valleys and electrons in the Γ valley becomes less efficient due to the large difference in effective masses. This causes the fast partial recovery seen in Fig. 4.4, since $\sim 80\%$ of the

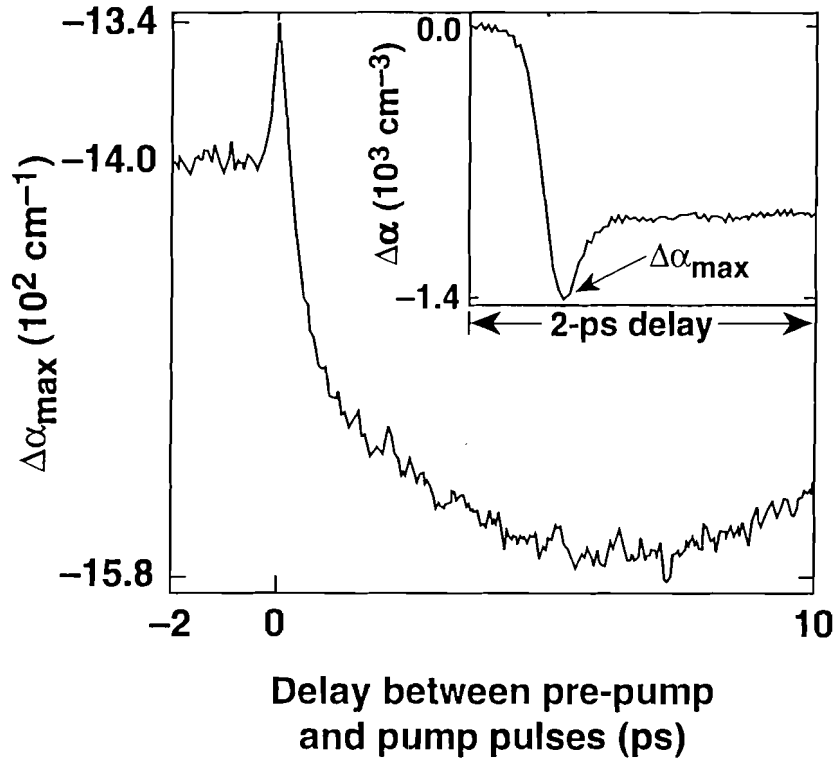
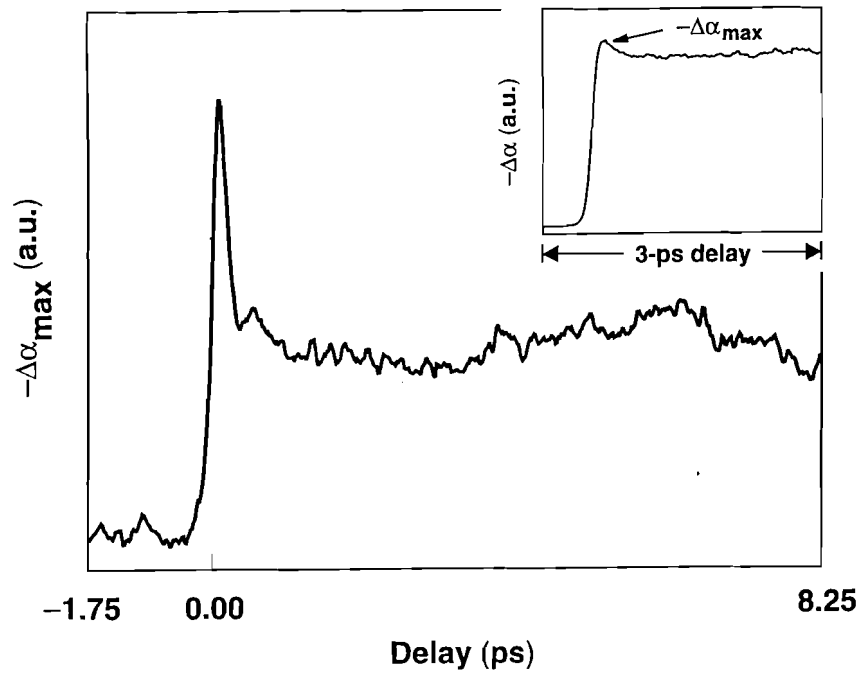


Fig. 4.5 Similar measurements as in Fig. 4.4 but at higher carrier densities ($N \sim N_{\text{pre}} \sim 5 \times 10^{18} \text{ cm}^{-3}$). The presence of a thermalized electron distribution at high temperatures leads to a dramatic reduction of electron-electron scattering.

pre-pump injected electrons have transferred to the satellite valleys and only 20% of the pump can interact efficiently with the pre-pump electrons. At later time delays, the pre-pump carriers return to the Γ valley forming a colder thermalized distribution. When the pump injected hot electrons interact with this colder distribution, the change in momentum involved is larger than when the two distributions occupy states with similar energy. In this single-particle picture [19] scattering with large momentum exchange is less efficient thus leading to the slow decay of the observed signal. When the injected carrier density is two orders of magnitude higher, we again see an increase in electron-electron scattering when pump and pre-pump overlap temporally on the sample, a result consistent with the sublinear change of $\Delta\alpha_{\max}$ with density. At this high density enhanced phase-space filling also contributes to the fast recovery. Band gap renormalization does not contribute significantly to the observed behavior since it is primarily a band edge phenomenon. The so:c carrier distribution injected by the pre-pump is of the order of $\sim 10^{18} \text{ cm}^{-3}$. As this distribution thermalizes, it populates the states with momentum below the as-injected pump distribution, leading to increased phase space filling and therefore less electron-electron scattering.[20] In addition, increased screening at these high densities can also reduce the electron-electron scattering rate. As the carriers return to the Γ valley, state filling and screening lead to further reduction of electron-electron interaction which causes the large plateau.

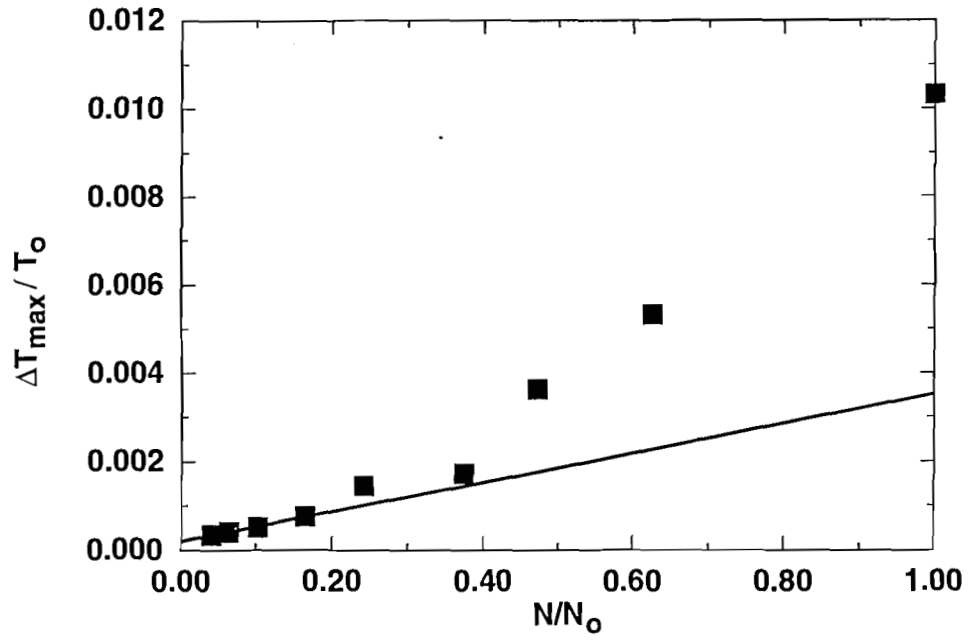
When 2 eV photons are used to excite electrons in GaAs, intervalley scattering is unavoidable, complicating the interpretation of three-pulse experiments. In order to examine electron-electron scattering without this additional complication we performed experiments on an intrinsic $\text{In}_{0.5}\text{Ga}_{0.5}\text{P}$ thin film. The bandgap of this material was determined by photoluminescence measurements to be 1.89 eV. As a result the electrons are excited with ~ 70 meV excess energy and cannot transfer to the satellite valleys.

Figure 4.6 shows how the maximum change in absorption is affected by the pre-pump pulse. When pre-pump and pump pulses overlap temporally, we observe a sharp decrease in $\Delta\alpha_{\text{max}}$ (increase in ΔT_{max}), i.e. a reduction in electron-electron scattering. This behavior is followed by a fast partial recovery taking place in ~ 0.3 ps and then a long lasting plateau. It is difficult to explain the behavior at early time delays. Due to the fact that this is a three-beam experiment, two beams are of the same polarization and therefore, coherent artifact can contribute to the initial rise of the signal. Additionally, for excitation close to the band edge, band gap renormalization also complicates the results. First, band gap re-normalization caused by the pre-pump, induces an effective increase to the pump and probe photons which now probe higher densities of states. This results in a stronger bleaching. Second, this increase of the density of states increases the phase space available for relaxation. Reduced electron-electron scattering due to phase-space filling is believed to play a significant role at later times. We also performed conventional pump-probe measurements at injected carrier densities



Z1658

Fig. 4.6 Three-pulse data taken on an $\text{In}_{0.5}\text{Ga}_{0.5}\text{P}$ thin film at $N \sim N_{\text{pre}} \sim 8 \times 10^{17} \text{ cm}^{-3}$. The behavior is opposite than that observed in GaAs, due to state filling and bandgap renormalization.



Z1659

Fig 4.7 Superlinear behavior of the maximum change in transmission as a function of the injected carrier density due to bandfilling.

varying from 2×10^{16} - 8×10^{17} cm^{-3} and measured the variation of ΔT_{max} with the carrier density as depicted in **Figure 4.7**. The behavior of ΔT_{max} is strongly superlinear, a result reinforcing the hypothesis that reduced electron-electron scattering is caused by phase-space filling. A similar superlinear behavior was observed in heavily doped n-type GaAs [18] pumped at 2 eV.

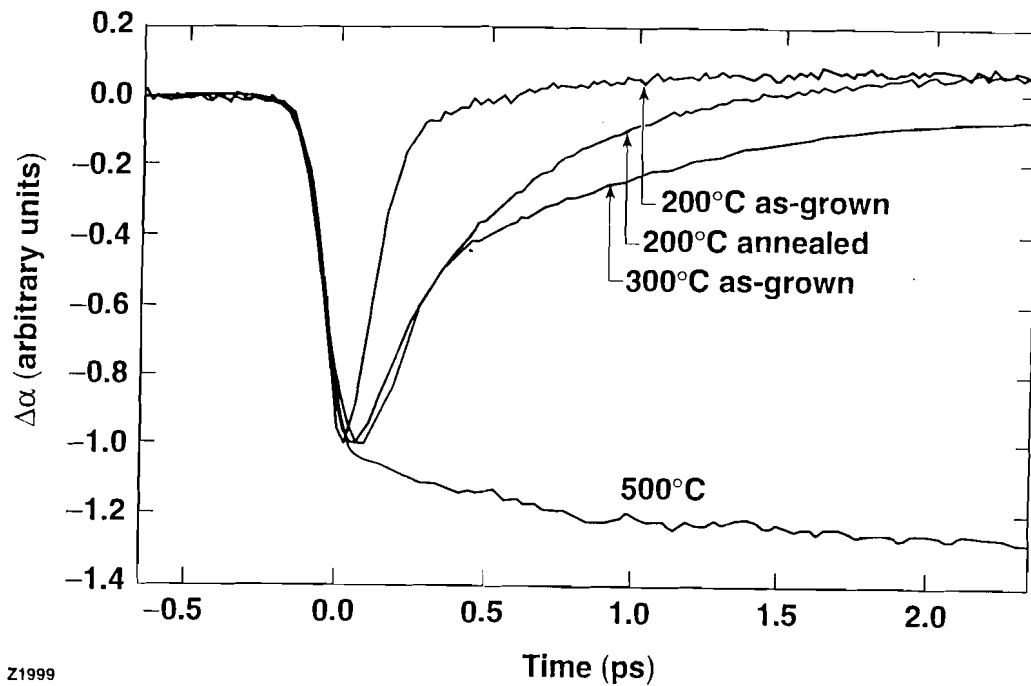
4.4 Carrier Dynamics In Low Temperature Grown GaInP

In the previous paragraph we investigated the properties and optical response of conventionally grown GaInP. We found that for excitation at 2 eV, carrier relaxation is evident only at low injected carrier densities due to band filling. Here, our goal is to perform similar measurements on material grown at low substrate temperatures and compare its behavior to that of conventionally grown GaInP.

The samples that were used in this study were grown by gas source molecular beam epitaxy (GSMBE) at substrate temperatures of 300°C and 200°C. Part of the 200°C grown sample underwent a modest *in situ* annealing at 450°C for 10 min under P overpressure. X-ray diffraction measurements showed all samples to be of good crystalline quality. Their thickness was 0.5 μm for the 300°C sample which is equal to approximately one absorption length for 2 eV photons,

and 1 μm for the samples grown at 200°C. The LT-grown samples did not show any CW luminescence. Their nominal bandgap is assumed to be 1.89 eV.

Figure 4.8 shows the results of differential absorption measurements performed at 2 eV following injection of $\sim 10^{19} \text{ cm}^{-3}$ carriers with a 2 eV pump. The trace of the 500°C sample is included for comparison and shows no recovery after carrier injection due to band filling and phase space filling.[21,22] When the growth temperature is lowered, a much faster response is observed. The recovery of the bleaching is bi-exponential and leads to a small induced absorption plateau in all samples. This plateau does not decay for tens of picoseconds and has also been observed in differential transmission measurements close to the band edge of LT-GaAs[23] and LT-InP.[24] The existence of this induced absorption plateau, is attributed to photo-ionization of the defect centers after trapping of the photoexcited carriers. The fact that it is a long-lived component, indicates that the ultrafast response in LT-GaInP, similarly to what has been seen in LT-InP and LT-GaAs, corresponds to carrier trapping and not carrier recombination which takes place in a time scale of tens of picoseconds. In the 300°C as-grown sample, a time constant of ≤ 200 fs is extracted for the fast component, and it describes the dwell time of the carriers in the as-excited states. The slower component which is 0.9 ps, is attributed to carrier trapping as in the case of LT-InP grown at 200°C and 300°C.[24] When the growth temperature is lowered even further to 200°C, we observe the fastest response. This ultrafast relaxation is probably due to impurity scattering. The component describing carrier relaxation in the as-grown sample is



Z1999

Fig. 4.8 Bleaching at 2 eV in three samples grown at: 500°C, 200°C as-grown, 300°C as-grown and 200°C annealed at 450°C for 10 min. For the samples grown at lower temperatures the trapping times are 350 fs (see text), 900 fs, and 700 fs correspondingly.

found to be 50 fs (deconvoluted). It is difficult, however, to extract the carrier trapping time from a biexponential fit, in the case of the 200°C as-grown sample, since carrier relaxation dominates the recovery of the signal at early time delays. This is due to the existence of a large band tail, which increases the phase space available for carrier relaxation, as is evident by the observation of a small bleaching component even at a probe photon energy of 1.82 eV (more than 70 meV below the nominal band gap). This band tail is the result of the large density of point defects due to the growth at low substrate temperatures.

A modest anneal of the 200°C grown sample at 450°C for 10 minutes, slows the 2 eV optical response appreciably. The fast component is found to be again ≤ 200 fs while the slower component is 0.7 ps. This slower response after annealing is a direct indication that the fast response in LT-GaInP is due to the large density of point defects. No formation of phosphorus precipitates has been observed in LT-GaInP even after an 1 hour anneal at 600°C.[3] In contrast, the concentration of point defects is reduced, as is evident by the smaller strain observed in the annealed sample. [3]

In order to extract the carrier trapping time in the 200°C, as-grown sample, we compare the experiments performed at ~ 80 meV above (620 nm probe) and ~ 240 meV below (750 nm probe) the nominal conduction band edge. These measurements are displayed in **Figure 4.9**. Both traces are normalized to their peak values for comparison. The signal at 620 nm is characterized by a pulse-width limited rise time, commensurate to the convolution of the pump and probe pulses.

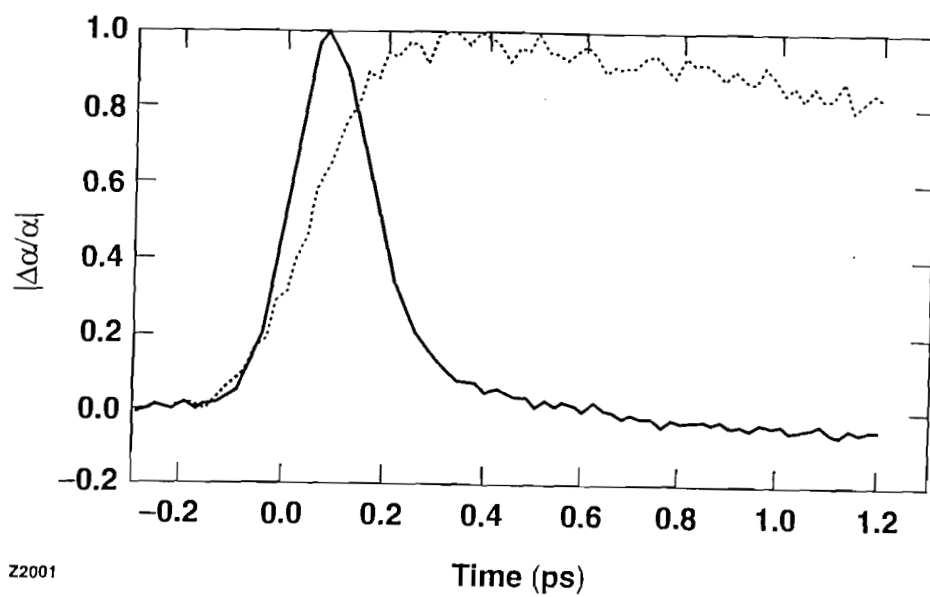


Fig. 4.9 An ultrafast recovery of 50 fs is observed in the as-grown 200°C sample at early time delays. The trapping time, which is found to be 0.35 ps, is better resolved by a comparison of the 620 nm and the 750 nm curves. Both traces are normalized to their respective peaks.

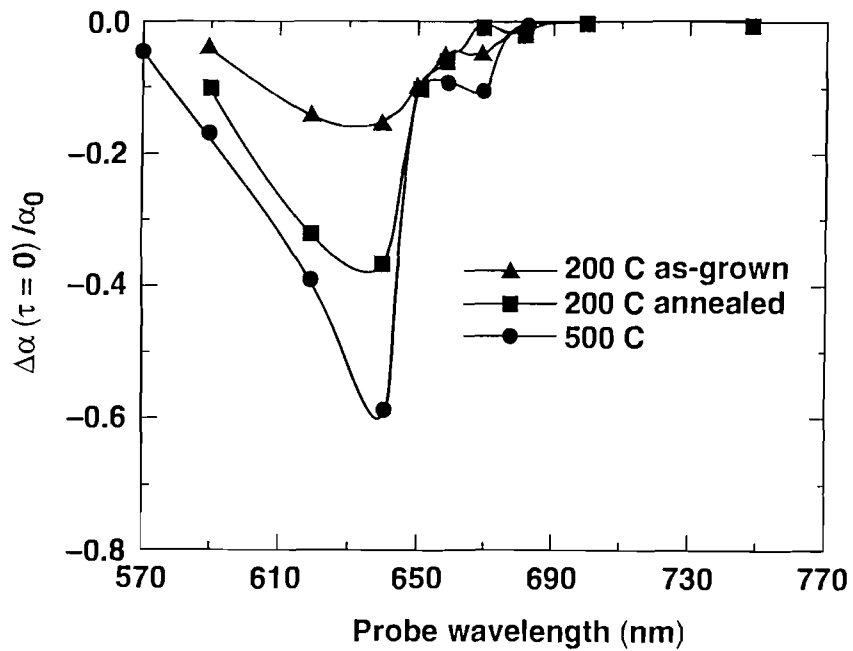
At 750 nm, on the other hand, we observe a much slower increase in absorption which reaches its maximum value with a rise time of ~ 0.35 ps. Identical temporal behavior has also been observed in this sample at a probe wavelength of 700 nm (~ 120 meV below the nominal conduction band edge). The 750 nm probe photons are well below the nominal conduction band edge and also not energetic enough to probe the band tail states. As the photoexcited carriers get trapped, a new absorption channel opens with the re-excitation of the trapped carriers by probe photons, leading to the absorption increase observed at 750 nm. The rise time of the induced absorption at this wavelength, reflects the carrier trapping time. We conclude, therefore, that the trapping time in the 200°C as-grown sample is 0.35 ps. The photo-ionization cross-section at 750 nm is found to be 10^{-16} cm^2 , similar to what we found for LT-InP.

4.5 Spectral Hole Burning In Conventionally And Low Temperature Grown GaInP

When InP is grown at low substrate temperatures, no spectral hole can be observed with an ~ 80 fs time resolution. In Chapter 3 we found that the rise time of the band edge luminescence was pulse width limited for the sample grown at 200°C . This was attributed to a combination of ultrafast relaxation mechanisms such as carrier-carrier scattering and defect ionization scattering. The case of LT-

GaInP turns out to be quite different. Even though we excite low in the conduction band and the injected carrier density is high, we are able to observe spectral hole burning in this material.

In **Figure 4.10**, we show the amplitude of the absorption bleaching at the peak of the excitation pulse normalized over the linear absorption, i.e. $\Delta\alpha(\tau = 0 \text{ fs}) / \alpha_0$, as a function of the probe wavelength for three samples: the 500°C grown and the 200°C as-grown and annealed layers. All samples show a clear spectral hole burning peaked at 640 nm, instead of 620 nm which is the excitation energy. This is due to significant carrier-carrier scattering at these high injected carrier densities which leads to a spreading of the carrier distribution during photo-excitation. Additionally, the spectral extend of the pump pulse leads to an overlap of the electron distributions from the heavy- and light-hole bands. This overlap combined with the strong carrier-carrier scattering at the high injected carrier density conditions of our measurements, causes the peak of the carrier distribution to be at 640 nm. The sample grown at 500°C shows a peak bleaching of ~60%. When the growth temperature is lowered to 200°C, the peak bleaching is reduced by more than a factor of 6, to less than 10%. This is attributed to an ultrafast carrier scattering mechanism, such as impact ionization of defects, which largely spreads the carrier distribution within our time resolution. Similar behavior has been observed in pump-probe measurements on LT-InGaAs. After a modest annealing at 450°C for 10 min, a partial recovery of the spectral hole peak amplitude to ~40% is observed. This is due to a reduction of the density of point



Z2015

Figure 4.10 Contrary to LT-InP (Ref. 10), Spectral hole burning is observed in LT-GaInP and is more pronounced in the normally grown sample. Its amplitude reduces by more than a factor of 6 when a large density ($>10^{19} \text{ cm}^{-3}$) of point defects is present, and recovers partially after annealing the sample at 450°C for 10 min.

defects introduced by the low temperature growth, as can also be seen by the slower recovery of the bleaching signal in Figure 4.8.

A similar ultrafast spreading of the as-excited carrier distribution has also been observed in the case of 200°C grown LT-InP.[24] No spectral hole was observed in this material as was evident by the pulse-width limited rise time of the band edge luminescence after excitation at 2 eV with 80 fs pulses.

4.6 Carrier Trapping vs Recombination in Low Temperature Grown GaInP

In order to distinguish between carrier trapping in the defect levels and carrier recombination, we performed experiments in which both pump and probe are well below the conduction band edge of GaInP. From resistivity measurements, the activation energy (at T~0 K) of the dominant donor in as-grown GaInP is 0.48 eV below the conduction band edge. With 840 nm photons (~0.42 eV below the band edge) we can therefore directly probe the defect states. After annealing, the situation becomes a bit more uncertain. The room temperature resistivity is very high and its value ($\sim 10^9 \Omega\text{cm}$) as well as the activation energy (~0.8 eV) are extrapolated from measurements at higher temperatures.[2]

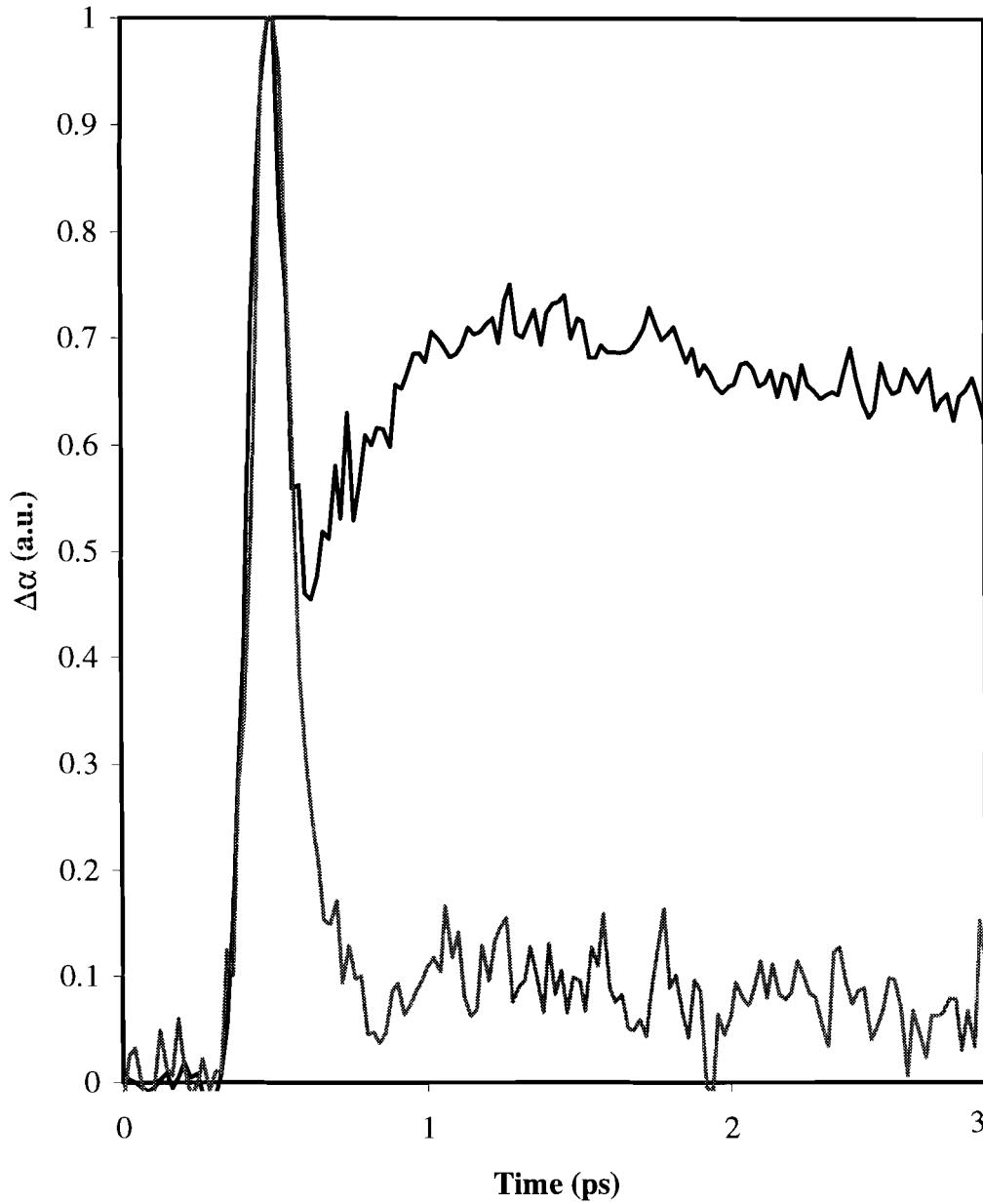


Figure 4.11 Comparison of the response of the 300°C as-grown sample and of that of the normally grown sample with both pump and probe at 840 nm. Two-photon absorption is the major contribution to the signal at early time delays for both samples. Free carrier absorption and photo-ionization of the traps takes over at longer times.

In **Figure 4.11** we show the results of differential absorption measurements performed with both pump and probe at 840 nm on the 500°C and 300°C as-grown samples. Both layers show an increase of absorption after photoexcitation. In the 500°C grown sample, the signal is dominated by two photon absorption (TPA), followed by a small absorption plateau due to free carrier absorption (FCA). By solving

$$\frac{d}{dz} I_p = -\beta_2 I_p I - \frac{1}{3} \sigma N I_p \quad (1)$$

where Gaussian transverse mode profiles are assumed, I and I_p are the pump and probe intensities, β_2 is the TPA coefficient, σ is the free carrier absorption cross section, we can determine the values of β_2 and σ . The carrier concentration N , is given by

$$N(t) = \frac{\beta_2}{4\hbar\omega} \int_{-\infty}^t I^2(t') dt' \quad (2)$$

In (1) we assumed that the linear absorption is negligible at the wavelength used and in (2) that there are not memory effects between pulses. We determine the values of the TPA coefficient to be $\beta_2 = 3.3 \text{ cm/GW}$, in good agreement with the $\beta_2 \sim E_g^{-3}$ scaling law,[25] and the induced absorption cross section to be $\sim 10^{-16} \text{ cm}^2$. This value is about an order of magnitude larger than what has been observed for FCA in the case of GaAs[26] at similar $\hbar\omega / E_g$ ratios, where $\hbar\omega$, is the photon energy and E_g is the bandgap energy of the material. This is probably due to the existence of a small density of defects in the epilayer[27] whose photo-

ionization cross section, being larger than the FCA cross section, dominates the calculated value of σ .

In the case of the 300°C sample, TPA dominates the signal at early time delays as can be seen from the short-lived peak around $\tau \sim 0^+$ fs. A slower rise of the absorption follows at later time delays and it is attributed to photoionization of the defects after trapping of the injected carriers. The time it takes for this slow increase in absorption to reach its maximum value is ~ 0.8 ps, in good agreement with the slow decay component of 0.9 ps observed in the bleaching measurements. The signal does not recover for tens of picoseconds, indicating that carrier recombination is much slower than carrier trapping. This is in agreement to our 2 eV-pump measurements where a long-lived induced absorption plateau has been observed.

The corresponding measurements for the 200°C as-grown and annealed samples are depicted in **Figure 4.12**. The as-grown 200°C sample shows a similar trend as its 300°C grown counterpart. The absorption increases via a pulsewidth limited rise, followed by a slower increase which leads to a maximum at ~ 0.35 ps after photo-excitation. After annealing, the 200°C sample shows a very similar behavior to that of the 500°C sample, indicating a large reduction in the density of point defects. This is in agreement with our observation of a slower response at 2 eV.

For both the 300°C and the 200°C as-grown samples, the increase in absorption does not recover appreciably within 3 ps due to the carrier

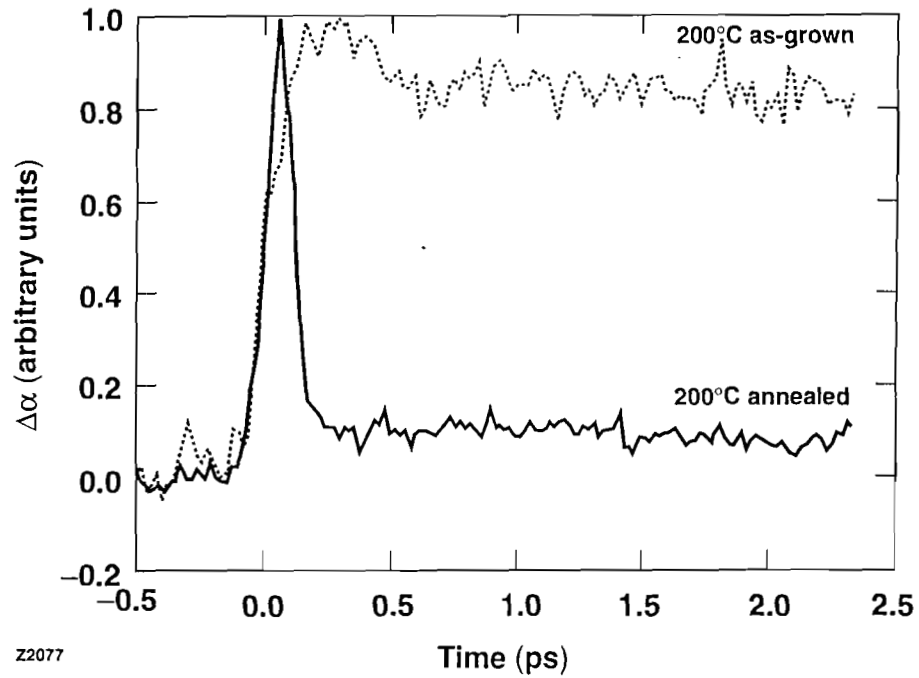


Figure 4.12 Similar measurements as in Figure 4.11 but for the 200°C as-grown and annealed samples. Even a modest anneal of 10 min at 450 °C reduces the number of traps and the response of the material is very similar to that of a conventionally grown sample.

recombination being much slower than carrier trapping. Similar behavior has been found in LT-GaInAs and LT-GaAs. The photo-ionization cross-section of the traps in the 200°C as-grown sample is estimated to be $\sim 5 \times 10^{-16} \text{ cm}^2$.

4.7 Conclusions

In this chapter we have presented the results of differential absorption measurements at energies above and below the bandgap, on $\text{Ga}_{0.51}\text{In}_{0.49}\text{P}$ grown at 500°C, 300°C and 200°C. Due to the excitation low in the conduction band, only a small relaxation of the injected carriers is observed at low densities in the conventionally grown material. At high injected densities a slow increase of the bleaching is observed, probably due to a slow interband relaxation of light holes. Bandgap renormalization and Coulomb enhancement play also a role in the carrier dynamics. Under these experimental conditions, bandgap renormalization is more important since Coulomb enhancement is a band edge effect. Band filling together with renormalization of the band edge, lead to behavior opposite than what is observed for experiments where excitation high in the conduction band takes place.

When the material is grown at low temperatures, a high density of defects is present. These defects are probably P_{In} and are of a density $> 10^{19} \text{ cm}^{-3}$, since no saturation is observed in the response of the sample grown at the lowest

temperature. Trapping of the photoexcited carriers, in the low temperature grown samples, takes place at sub-picosecond time scales with time constants of 0.35 ps and 0.9 ps for the as-grown 200°C and 300°C samples, and of 0.7 ps for the 200°C annealed sample. In contrast, a study below the gap, with 880 nm photons, shows a long (>10 ps) recombination time. Re-absorption of the trapped carriers by the probe photons leads to induced absorption with a cross section of $\geq 10^{-16}$ cm². A modest anneal of the 200°C sample, slows its response indicating that the point defects are responsible for the sub-picosecond trapping times. In contrast to what has been observed in the case of LT-InP, the burning of a spectral hole is observed in LT-GaInP.

References

1. K. H. Bachem, Th. Lauterbach, M. Maier, W. Pletschen, and K. Winkler, *Inst. Phys. Conf. Ser.* **120**, 293 (1991).
2. D. C. Look, Y. He, J. Ramdani, N. El-Masry, and S. M. Bedair, *Appl. Phys. Lett.* **63**, 1231 (1993).
3. Y. He, J. Ramdani, N. A. El-Masry, D. C. Look, and S. M. Bedair, *J. Electron. Mat.* **22**, 1481 (1993).
4. C. Alibert, G. Bordure, A. Laugier, and J. Chevalier, *Phys. Rev. B* **6**, 1301 (1972).

5. H. C. Casey, and M. B. Panish, *Heterostructure Lasers* (Academic, New York, 1978), part A.
6. J. E. Bair, D. Cohen, J. P. Krusius, and C. R. Pollock, *Phys. Rev. B* **50**, 4350 (1994).
7. M. Ulman, D. W. Bailey, L. H. Acioli, F. G. Vallée, C. J. Stanton, E. P. Ippen, and J. G. Fujimoto, *Phys. Rev. B* **47**, 10267 (1993).
8. T. Gong, P. Mertz, W. L. Nighan Jr., and P. M. Fauchet, *Appl. Phys. Lett.* **59**, 721 (1991).
9. T. Gong, P. M. Fauchet, J. F. Young, and P. J. Kelly, *Phys. Rev. B* **44**, 6542 (1991).
10. R. Tommasi, P. Langot, and F. Vallée *Appl. Phys. Lett.* **66**, 1361 (1995).
11. B. R. Bennett, R. A. Soref, and J. A. Del Alamo, *IEEE J. Quantum Electron.* **QE-26**, 113 (1990).
12. D. W. Snoke, D. W. Rühle, Y. C. Lu and E. Bauser, *Phys. Rev. B* **45**, 10970,(1992).
13. T. Elsaesser, J. Shah, L. Rota and P. Lugli, *Phys. Rev. Lett.* **66**, 1757, (1991).
14. J. F. Young, T. Gong, P. J. Kelly and P. M. Fauchet, submitted to *Phys. Rev. B*
15. P. C. Becker, H. L. Fragnito, C. H. Brito Cruz, R. L. Fork, J. E. Cunningham, J. E. Henry and C. V. Shank, *Phys. Rev. Lett.* **61**, 1647, (1988).

16. W. H. Knox, D. S. Chelma, G. Livescu, J. E. Cunningham and J. E. Henry, Phys. Rev. Lett. **61**, 1290, (1988).
17. T. Gong, P. M. Fauchet, J. F. Young and P. J. Kelly, Phys. Rev. B **44** 6542, (1991).
18. J. F. Young, T. Gong, P. M. Fauchet, and P. J. Kelly, Phys. Rev. B **50**, 2208 (1994).
19. plasmon emission is negligible at these carrier densities since $\hbar\omega_p \sim 8$ meV.
20. D. C. Scott, R. Binder, and S. W. Koch, Phys. Rev. Lett. **69**, 347, (1992).
21. T. Gong, W. L. Nighan Jr, and P. M. Fauchet, Appl. Phys. Lett. **57**, 2713 (1990).
22. J. E. Bair, D. Cohen, J. P. Krusius, and C. R. Pollock, Phys. Rev. B **50**, 4355 (1994).
23. E. S. Harmon, M. R. Melloch, J. M. Woodall, D. D. Nolte, N. Otsuka, and C. L. Chang, Appl. Phys. Lett. **63**, 2248 (1993).
24. Y. Kostoulas, L. J. Waxer, I. A. Walmsley, G. W. Wicks, and P. M. Fauchet, Appl. Phys. Lett. **66**, (1995).
25. E. W. Van Stryland, H. Vanherzeele, M. A. Woodall, M. J. Soileau, A. L. Smirl, S. Guha, T. F. Bogges, Opt. Eng. **24**, 613 (1985).
26. A. S. Jordan, J. Appl. Phys. **51**, 2218 (1980).
27. R. E. Viturro, J. D. Varriano, and G. W. Wicks, Mat. Res. Soc. Symp. Proc. **325**, 513 (1994).

CHAPTER 5**Femtosecond Carrier Dynamics In Low Temperature-Grown
GaAs****5.1 Introduction**

Many semiconductor optoelectronic devices, such as photoconductive switches and photodetectors, must operate in the multi-GHz regime. This requires a photoinjected carrier lifetime of ~ 1 picosecond, which can be achieved with appropriate defect engineering. There are at least two important challenges. One is to identify the defects and the necessary density level that not only produce such an ultrafast response time but also yield acceptable electrical properties and long term stability. The second is to understand the detailed role of the defects and eventually manipulate them to achieve the desired functionality.

In the previous chapters we have investigated the dynamics of carriers in InP and GaInP grown at low substrate temperatures. The electrical properties of these materials are quite different. InP, when grown at low substrate temperatures, is heavily n-type both as-grown and annealed. This severely limits its optoelectronic applications. GaInP, on the other hand, is highly resistive in both forms. In spite of these differences, their optical response appears to be qualitatively the same at the lowest growth temperatures. This naturally leads to a

comparison with LT-GaAs, a material that has been more extensively studied and characterized. As growth temperature is reduced, more As is incorporated in the material during epitaxial growth, which leads to a high density of point defects that form a defect band with an average energy of 0.75 eV below the conduction band edge. In a sense, LT-GaAs is an intermediate material between LT-InP and LT-GaInP. As-grown, it is of low resistivity (0.3-20 Ωcm) due to nearest neighbor hopping of holes in the defect band, and, like LT-InP, of limited use in electrooptic applications. After annealing at $\sim 600^\circ\text{C}$ for 10 min, its resistivity increases by a several orders of magnitude (up to $10^6 \Omega\text{cm}$) and As clusters appear. This is the form of the material that is useful and has generated so much interest.

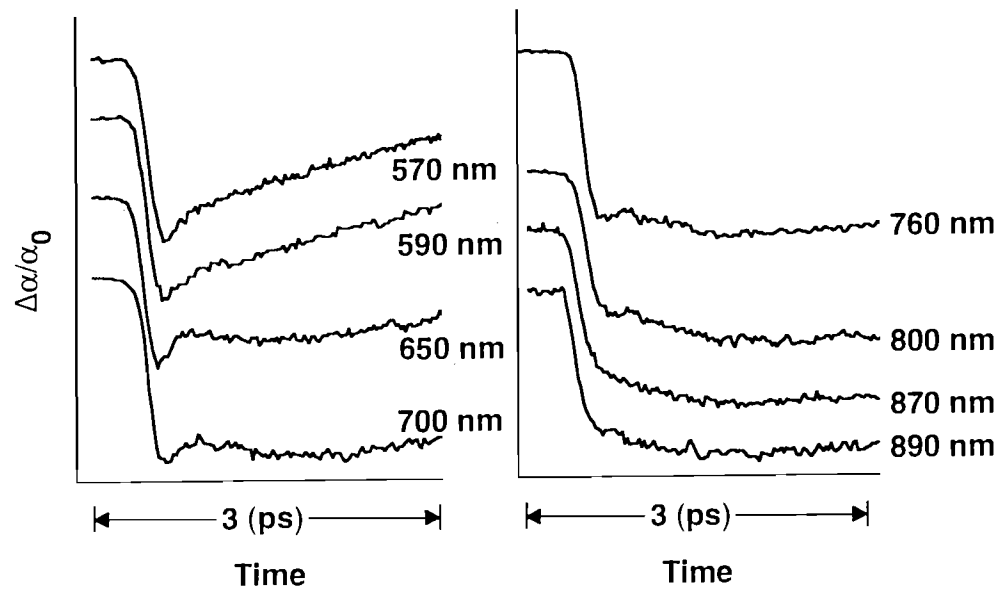
In this chapter we make use of the 2-eV-pump/WLC-probe system in order to investigate carrier dynamics in two samples grown at temperatures of 250°C and 195°C . After growth, part of the 195°C sample is annealed at 600°C for 10 minutes in As overpressure in order to investigate the effects of annealing in the optical response. We also present some preliminary experiments performed with a ~ 100 fs, 1.53-eV-pump/WLC-probe laser system on the above samples as well as on a normally grown GaAs layer.

5.2 LT-GaAs grown at 250°C

The results of the pump-probe measurements performed on the sample grown at a substrate temperature of 250°C are presented in **Figure 5.1**. The

injected carrier density is $\sim 8 \times 10^{18} \text{ cm}^{-3}$. The probe wavelength is varied from 570 nm to 890 nm, which corresponds to ~ 31 meV below the room temperature band edge of normally grown GaAs. The behavior of the sample resembles that of a conventionally grown material throughout the range of wavelengths studied. At the shortest wavelengths (570 nm and 590 nm), we observe a small partial relaxation in the first 200 fs. A slower time constant takes over at longer times. Intervalley transfer together with LO-phonon emission causes the fast relaxation. Combining the Γ -X,L scattering time of ~ 120 fs and the e-LO phonon emission time of 180 fs yields an effective initial scattering time of 65 fs. As a result only less than 35% of the *total* excited electrons ever accumulate in the as-excited states for 2 eV excitation [1]. Most of them have already scattered away within the pulse width since the effective initial scattering time is about half the pump pulsewidth at room temperature. After the first ~ 200 fs (without deconvolution) the spin-split-off probe will make a major contribution to the signal by monitoring bandfilling and cooling of the Γ -valley electron distribution [1].

As the probe photon energy becomes smaller (longer wavelengths), a slow increase in the observed bleaching appears after ~ 1.5 ps. It becomes visible at 650 nm and increases in magnitude up to 800 nm probe wavelength. It is due to the return of the carriers from the L-valley and their relaxation towards the bottom of the conduction band. About 80% of the electrons in the X valley transfer to the L-valley and only 20% to the Γ -valley [2]. The X-to-L transition takes place in ~ 130 fs [2] at room temperature while the L-to- Γ transition takes ~ 2 ps, which



Z1901

Figure 5.1 Pump-probe using the 2-eV-pump/WLC-probe system on LT-GaAs as-grown at 250°C.

is comparable to our observations.

As the probe wavelength is increased to 870 nm and 890 nm, the slow rise of the bleaching completely takes over. This behavior is commensurate with what has been observed in GaAs grown at high temperatures ($\sim 500^\circ\text{C}$) and it is due to band filling from the carriers returning from the satellite valleys. We do not see any short lived increase in absorption around $\tau \sim 0$ fs which has been attributed to band gap renormalization in the case of the conventionally grown material. Bleaching due to band filling dominates the signal even at $\tau \sim 0$ fs, indicating that a strong scattering mechanism has extended the carrier distribution close to the band edge. This is in agreement to what we have observed in other materials such as LT-InP and LT-GaInP. Similar results have been seen in the case of LT-GaInAs.

The absorption plateau at longer time delays, which has been seen in LT-InP and LT-GaInP and is attributed to re-absorption of the probe photons by the trapped carriers, is not observed within the 3 ps time window shown in Figure 5.1. We performed experiments at time delays of up to 15 ps but we were not able to see any induced absorption.

We need to note that there is some uncertainty of the order of 50 K, in determining the temperature of the substrate during growth. A higher growth temperature leads to a lower density of point defects. This low defect density, in turn, can be saturated at our experimental conditions of high injected carrier densities, leading to an optical response that resembles that of the conventionally grown material. This would put an upper bound to the defect density in this sample

at $\sim 10^{18} \text{ cm}^{-3}$. Saturation of the traps at high injected carrier densities has also been observed in LT-InP grown at 300°C (chapter 3). Unfortunately, it is difficult to test this hypothesis with the 2-eV-pump/WLC-probe system since a reduction of the injected carrier density leads to fast deterioration of the signal-to-noise ratio due to the low repetition rate of the laser system.

5.3 LT-GaAs grown at 195°C

When the growth temperature is lowered from 250°C to 195°C , the transient behavior changes appreciably. At this very low growth temperature, a total density of defects of 10^{20} cm^{-3} has been reported, mostly comprised of As antisite defects. Of these, 5% are ionized leading to a hole density of $5 \times 10^{18} \text{ cm}^{-3}$ in the defect band. The result of the measurements using the 2-eV-pump/WLC-probe system are depicted in **Figure 5.2**. From 570 nm to 750 nm the response of the sample is qualitatively the same. A fast relaxation is observed in the first 200 fs, followed by a slower component of ~ 2 ps (without deconvolution). This is a much faster response than what has been observed in the conventionally grown material at these high injected carrier densities. For example, after a fast partial relaxation due to intervalley transfer, the signal at 2 eV is dominated by the spin-split-off transition. At high injected carrier densities, this transition is saturated leading to a plateau that does not recover for tens of picoseconds. In LT- GaAs, as in LT-InP, the bleaching signal gives way to an induced absorption plateau at about 3 ps after

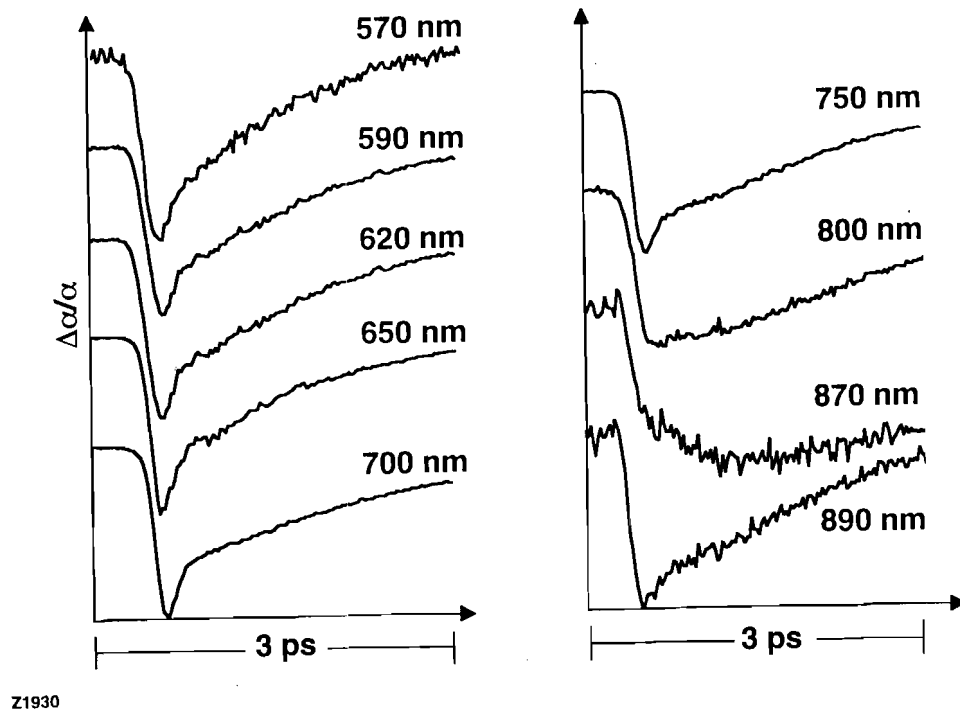


Figure 5.2 Pump-probe using the 2-eV-pump/WLC-probe system on LT-GaAs as-grown at 195°C (see text for details).

the maximum bleaching.

At about 31 meV below the band gap (890 nm) we observe a fast recovery of the signal. At this probe wavelength, the kinetic energy of the carriers is negligible and the decay time observed is due to carrier trapping. A single exponential fit of the data, shown in **Figure 5.3**, yields a trapping time of 1.4 ps.

Annealing the 195°C-grown sample at 600°C for 10 min under As overpressure changes the optical response towards that of the conventionally grown material. The results of our experiments using the 2-eV-pump/WLC-probe system are shown in **Figure 5.4**. The bleaching at the shortest wavelengths (590 nm - 620 nm) recovers through two components, in a manner similar to what has been observed in the case of the as-grown 250°C sample. At 650 nm a slow increase of the bleaching is observed, which keeps increasing in amplitude up to the 800 nm probe wavelength. This component is due to the relaxation of the carriers excited at 2 eV to the bottom of the conduction band and also to the return of the carriers from the satellite valleys. At 870 nm, which corresponds to the room temperature unperturbed band edge of high temperature grown GaAs, the slowly increasing component completely takes over. When the probe wavelength is increased even further to 890 nm, an increase of the absorption is observed around zero time delay. This initial increase of absorption below the band edge is attributed to band gap renormalization and plasma screening of Coulomb interactions. A similar observation was made by Shank et al. at low temperatures and with 0.5 ps time resolution and by Gong et al. at room temperature and sub-

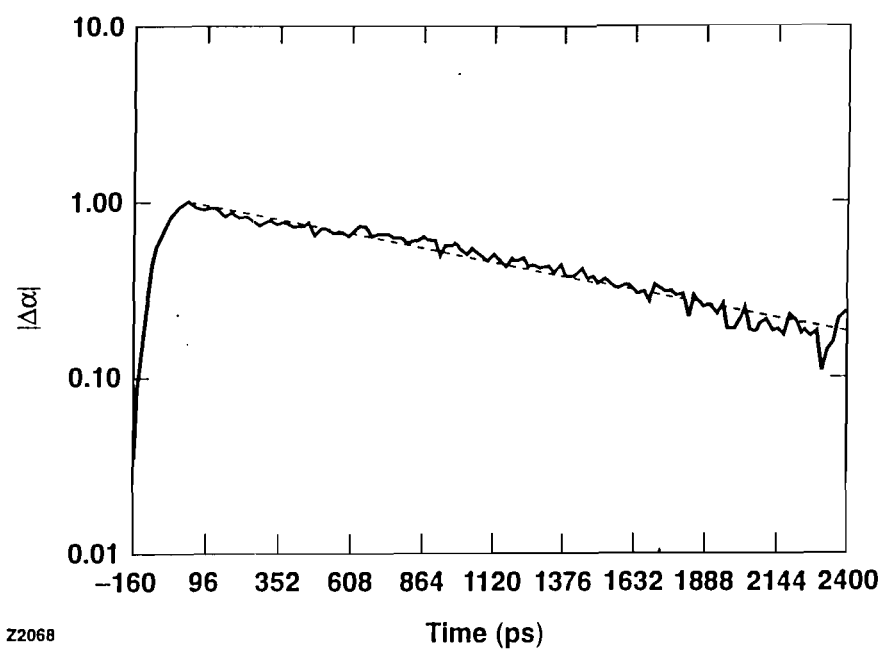


Figure 5.3 Single exponential fit of the 890 nm probe trace of the LT-GaAs as-grown at 195°C. The carrier trapping time is found to be 1.4 ps.

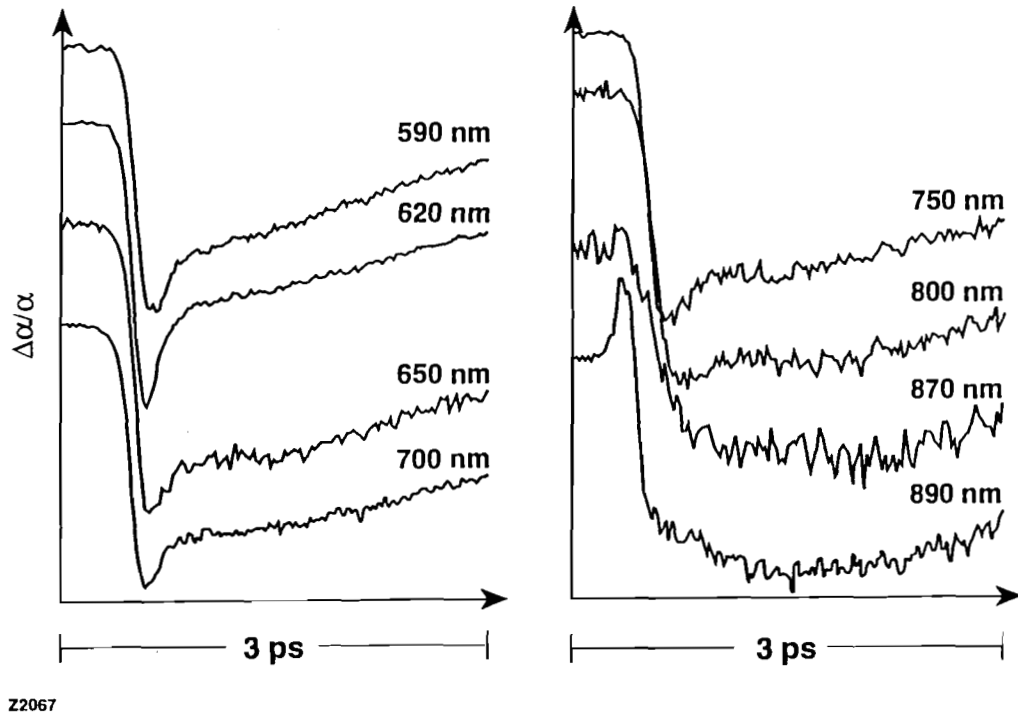


Figure 5.4 Pump-probe using the 2-eV-pump/WLC-probe system on LT-GaAs as-grown at 195°C and annealed under As overpressure at 600°C for 10 min. The response is similar to that of the normally grown material, indicating that the density of traps is significantly reduced.

100 fs time resolution. The subsequent decrease of absorption indicates that the states near the re-normalized band edge become filled. Bandgap renormalization is not observed at 860 nm (20 meV above the unperturbed band edge) because the large negative $\Delta\alpha$ produced by plasma screening offsets the small positive $\Delta\alpha$ due to band gap renormalization. The fact that bandgap renormalization does not take place in the as-grown sample is probably due to the existence of a large band tail. This lack of bandgap renormalization was first observed in α -Si:H [Fauchet et al. J. Non Cryst. Solids (1992)], an other material with a large density of bandtail states.

In **Figure 5.5** we compare the behavior of the three samples around the band edge (excitation at 2 eV) with that of a conventionally grown material. In the case of the conventionally grown GaAs bandgap renormalization leads to increased absorption at $\tau \sim 0$ fs, followed by band filling at longer time delays at 880 nm and 900 nm. At 860 nm no increase in absorption is observed at $\tau \sim 0$ fs. Instead, only a slow increase in bleaching is seen which is also present at the longer wavelengths of 880 nm and 900 nm. The slow rise time of the bleaching corresponds to the time the photo-injected carriers take to relax to the bottom of the conduction band. The sample grown at 195°C and annealed shows qualitatively the same behavior at 890 nm: at $\tau \sim 0$ fs an increase in absorption is observed due to bandgap renormalization, followed by a slow rise of the bleaching at longer time delays. The annealing leads to a significant reduction of the density of point defects and therefore to a behavior that resembles more that of the conventionally grown

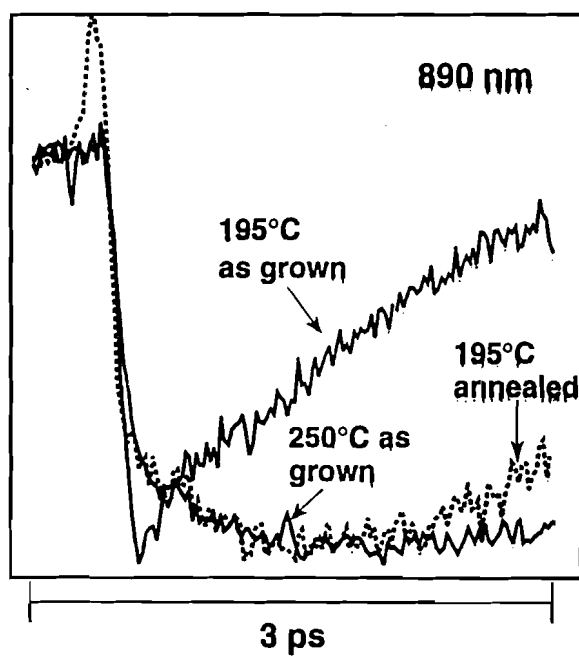
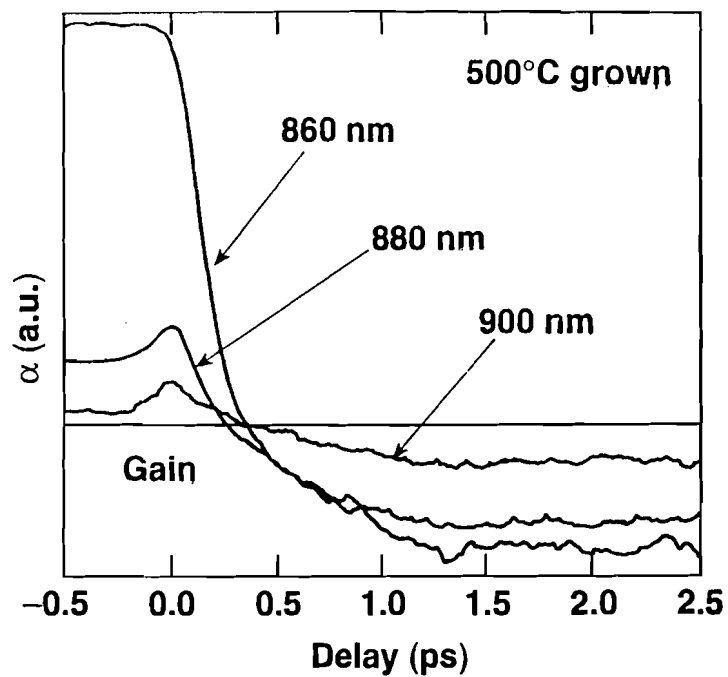


Figure 5.5 Comparison of the bandedge response of four samples grown at different conditions: 500°C, 250°C as-grown, 195°C as-grown, and 195°C annealed.

material. The behavior of the 250°C as-grown sample is very similar to the normally grown, and the 195°C grown and annealed samples apart from one difference: no bandgap renormalization is evident at $\tau \sim 0$ fs. The behavior of the as-grown 195°C sample, on the other hand, is drastically different from that of the above mentioned samples. The maximum of the bleaching is reached within the pulse width, indicating a carrier distribution that extends to the bottom of the conduction band within our time resolution. Thus no spectral hole burning should be observed in this sample, in agreement to what we have observed in the case of the LT-InP. As in the 250°C sample, no renormalization of the band edge is observed in the 195°C as-grown sample, and the existence of a large bandtail is believed to play an important role in this effect.

5.4 Carrier Dynamics Near and Below the Band Edge

In order to investigate the trapping dynamics of carriers in LT-GaAs, experiments were performed with an amplified Ti:Sapphire laser system producing ~ 80 fs pulses centered at 800 nm (1.55 eV). The pulses are amplified by means of a regenerative amplifier to several hundred μJ at a repetition rate of 1 kHz. A small part of the amplifier output is used as the pump pulse while the rest is focused on a sapphire window in order to create a white light continuum from which we select the probe wavelengths by means of interference filters. The probe wavelengths used in our experiments range from 870 nm, which is the unperturbed band edge of

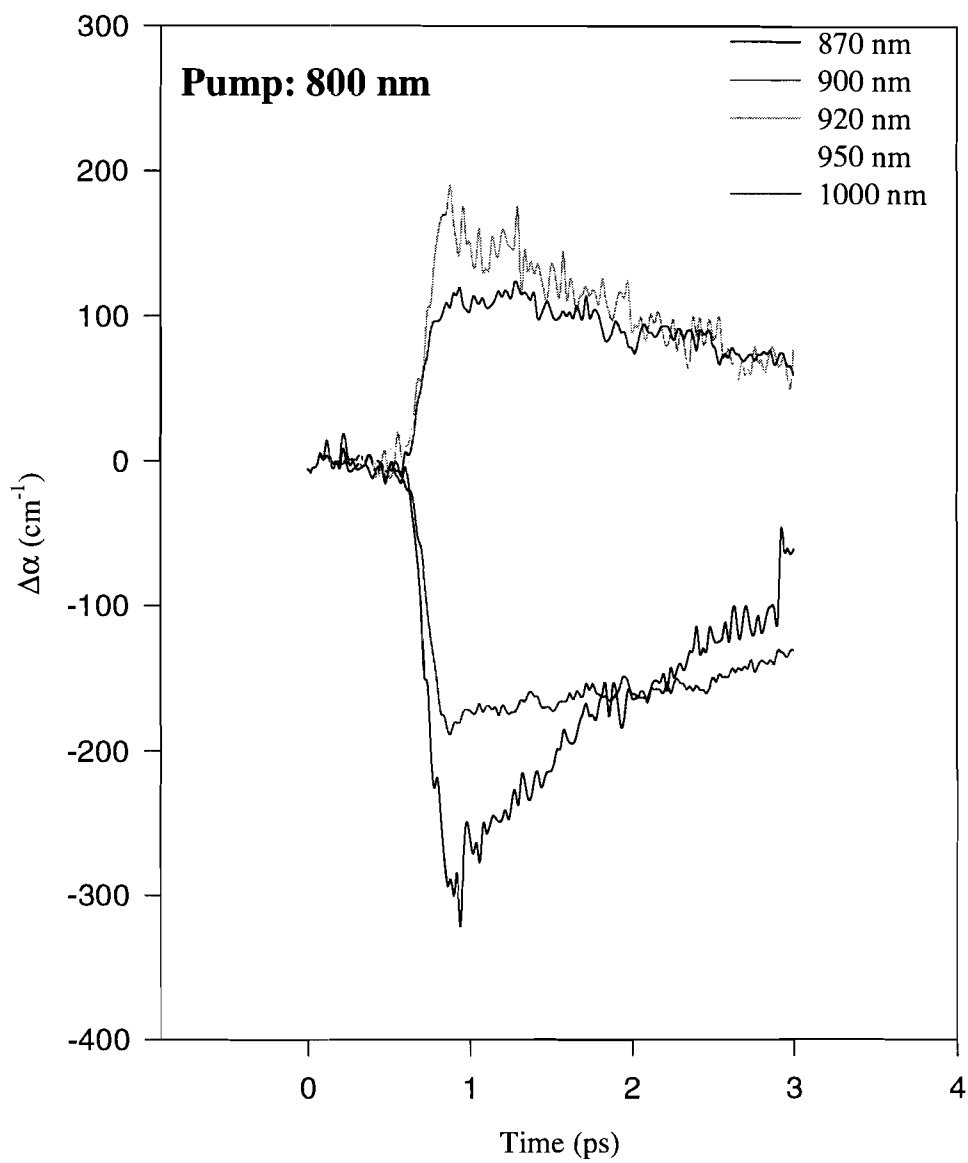


Figure 5.6 Pump-probe on the 195°C as-grown sample using the 1.55-eV-pump/WLC-probe system.

normally grown GaAs (1.425 eV), to 1000 nm (corresponding to ~ 1.24 eV). The growth of GaAs at low substrate temperatures introduces a large density of As_{Ga} antisite defects. Due to their large density, these defects form a band at the midgap of GaAs (0.75 eV below the conduction band). The long probe wavelengths achievable with the amplified Ti:Sapphire system offer an ideal tool in studying the dynamics of carriers in the defect states. In **Figure 5.6** we show the results of pump-probe measurements performed on the 195°C as-grown sample. The injected carrier in these measurements, as well as in the remaining experiments is of the order of $1 \times 10^{18} \text{ cm}^{-3}$. We observe bleaching at 870 nm and 900 nm. The recovery of the signal at 870 nm is described by a single exponential and the decay time is 1.7 ps. This is in good agreement with the 1.4 ps carrier trapping time deduced from our 2-eV-pump/WLC-probe measurements. No bandgap renormalization is observed as in the 2 eV excitation experiments. In a sense, the 2 eV pump measurements are a better indication that no bandgap renormalization is observed in this material. This is so because the injected carrier density in the 800 nm excitation experiments, is of the order of the density of states from the bottom of the band to the excitation energy, and therefore band filling contributes mostly to the observed absorption changes. At the longer wavelengths of 920 nm, 950 nm, and 1000 nm there is only induced absorption. This absorption is due to the photo-ionization of the trapped carriers from the defects.

In **Figure 5.7** we show the results of the same measurements performed on the 195°C grown and annealed sample. Bleaching is observed at 870 nm and 900 nm while induced absorption dominates at the longer wavelengths. A small

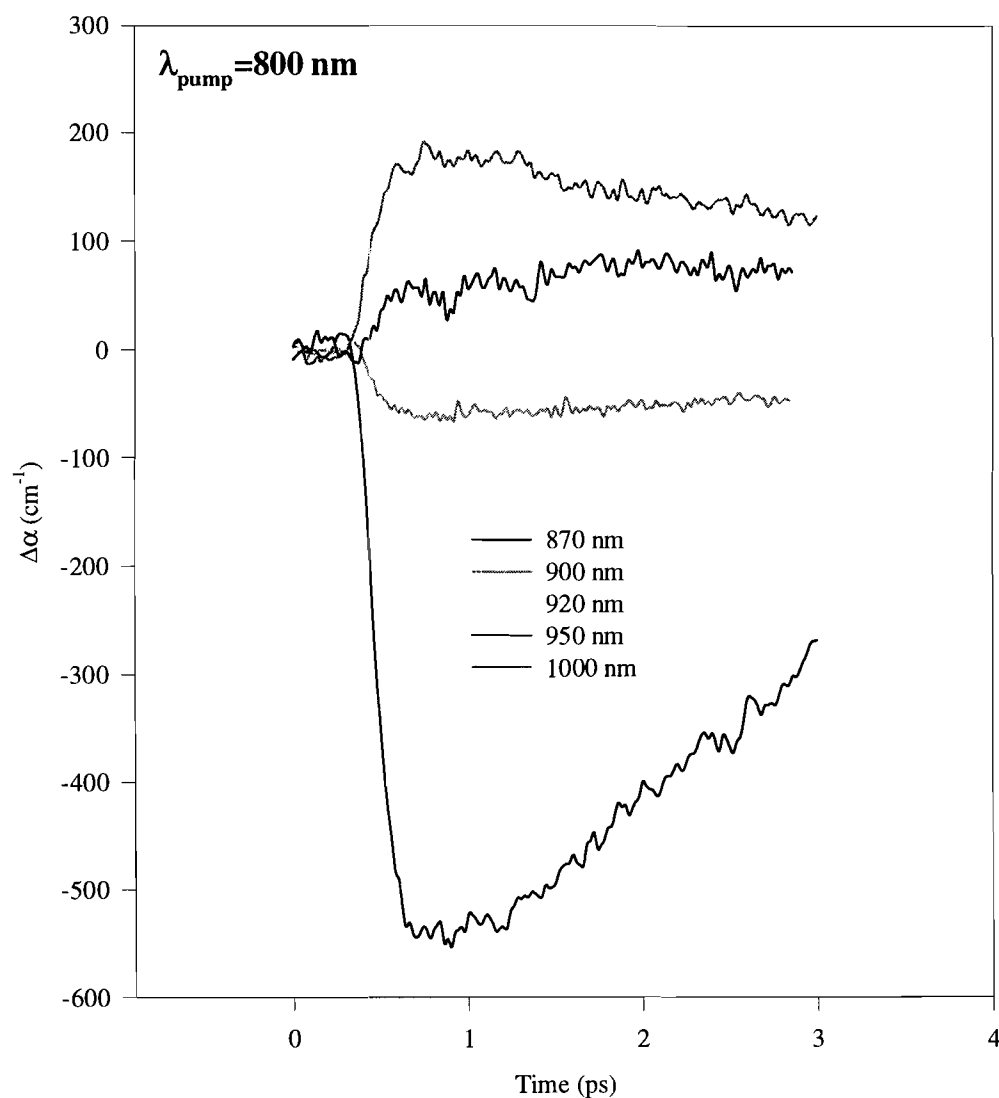


Figure 5.7 Pump-probe on the 195°C annealed sample using the 1.55-eV-pump/WLC-probe system.

increase of absorption is observed around zero time delay at the wavelengths of 870 nm and 900 nm (it is clearly obvious when the traces are plotted individually). This is due to band gap renormalization and is visible in this sample since the annealing reduces the disorder and therefore the bandtail, as compared with the as-grown material. The recovery of the signal is slower than in the as-grown sample, which is consistent with the lower defect density. The photo-ionization cross-section at 1000 nm is found to be $\sim 5 \times 10^{-17} \text{ cm}^2$. The same experiments performed on the 250°C as-grown sample are shown in **Figure 5.8**. This material shows a different behavior than the samples grown at 195°C (as-grown and annealed). Bleaching is observed at 870 nm, 900 nm, 920 nm and 950 nm while induced absorption takes over at 1000 nm. A large induced absorption at 1000 nm indicates some resonance. It is possible that at this higher growth temperature, the defects are of a different nature than in the material grown at the lower temperatures. This can lead to some resonant enhancement of the absorption at this wavelength. Indeed there is some controversy as to where the defects levels are located in the bandgap. D. C. Look et al. [3] have measured an activation energy of 0.65 eV for material grown at substrate temperatures of 300°C, 350°C, and 400°C. Several other experiments have also suggested that the dominant donor in LT-GaAs is shallower than EL2 [4-8]. The results of these measurements performed on the normally grown material are shown in **Figure 5.9**. They were carried out at a smaller injected carrier density ($\sim 10^{17} \text{ cm}^{-3}$) than the previous measurements ($\sim 10^{18} \text{ cm}^{-3}$). There is bandgap renormalization at $\tau \sim 0$ fs at

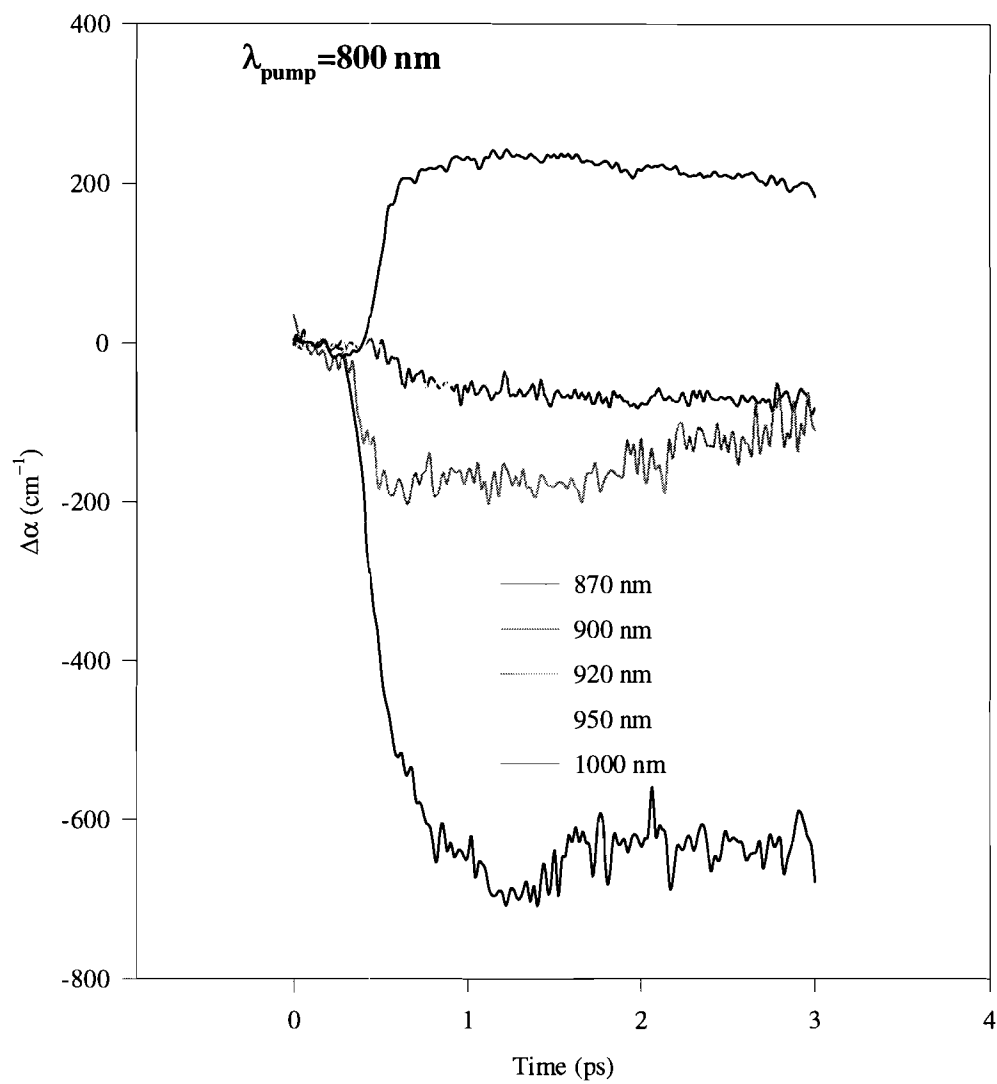


Figure 5.8 Pump-probe on the 250°C as-grown sample using the 1.55-eV-pump/WLC-probe system.

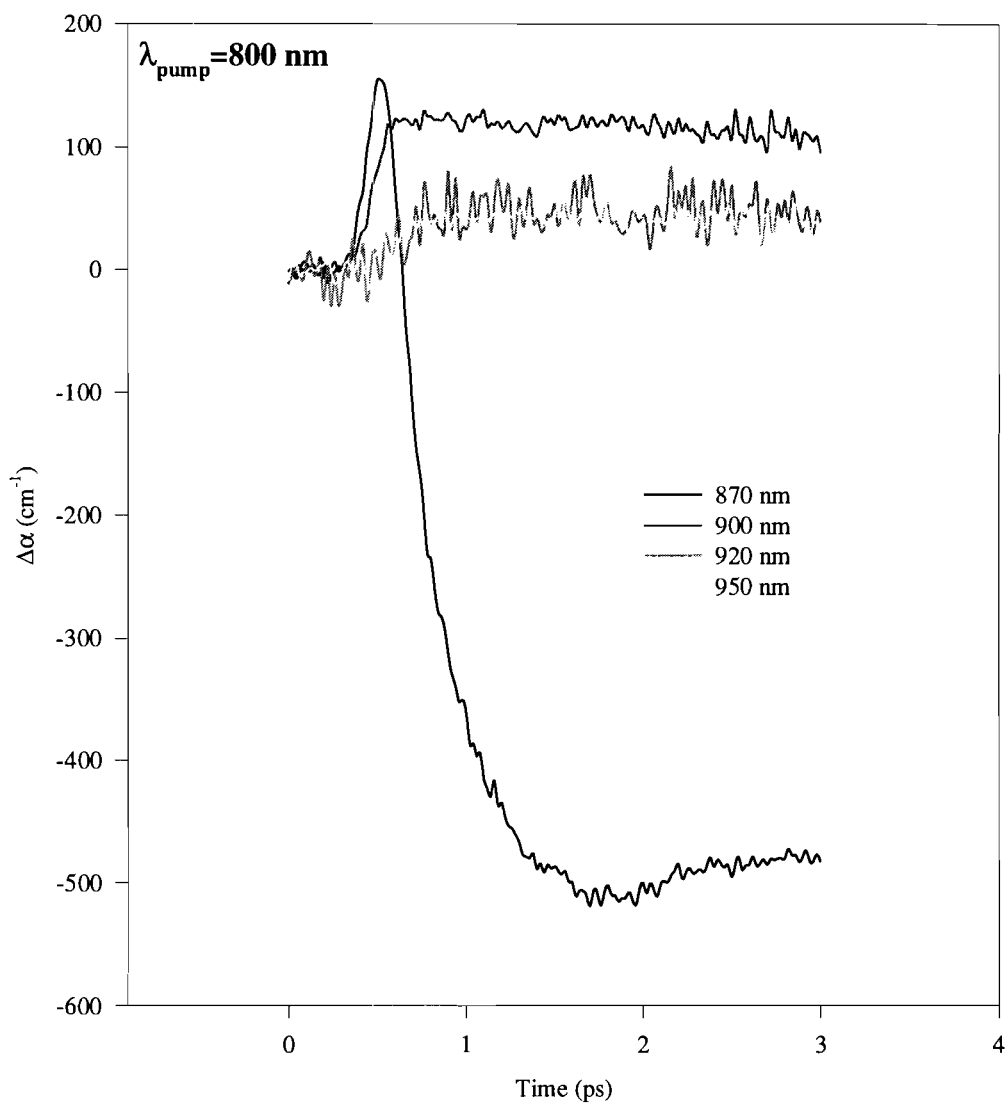


Figure 5.9 Pump-probe on the normally grown sample using the 1.55-eV-pump/WLC-probe system.

870 nm. This wavelength probes the bandedge of the normally grown material. As the carriers relax, band filling leads to bleaching. The relatively slow rise of the bleaching observed here is probably due to a combination of bandgap renormalization and Coulomb enhancement. Monte Carlo calculations which take into account these two mechanisms and dynamic screening, have shown that for a cooling distribution bandgap renormalization slows the observed relaxation while Coulomb enhancement accelerates it. The rest of the wavelengths indicate only induced absorption due to free carrier absorption.

In conclusion we have measured the dynamics of carriers in LT-GaAs using a 2-eV-pump/WLC-probe and a 1.55-eV-pump/WLC-probe systems. The carrier trapping time is found to be ~ 1.5 ps for the 195°C as-grown material. The large disorder in this material, increases the scattering of the photo-excited carriers leading to a carrier distribution that extends to the bottom of the conduction band within our time resolution. Additionally, no bandgap renormalization is observed in the as-grown material both at 250°C and at 195°C. It is recovered after annealing of the 195°C material which leads to a significant reduction of the disorder. The behavior of the material appears to be complicated when probing well below the conduction band edge. Both the sign and the magnitude of the absorption change indicate that the dominant defect may be different for different growth temperatures and annealing conditions. More detailed measurements on samples grown and annealed at different temperatures will shed light into these effects.

References

1. T. Gong, P. Mertz, W. L. Nighan, Jr., and P. M. Fauchet, *Appl. Phys. Lett.* **59**, 721, (1991).
2. S. Zollner, S. Gopalan, and M. Cardona *SPIE* vol. 1282, p. 78 (1990).
3. D. C. Look, *Thin Solid Films*, 2331, 61, (1993).
4. H. J. von Bardeleben, M. O. Manasreh, D. C. Look, K. R. Evans, and C. E. Stutz, *Phys. Rev. B*, **45**, 3372, (1992).
5. D. C. Look, D. C. Walters, C. E. Stutz, K. R. Evans, and J. R. Sizelove, *J. Appl. Phys.* **71**, 5981, (1992).
6. A. C. Warren, J. M. Woodall, P. D. Kirchner, X. Yin, F. Pollak, M. R. Melloch, N. Otsuka, and K. Mahalingam, *Phys. Rev. B*, **46**, 4617, (1992).
7. H. Shen, F. C. Rong, R. Lux, J. Pamulapati, M. Taysing-Lara, M. Dutta, E. H. Poindexter, L. Calderon, and Y. Lu, *Appl. Phys. Lett.*, **61**, 1585, (1992).
8. D. C. Look, J. T. Grant, and J. R. Sizelove, *Appl. Phys. Lett.*, **61**, 1329, (1992).
9. J. E. Bair, D. Cohen, J. P. Krusius, and C. R. Pollock, *Phys. Rev. B*, **50**, 4355, (1994).

CHAPTER 6

Conclusions and Future Directions

GaAs layers grown by molecular beam epitaxy (MBE) at substrate temperatures of 200°C-400°C, well under the normal growth temperature of 600°C, exhibit unique properties and can be profitably used in a variety of applications such as buffer layers for metal-semiconductor field effect transistors (FETs), gate insulator layers for metal-insulator-semiconductor FETs, and channel layers in fast photoconductive switches. The most outstanding features of LT-GaAs are very high point defect densities e.g. about 10^{20} As_{Ga} centers per cm^3 in the 200°C material and a large concentration ($\sim 10^{17}$ cm^{-3}) of As precipitates after annealing for 10 min at 600°C. Other III-V materials, such as AlGaAs, InAlAs, InGaAs, InP, GaInP, and GaP have also been grown at low substrate temperatures and some have shown promise for applications.

In this work we focused on three materials which have properties that span the spectrum of the observed material properties in LT III-V compounds: InP, GaInP, and GaAs. InP exhibits low resistivity in both its as-grown and annealed forms due to the fact that P_{In} , the dominant defect, has an ionization level degenerate with the conduction band. GaInP exhibits high resistivity both as-

grown and annealed while GaAs is low resistivity when as-grown and it becomes resistive after annealing.

How do these differences in electrical properties affect the optical response of the materials? We showed that all these compounds exhibit a very similar behavior: ultrafast scattering due to the disorder in the material spreads the carrier distribution within ~ 100 fs to the bottom of the conduction band which makes the observation of spectral hole burning at least problematic. In all cases, carrier relaxation is followed by carrier trapping with recombination taking place at longer time scales.

What happens to the carriers after photoexcitation? Is trapping or recombination the observed ultrafast response in these materials? The assumption implicit in most work up to now is that recombination is the cause of the fast response. Our pump-probe measurements in conjunction with up-conversion luminescence measurements show clearly that carrier trapping causes the fast response. The trapping times in these materials are measured to be ~ 350 fs for InP and GaInP, and 1.4 ps for GaAs. Carrier recombination is a much slower process that takes place in tens of picoseconds. This also leads to an induced absorption plateau due to re-excitation of the trapped carriers which can lead to complications in optoelectronics applications such as high bit rate optical communications components.

The course of this research has uncovered more questions than it has answered, as is often the case, and therefore much remains to be done. It is also

quite likely that new questions will arise faster than satisfactory answers can be obtained for the few questions presented here. What happens when excitation close to the band edge takes place? How does the behavior change? When the probe wavelengths are well below the band edge, the change in the index of refraction becomes significant. How large is the change in the index of refraction and how does its magnitude and sign correlate with the observed changes in the absorption coefficient? These are questions that can be answered with future experiments. A detailed study of the carrier dynamics as a function of annealing would also yield useful information about the physical effects determining the behavior of these materials. For example, it has been observed [1] that the intensity of midgap luminescence (1.39 eV and 1.24 eV) in LT-GaAs, increases with annealing. Time resolving the dynamics of this midgap luminescence will answer important questions about the changes occurring in the material after annealing.

Of direct technological implication would be materials that are of high resistivity, good crystalline quality, and have a bandgap that corresponds to 1.55 μm , an important wavelength for optical communications. In order to achieve that, changes in composition are necessary which unavoidably lead to changes in the position of the valence and conduction bands. Intuitively, the valence band is more rigid than the conduction. Upon any perturbation that causes changes in volume, the change in conduction band is larger than the change in valence band. Theoretical and experimental work confirm this picture: the change in bandgap energy is mostly due to changes in conduction band energy. Similar concepts apply

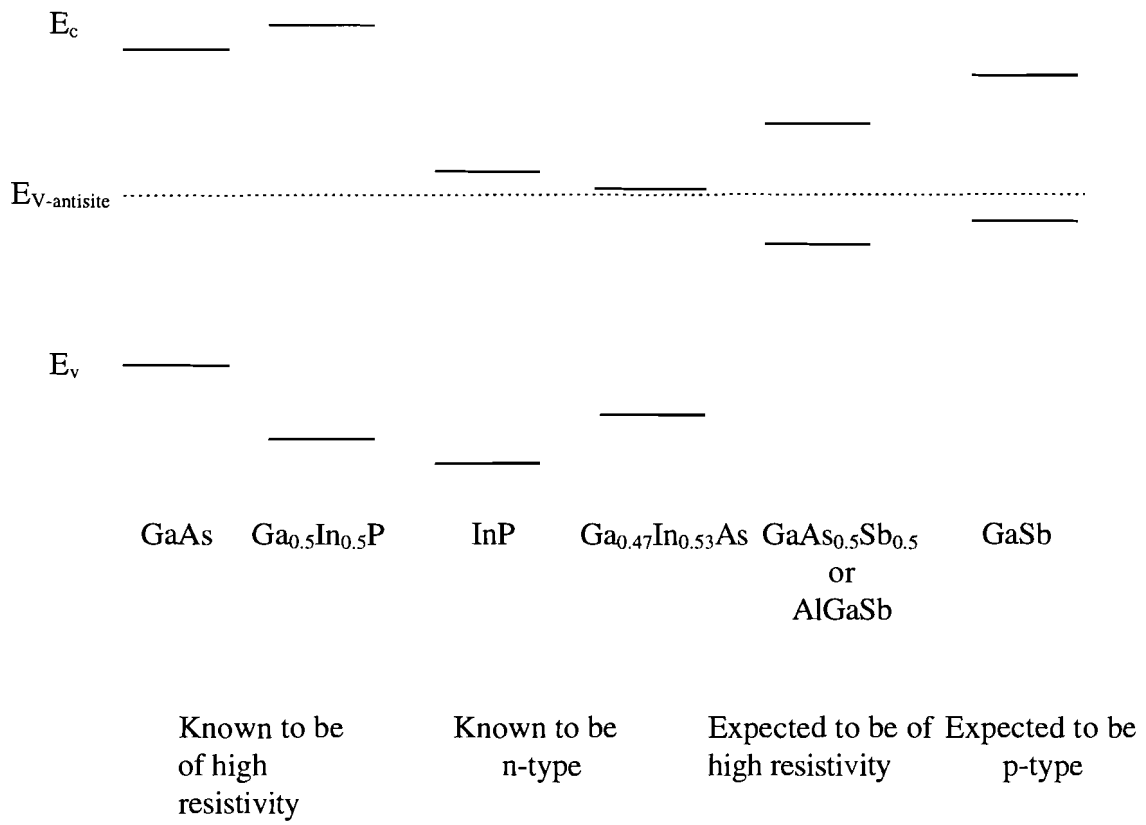


Figure 6.1 Schematic of the expected behavior of other III-V compounds grown at low substrate temperatures.

to shallow donor and acceptor states where the impurity potential is dominated by the long range (Coulomb) term. The case of the deep defects, which are dominant in LT materials, is different. A deep level originates from the central-cell defect potential which is very strong within the effective radius of the defect. It follows that as the material composition is altered to achieve smaller bandgaps, the position of the defects remains roughly unaltered. Therefore, appropriate defect engineering can lead to materials relevant to optical communications wavelengths. Some candidates can be seen in Figure 6.1 [2].

It is hoped that the techniques and observations presented in this thesis will help guide future endeavors in this rich and not yet fully explored field.

References

1. I. Ohbu, M. Takahama, and K. Hiruma, *Appl. Phys. Lett.* **61**, 1679, (1992).
2. G. Wicks, (private communication).